Dynamic ^{18}F-FDG positron emission tomography of xenografts in mice

Thomas Bandur Aleksandersen

Thesis submitted for the degree of
Master of Physics

Biophysics and Medical Physics
Department of Physics
UNIVERSITY OF OSLO

November 15th 2010

2010

Tittel

Thomas Bandur Aleksandersen

http://www.duo.uio.no/

Trykk: Reprosentralen, Universitetet i Oslo.

Abstract

Positron emission tomography (PET) is a medical imaging technique widely used for cancer diagnostics. The objective of this study was to investigate whether dynamic ^{18}F-FDG PET imaging could be used to characterize tumors and monitor treatment response.

In this study we have looked at human prostate and breast cancer xenografts in nude mice. The first set was the androgen sensitive CWR22 prostate cancer, where the untreated tumors were compared with tumors that had received a dose of 7.5 Gy. The second set compared the basal-like MAS 98.12 with the luminal-like MAS 98.06 xenografts of breast cancer.

By using different methods and techniques, a search for distinctions between groups have been conducted. It was first noticed that the very basic time activity curve (TAC) itself differed between the groups. For the latest time points, there was statistically significant differences between groups within each data set. Using a two-compartment pharmacokinetic model, rate constants describing FDG-uptake (k-parameters) have been estimated. These parameters represent some of the physiological conditions in the tumor; uptake and metabolism of glucose. For the CWR22 dataset, comparison of the mean k-parameters (treated tumors against untreated) yielded p-values of 0.06 for k1, the p-value 0.04 for k2 and the p-value 0.14 for k3. For the second dataset (MAS 98.12 against MAS 98.06) the same test yielded for k1 the p-value 0.06, for k2 the p-value 0.92 and for k3 the p-value $<< 0.01$. By investigating every percentile of the parameter and testing, eve lower p-values could in some cases be found.

By combining these parameters, an estimate of the metabolic rate of glucose (MRglc) can be obtained. The results showed that the treated CWR22 tumors were more metabolic active than the controls. We also found that the MAS 98.06 tumors had a higher metabolic rate of glucose than the MAS 98.12. Patlak plots can be used to calculate the MRglc as well and showed similar results; for the first data set a p-value $<< 0.01$. For the second data set a p-value $<< 0.01$ was found.

This study demonstrate that both by looking at the tumor as a whole and investigating the heterogeneity it might be possible to distinguish different tumors from one another using dynamic FDG-PET .

Acknowledgements

First of all I want to thank my supervisors Eirik Malinen and Therese Seierstad for their help, support and patience during this work. I would also like to thank Kathrine Røe for close collaboration on parts of the work. Thanks to Alexander Kristian for handling the animals used for this work and showing me the reins around the animal stall. Thanks to Hong Qu for reconstructing PET images. Thanks to all the students at the Biophysics group for fun times and support, especially to Siv for reading and commenting part of my thesis. Thanks to Radiumhospitalet for funding valuable courses and symposiums I attended. And finally thanks to family and friends for continuous support and encouragement.

Table of Contents

1 Introduction 1
1.1 Motivation and goals 2
2 Background 3
2.1 Basic principles 3
2.1.1 Photon interactions 3
2.2 Equipment of Radiotherapy 4
2.2.1 The linear accelerator 4
2.2.2 The cobalt machine 5
2.3 Positron emission tomography 5
2.3.1 Tracers 6
2.3.2 The tracer in the body 7
2.3.3 Annihilation 8
2.3.4 Photon detectors used for PET 11
2.3.5 Coincidence detection 14
2.3.6 The sinogram 15
2.3.7 Image reconstruction 17
2.3.8 Radiation dose to patients 18
2.4 Pharmacokinetics 18
2.4.1 Two-tissue compartment model 19
3 Experimental setup and procedures 21
3.1 The use of mice for this project 21
3.1.1 On the use of animals and the animal model 21
3.1.2 Implantation of tumors 22
3.1.3 Irradiation 22
3.1.4 PET assay 23
3.2 The tumors used 24
3.2.1 CWR22 24
3.2.2 MAS 98.12 and MAS 98.06 24
3.3 Image and data handling by the use of IDL 26
3.4 Metabolic rate of glucose and the Patlak plot 31
3.5 Statistical methods 33

3.5.1 Hypothesis testing and the students t-test. ... 33
4 Results ... 34
4.1 General investigations ... 34
4.1.1 Illustrations of dynamic series ... 34
4.1.2 Plasma function ... 35
4.1.3 Tumor curves ... 36
4.1.4 Distribution of pharmacokinetic variables ... 38
4.1.5 Investigation of the input parameters of the model ... 41
4.1.6 Adding a blood fraction parameter to the model ... 42
4.2 TAC ... 44
4.2.1 TAC for treated tumors against controls ... 44
4.2.2 TACs of the MAS 98.12 and MAS 98.06 tumors ... 45
4.3 Pharmacokinetic parameters ... 47
4.3.1 Median parameters of the CWR22 ... 47
4.3.2 Median parameters of the MAS 98.12 and MAS 98.06 ... 47
4.3.3 Histograms and percentile charts of CWR22 ... 48
4.3.4 Histograms and percentile charts of MAS tumors. ... 52
4.4 The Patlak plot and calculation of MRglc ... 56
4.4.1 Patlak and MRglc for CWR22 tumors. ... 56
4.4.2 Patlak and MRglc for MAS 98.12 and MAS 98.06 ... 57
4.5 Other investigations ... 57
4.5.1 Blood fraction of the tumors ... 57
4.5.2 Time dependant k-parameter histograms ... 58
4.5.3 Dependance on distance from centre of tumor ... 60
5 Discussion ... 62
5.1 General issues of diagnostic imaging ... 62
5.2 Specific issues for this study ... 63
5.2.1 Tumor delineation ... 63
5.2.2 The arterial input function ... 63
5.2.3 The CWR22 dataset ... 64
5.2.4 The MAS 98.12 and MAS 98.06 dataset ... 64
5.3 Investigations of the CWR22 data ... 64
5.3.1 The time activity curve ... 65

5.3.2 Pharmacokinetic model 66
5.3.3 Looking at the metabolic rate of glucose 66
5.3.4 TAC versus pharmacokinetics 67
5.4 Investigations of the MAS 98 xx data 67
5.4.1 The time activity curve 67
5.4.2 Pharmacokinetic modeling 68
5.4.3 Metabolic rate of glucose 68
5.4.4 TAC versus pharmacokinetics 68
5.5 Radial dependency 69
5.6 Conclusions 71
5.7 Further work 71
Index 72
Bibliography 73
Appendix 76

1 Introduction

In Norway, about 1/3 of total deaths are caused by cancer. For people aged between 45 and 74 years of age, cancer is the most common cause of death. Still, the actual chance of dying from cancer is reduced since 1997. (1)

Cancer is developed from cells that have lost the ability to control their cell division and self-elimination mechanics (apoptosis). The cancer cells will therefore multiply rapidly and a large lump of cells (tumor) will eventually be formed. Some tumors stop their growth when they reach physical limitations and are characterized as benign. Other tumors however will invade surrounding tissue and are characterized as malign. In order to maintain growth the tumor need blood vessels for nutrition and oxygen. They have therefore the ability to provoke angiogenesis, the recruitment of new blood vessels. With a makeshift blood network the tumor will be able to grow larger, and will also have a way of spreading to other regions of the body. The phenomenon is called metastasis and is a major challenge in cancer treatment. (2)

There are several different ways of treating cancer, and radiotherapy is one of them. The discovery of x-rays in 1895 by Wilhelm Röntgen and the discoveries of radium and polonium by Marie Curie was the beginning of radiotherapy. Thus radiotherapy of cancer has been present for more than 100 years. At first radium was mainly used for treatment, followed by cobalt and cesium units in the 1950s. The medical linear accelerators have been in use since the 1940s and are the standard in modern clinics. (3) Other treatment methods include brachytherapy which is radioactive metals placed inside or close to the tumors. Chemo and hormone therapy is other methods where medicinal drugs are involved. Surgery is still the most used method for treating cancer. All these modalities have strengths and weaknesses, but they can be combined for more effective treatment. For instance, external radiotherapy may be given after surgery to deal with possible residual disease.

The development of modern imaging techniques like computed tomography, nuclear magnetic resonance imaging and positron emission tomography (PET) have contributed to better treatment planning and tumor delineation in radiotherapy. PET is a diagnostic imaging technique that have several different applications regarding cancer. It can be used to find tumors in the body, especially useful if there is a chance that a primary tumor discovered has spread to different locations. Furthermore, PET may be used to help distinguish malign tissue from benign tissue and define the stage of the disease. Also, PET may aid further characterization of tumors, which can be used to identify radioresistant regions within tumors in need of elevated radiation doses, and then monitoring response of the therapy. After

ended therapy PET can be used to examine the any remains of the tumor and evaluate the chance of successful treatment.

Apart from cancer, PET is used for several studies of the brain; it can be used to examine patients suffering from epilepsy, mapping of damaged tissue due to Parkinson's disease and it is a useful tool for finding early signs of dementia. (4)

The basic principle of PET is the use of a positron emitter attached to a tracer molecule. The tracer is injected into, and thus distributed within, the patient. Normally, after around 1 hour, the patient is ready for examination. The PET machine consists of a ring of detectors, all facing the centre. When the radioactive material inside the patient decays, it emits positrons. The positrons will very quickly interact with an electron, resulting in a subatomic explosion, sending off two photons in opposite directions. If both of these photons manage to escape the body of the patient, they might interact with the surrounding ring of photon detectors. A computer will log the time of event and what pair of detectors that registered the event. The data is stored in a matrix called a sinogram. Several different techniques can be applied to reconstruct the images and produce a representation of where all events occurred. (5)

1.1 Motivation and goals

As cancer is a disease that is different from patient to patient in biological characteristics, it is important to learn about factors that e.g. determine treatment outcome. To date, biopsy is a common way to investigate a given tumor. But it is known that tumors display heterogeneity, thus a few sample cells might not be enough to give a complete understanding of the entire tumor. Tumor treatment response is also a variable across patients. If this can be assessed early it will be possible to adjust the treatment plan accordingly. In this work, tumor information from dynamic FDG-PET imaging was investiated, both for assessing radiation response and for characterizing different tumors in mice.

2 Background

2.1 Basic principles

2.1.1 Photon interactions

For the purpose of radiotherapy and PET imaging, one must be familiar with the basic physics governing the movements of photons through matter. That the photons interact with matter and deposits energy is the crucial point in radiotherapy. In PET the most important part is to construct efficient photon detectors.

There is several different ways a photon can interact with matter; photoelectric effect, Rayleigh or Compton scattering and Pair production. The chance of interaction is determined by the energy of the photon and the density (or effective atom number) of the medium it is traversing. Below in Figure 1 is a graph describing the relative probability of the different interactions.

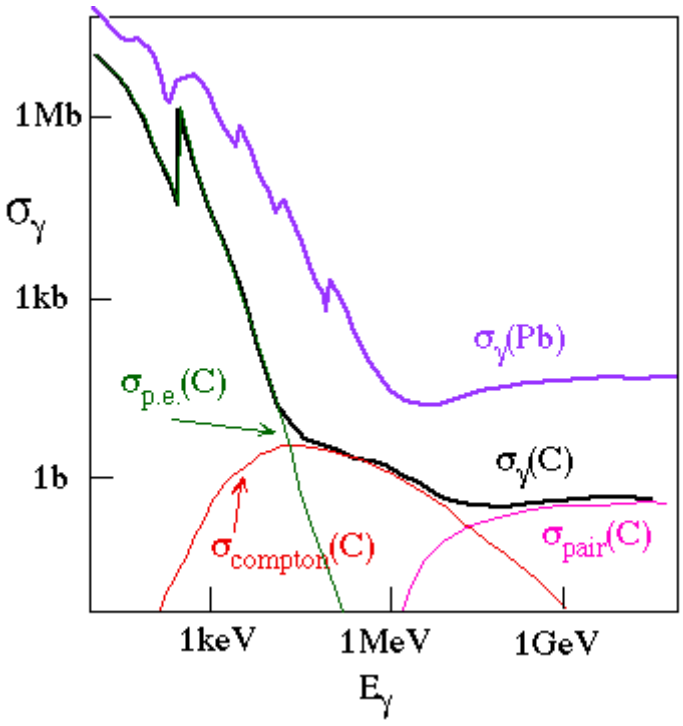

Figure 1: Photon interactions dependent on photon energy (courtesy of University of Toronto, Ca).

As shown above, the photoelectric effect is dominant for low energies. The entire photon can be absorbed by an electron, which escapes the atom/molecule it was bound to. The molecule will end up in an energetically unstable state., and may rearrange its electrons and emit characteristic radiation in form of a new photon.

If the photon is subject to Rayleigh scattering it will change its direction but retain all its energy. When undergoing Compton scattering however, it will interact with a free electron and give it considerable energy. Because of this the photon itself will lose energy and change its direction. As momentum and energy is conserved during such an elastic collision, there exist a relationship between the energy and scattering angle of the new photon;

$$E_{sc} = \frac{m_e c^2}{\frac{m_e c^2}{E} + 1 - \cos\theta}$$

where E is the energy of the original photon, E_{sc} energy of the scattered photon, c the speed of light, m_e the mass of electron and θ the scattering angle.

Finally, in pair production a high energy photon (minimum energy 1.022 MeV) interacts with a nucleus and produces a pair consisting of an electron and a positron. These particles will mainly be spread forward in the direction the photon was heading. (6)

2.2 Equipment of Radiotherapy

2.2.1 The linear accelerator

As photons from an ordinary X-ray tube does not have enough energy to efficiently reach deep into tissue, a new type of machine had to be developed in order to produce higher energy photons. The linear accelerator (linac) can produce electrons with energy of more than 20MeV, where the electrons gain energy by interacting with a synchronized radio-frequency electromagnetic field. The electrons originate from an electron gun and then moves into a long tube, the accelerating waveguide. Inside this tube, the electrons ‘surf’ on the microwaves and gain more and more speed. The tube is usually too long to practically point down towards to the patient, and a bending magnet is thus applied to change the direction of the electrons. The electrons themselves can be used for therapy, or they can bombard a target to form high energy x-rays. It should be noted that the x-rays generated from this machine will have a spectrum of energies. The x-rays will then be shaped into an uniform treatment field of selected size. If the linac got a multileaf collimator (MLC) as well, the field can be shaped to better fit the extent of the tumor. Dosimeters are placed in the head of the linac in order to measure the treatment dose. (7) An illustration of the linac is shown in Figure 2.

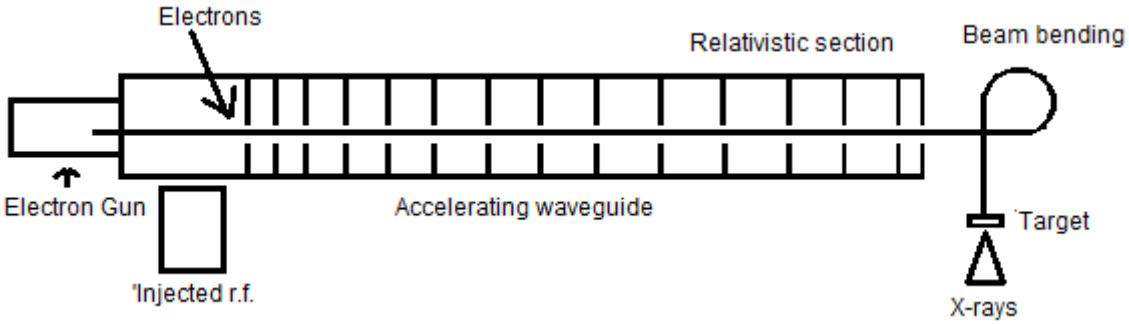

Figure 2: Schematic diagram of a linear accelerator designed for radiotherapy used in x-ray mode. (7)

2.2.2 The cobalt machine

As opposed to the intricate design of the linear accelerator, cobalt machines are fairly simple. The radiation comes from a radioactive source emitting high energy gamma rays (and some low energy beta rays). The energy of the photons is mostly monochromatic and is either 1,173 MeV or 1,333 MeV. The source is placed in the head of the unit which must be able to shield the surroundings from the source and make sure the beam is collimated to the correct size. As the radiation from this machine is always “on”, safety measures to avoid radiant contamination must be strict.

2.3 Positron emission tomography

Positron emission tomography is a relative new imaging modality and came into use in the 1980s. The basic principle is a radioactive tracer that emits positrons, a ring detector that can catch the annihilation photon pairs and electronics to make sense of it. The following chapter will review some of these aspects. In Figure 3 the basic PET setup is displayed.
Most of the information in this chapter is based upon the work of Michael E. Phelps (5).

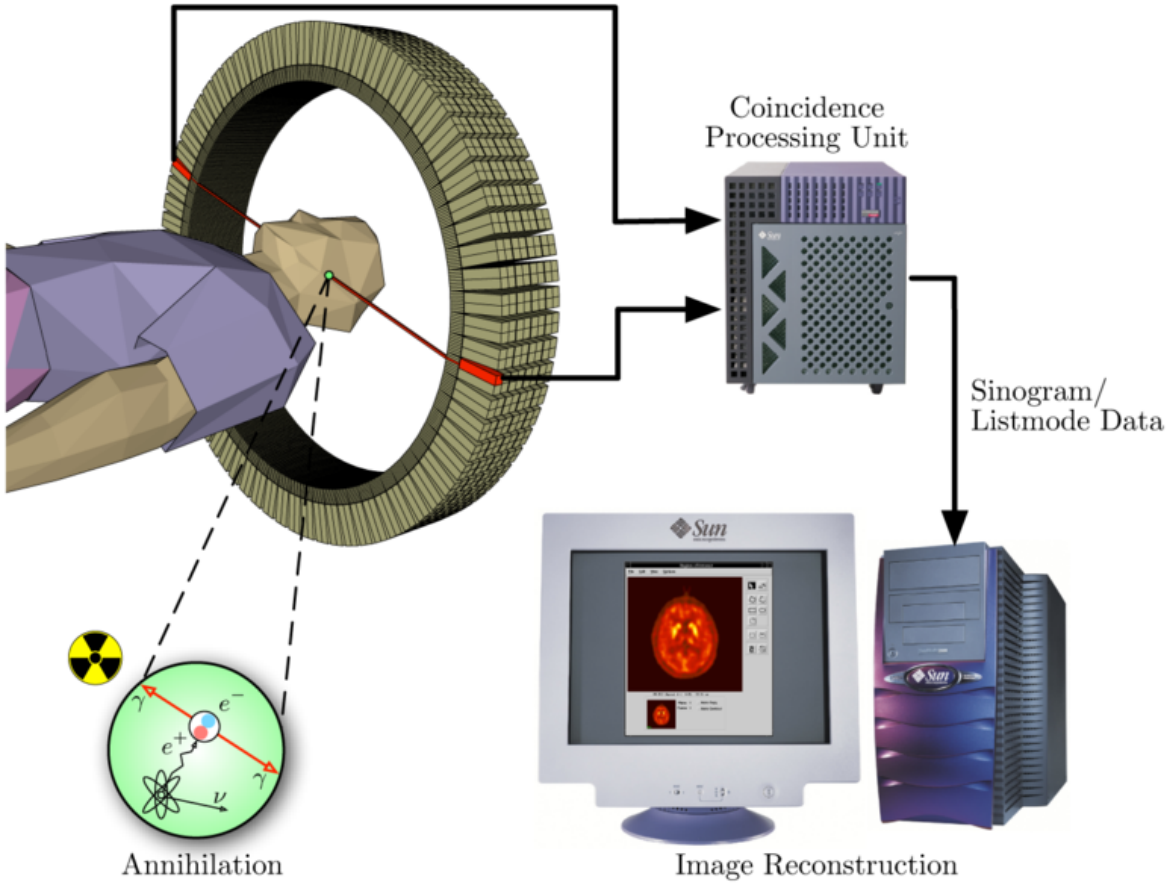

Figure 3: The basic steps in order to produce a complete PET image (Wikipedia).

2.3.1 Tracers

The tracer in PET consists of two equally important parts. The first part is a to select a suitable molecule that is incorporated by the cells in the human body, a *tracer*. A PET survey will show you the distribution of this tracer in the body. To monitor metabolic activity for instance, glucose (or glucose analogues) can be used. The next task is to find a radioactive isotope that can be attached to the molecule without changing its properties too much. This can be done by removing a small group of atoms and replace it with an isotope with similar atomic weight and electron structure. It is vital that the body can still recognize and use the molecule as if it was of original structure. The isotope should primarily emit positrons. All other radiation emitted would be useless for the survey and also irradiate the patient. It is also important to consider the physical and biological half time of the isotope. If the half time is very short, a lot of the activity would be spent on the way from cyclotron (see below) to the patient. If it is too long, little activity would be shown when imaging the patient. For example, ^{18}F has a half time of 110 minutes, which is considered to be quite suitable for the purpose of PET.

The glucose analogue 2- deoxy -2 -[^{18}F]-fluoro-D-glucose (FDG for short) is a molecule that can be used to look for cancerous growth as it monitors metabolic activity. The isotope ^{18}F is produced from ^{18}O -water that is bombarded by 16MeV protons from a cyclotron. Synthesis of the complete molecule is performed according to the routines presented in the article by Joanna S. Fowler and Tatsuo Ido. (8). In a model of the molecule and where the ^{18}F atom has replaced an OH group compared to glucose is shown.

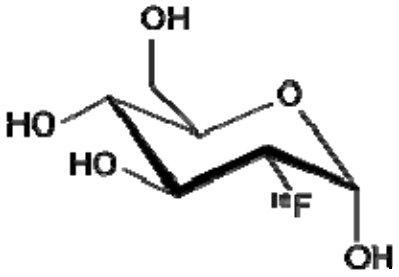

Figure 4: A representation of the FDG molecule (Wikipedia)

As will be shown there is also a high metabolic activity in the brain, kidneys, and intestines. The bladder will also accumulate FDG. Therefore other tracers / methods might be considered to look for cancer in these regions. But if one wait for about 3 hours after injection, it might still be possible to distinguish tumors here. When ^{18}F decays, it turns into a heavy oxygen atom with negative charge, which quickly attracts a positive hydrogen core. This new molecule is harmless and can in normal cells be used for further metabolism. (9). FDG is the most commonly used PET tracer, and is used in more than 90% of all surveys worldwide and exclusively in Norway (4).

2.3.2 The tracer in the body

The tracer (FDG) is intravenously injected into the patient and will be transported in the blood stream as normal glucose. When the FDG reach the capillary blood vessels, it will leave the blood and move into the space in between the cells. GLUT transporters help pulling the tracer into the cells. An illustration of this is given in Figure 5.

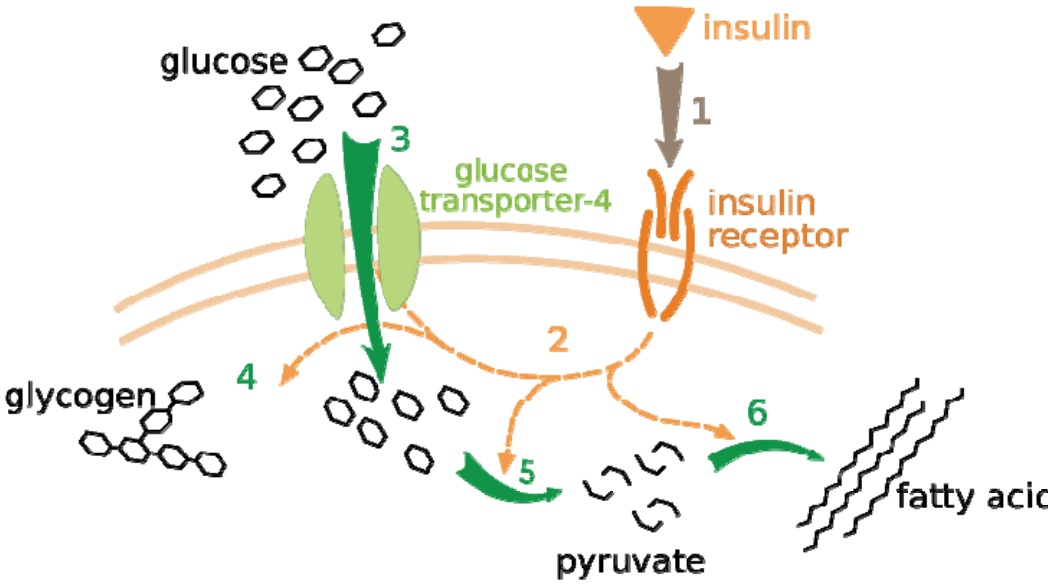

Figure 5: Transportation of glucose and FDG across the cell membrane (Wikipedia).

When FDG enters the cell, it may undergo glycolysis. The first step is phosphorylation by hexokinase and ATP, and this reaction is illustrated in Figure 6. However, the fluor atom stops further metabolism of the molecule. Thus the FDG will remain inside cells for a longer time. This attribute is very much desired for the imaging process.

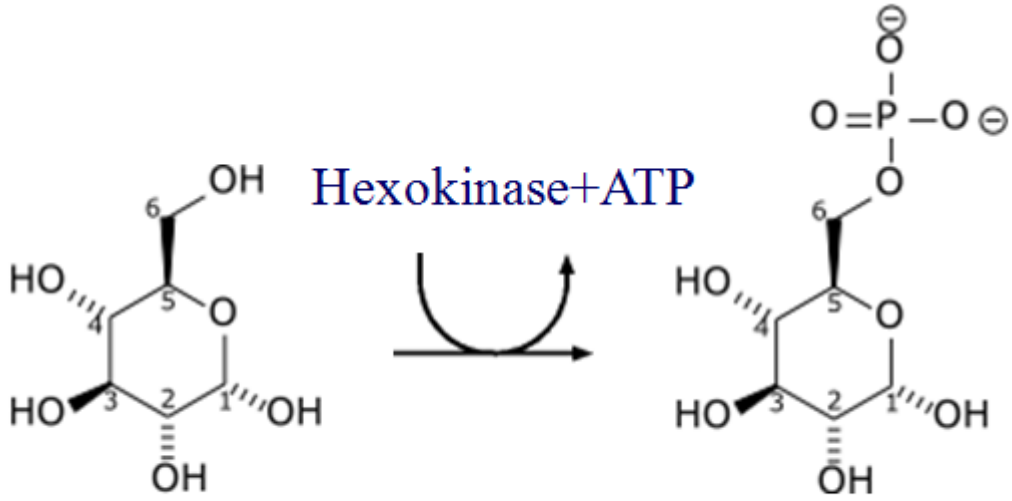

Figure 6: The phosphorylation reaction of glucose (Wikipedia). Note that for FDG the second OH group is replaced by ^{18}F.

2.3.3 Annihilation

^{18}F atoms will emit positrons and revert to ^{18}O. This will subsequently cause annihilation of a positron and electron which will result in two high energy photons. An assumption is made that the positron annihilate at the site of FDG, and that the photons produced travel in exact

opposite directions. This is not exactly true. The positron emitted from a radioactive nuclide will have a component of kinetic energy. The positron is therefore able to travel for a certain distance before it interacts with an electron. The probability of interaction is inversely dependent on the speed, and it is intuitive that positrons of higher energy will travel for longer. It follows that the distance is dependent on the radionuclide used for a PET. For ^{18}F the maximum energy an emitted positron can possess is 635 keV. This is relative small compared to other radionuclides used. The distribution function for the distance traveled have a full with half maximum (FWHM) of 0.1 mm and full width tenth maximum (FWTM) of 1.0 mm. This means that most of the positrons travel less than a millimeter, but they can travel further. This effect cause image blurring and limit the spatial resolution that could theoretically be possible for PET. Strong magnetic fields can reduce these effects (10) but is not practical to implement.

Another problem is that both the positron and the electron interacting have a bit of kinetic energy, and therefore the scatter angle between the resulting photons is not exactly 180^o. It will instead be a roughly Gaussian shaped distribution around 180^o with a FWHM of about 0.5^o. The blurring due to this effect can be estimated as:

$$\Delta_{nc} = 0.0022 \times D$$

Where D is the diameter of the PET scanner. For the moment these effects are relative small compared to the typical resolution of a clinical PET scanner. An illustration of these effects is provided in Figure 7. The problem of photon interactions within the body is discussed later in chapter 2.3.5.

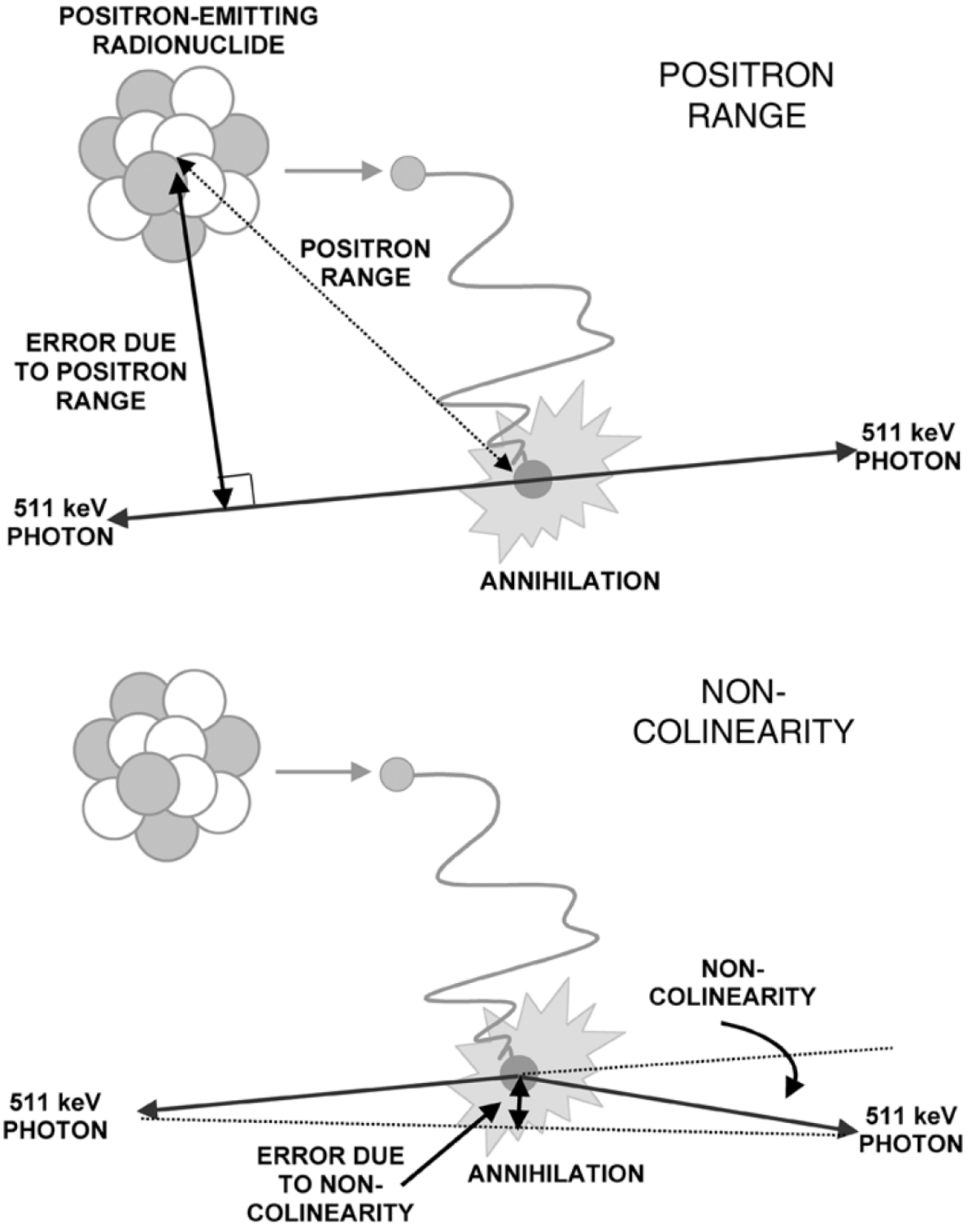

Figure 7: Illustration of errors due to positron range and non-colinearity. (5)

2.3.4 Photon detectors used for PET

The detectors are a vital part of the PET scanner and need to have several specified properties. They need to be able to efficiently detect photons with energy of 511 keV and it is also useful if they can detect the actual energy of the incoming photons. If so, scattered photons can be discarded. A precise measurement of the spatial location of the interaction improves the spatial resolution of the images. The ability to determine when the photons hit the detector is crucial in order to pair photons that spawned from the same interaction. Scintillation detectors are used for most present PET scanners. They consist of a dense crystalline scintillator material where photons interact. When a photon interacts with this kind of material visible light is emitted. This light can then be recorded as an electrical current at the end of a photomultiplier tube (PMT). See Figure 8 for an illustration of this setup.

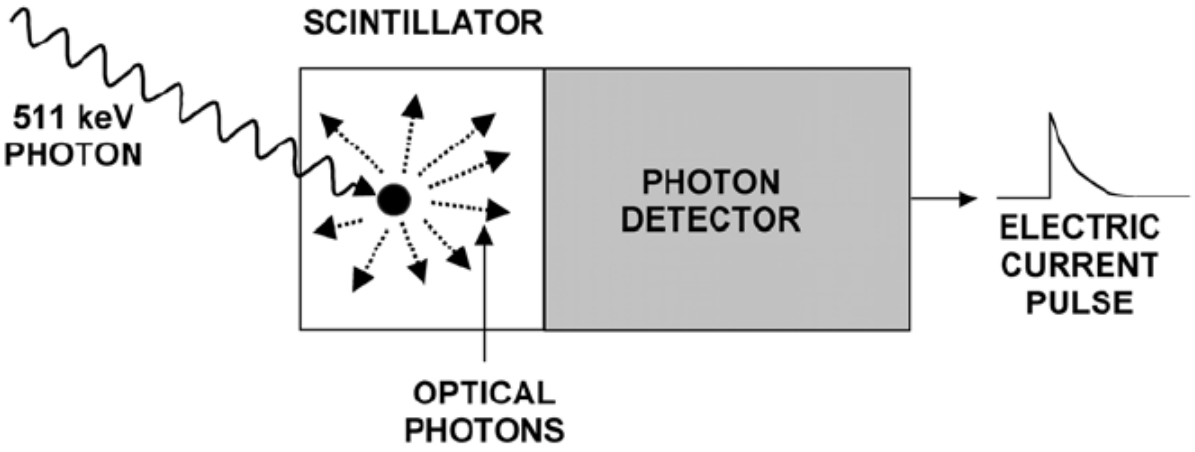

Figure 8: The basic components of a scintillation detector. (5)

Scintillators will emit light in the visible spectrum when high-energy photons deposit their energy in them. They are therefore transparent and dense, allowing the light a chance to escape and increasing the chance of interaction with high-energy photons. The amount of light emitted is proportional to the energy deposited in the scintillator. However, the light is emitted equally in all directions, so not all reach the second photon detector. Even though a single high-energy photon causes the emission of a wave of lower energy photons, only one electric pulse is recorded. The amplitude of the pulse will be related to the energy of the interacting photon. Because of this it is possible to reject low energy photons that have been scattered in the body.

For PET imaging dense, inorganic solid scintillators are chosen. Even the materials with high stopping power must be several centimeters thick in order to efficiently stop a larger percentage of incoming photons. The stopping power is therefore a major factor when considering different scintillators. “The brightness of the scintillator (the number of light

photons produced per 511 keV interaction) is important because the integrated light signal from the scintillator is used in several different ways. In many detectors, the relative amplitudes of the signals seen by adjacent light sensors viewing a piece of scintillator are used to determine the location of the interaction." Unfortunately, not all the light photons are detected. This causes fluctuations in the output which are governed by Poisson counting statistics.

Accurate measurements of when photons interact with the scintillator are important because of the coincident detection of the two annihilation photons. The accuracy of timing is dependant on the decay time of the scintillator and its brightness. "A fast, bright scintillator will produce a signal with less timing variation than a slow, dim scintillator."

Most PET scanners use photomultiplier tubes (PMT) as the photon detector to convert scintillation light into an electrical pulse. At the entrance of the tube, a photocathode is placed. When a light hits the cathode, a loose electron will be given enough energy to launch itself off the cathode. It will then be directed towards a positively charged electrode, called a dynode. The electric potential difference will give it enough speed to bounce off the electrode and head towards the next dynode. Each time the electron bounce off a dynode, it knocks off 3-4 other electrons as well. This will rapidly increase the number of loose electrons that will finally strike an anode at the end of the tube. This will cause an electric current which is the new output signal. Se Figure 9for an illustration of a PMT.

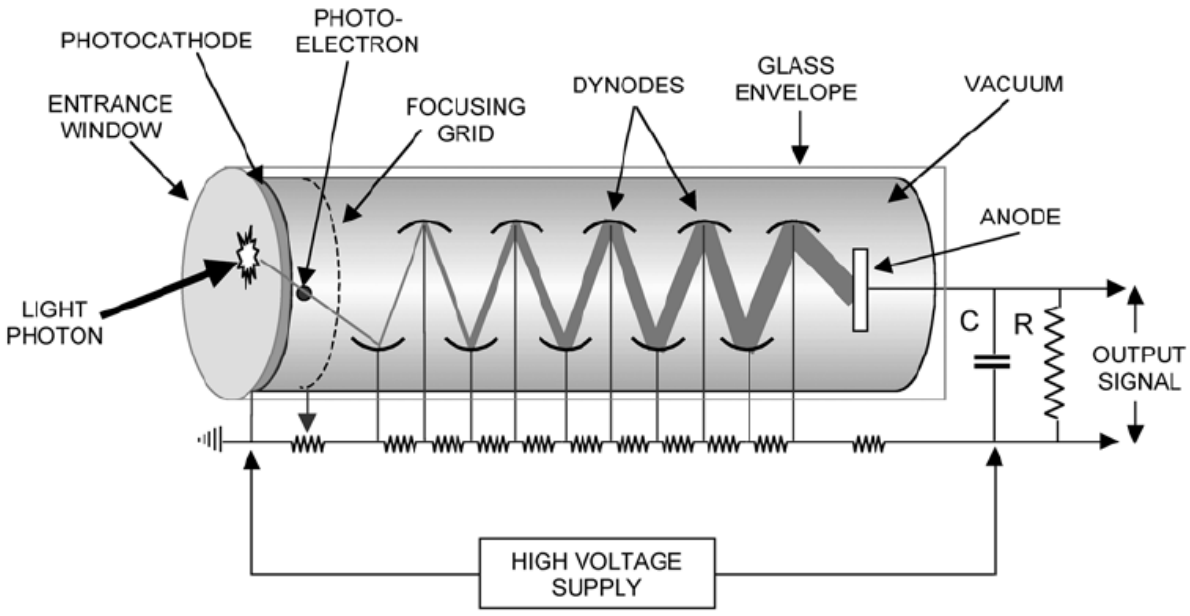

Figure 9: A schematic of the basic photomultiplier tube. (5)

Some of the PMT models available are multichanneled and position sensitive. Still, most PET scanners use single-channel PMTs with sizes ranging from 1 to 5 cm in diameter.

“The advantages of MPTs are their high gain, which leads to high signal-to-noise pulses, their stability and ruggedness, and their fast response. “

By arranging scintillator crystals and PMTs together, a block detector can be created. This design was proposed by Casey and Nutt (11), and the majority of PET scanners use this design. This consists of a relatively large block of scintillator material (typically 4 x 4 cm in area and 3 cm deep). This block got cuts filled with reflective material to make it into a say 8 x 8 array of detector elements. This is then attached to four PMTs, see Figure 10

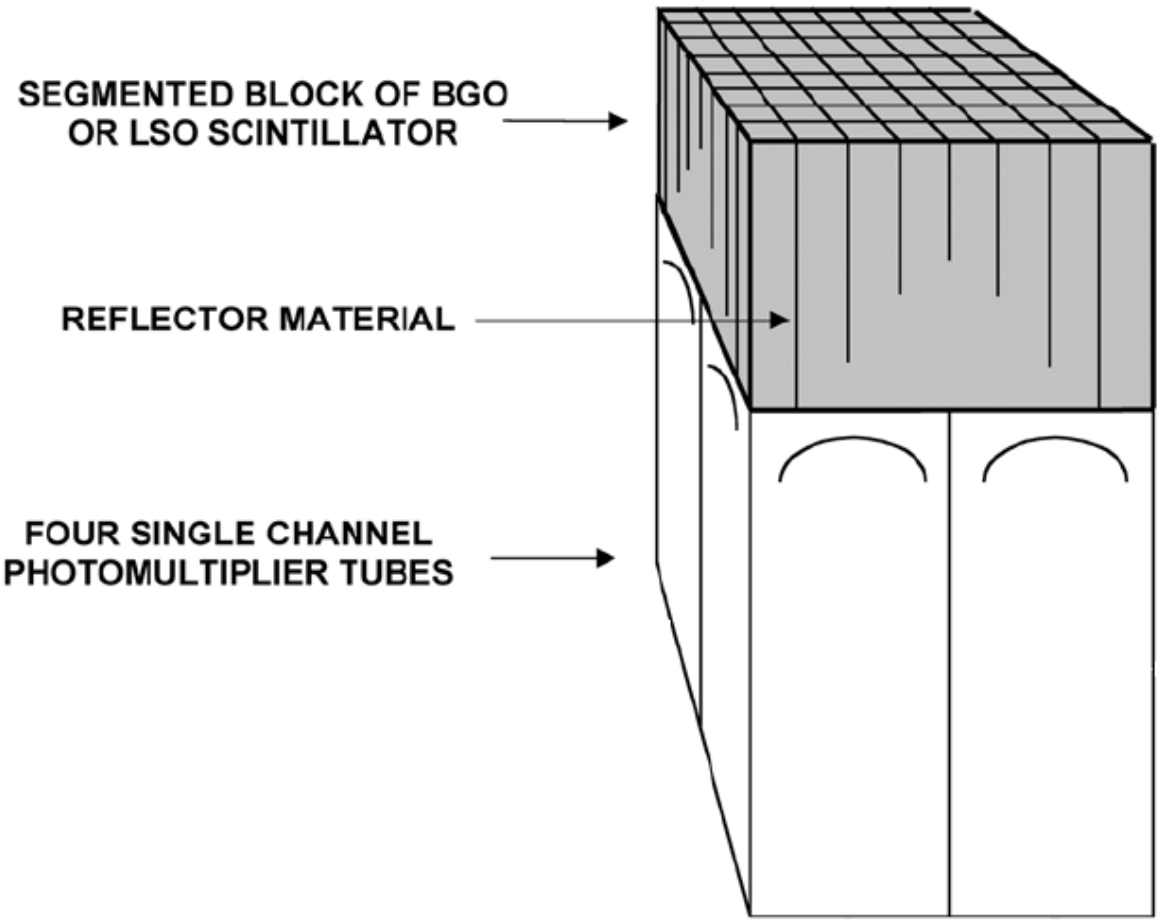

Figure 10: The design of the block detector. (5)

The depth of the cuts varies across the block in order to share the light between the PMTs. As illustrated, in the middle, the cuts are shallow, allowing all PMTs light. Thus one can determine the actual entrance in the 8x8 array by looking at the relative light in the four PMTs. By doing this one catches two flies in one go. This reduces the number of expensive PMTs used and the spatial resolution can be improved to a certain level.

2.3.5 Coincidence detection

In PET, coincidence detection is used rather than absorptive collimation to determine the location of the emitted photons. The basic principle is that when an annihilation event occurs, two photons will be emitted in opposite directions. If both are caught by the detectors, the event will be recorded. It is then assumed that the event occurred somewhere along the line that goes from one detector to the other. The detector pair and time of event is stored for each accepted coincidence. Under ideal circumstances the photons hits the detectors simultaneously, but this is not always the case. Therefore a time window in which two occurrences can be recorded as a pair is in place. This window depends on the scintillator material used and is mainly in the order of a few nanoseconds. If the window is too big however, the chance of recording another random event increases. This will lead to false coincidences. The different types of coincidences that might occur are described in the picture below.

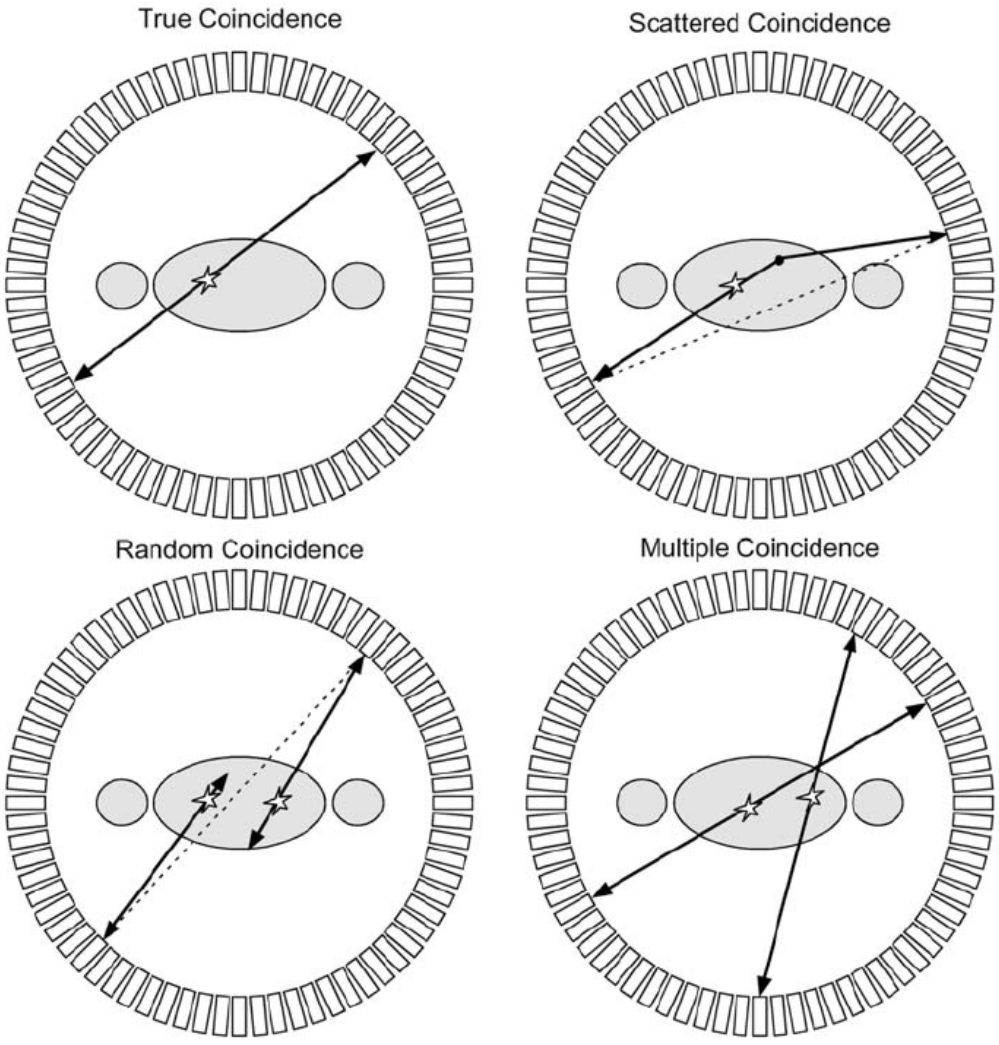

Figure 11: The situations that might be recorded as events. (5)

The scattered coincidences cause a displacement of the actual event. The fraction of these events can range from 15% to over 50% of the total data and are also the most difficult to correct for. The random coincidences cause worse errors and form a background noise that should be removed whenever possible. The rate N_R of these occurrences can be calculated;

$$N_R = 2\tau N_1 N_2$$

Where τ is the width of the logic pulses produced when a photon is absorbed in the detector (2τ is the usual coincidence timing window.) $N_{1,2}$ are the individual photon detection rates in a pair of detectors. When more than two photons are recorded simultaneously they are usually discarded, but in some circumstances it is considered better to choose a random pairing instead.

2.3.6 The sinogram

"A simple Pet-system consisting of 32 individual detectors in a ring, scanning an object with a 2-Ddistribution of radioactivity denoted by a(x,y) (Figure 12).

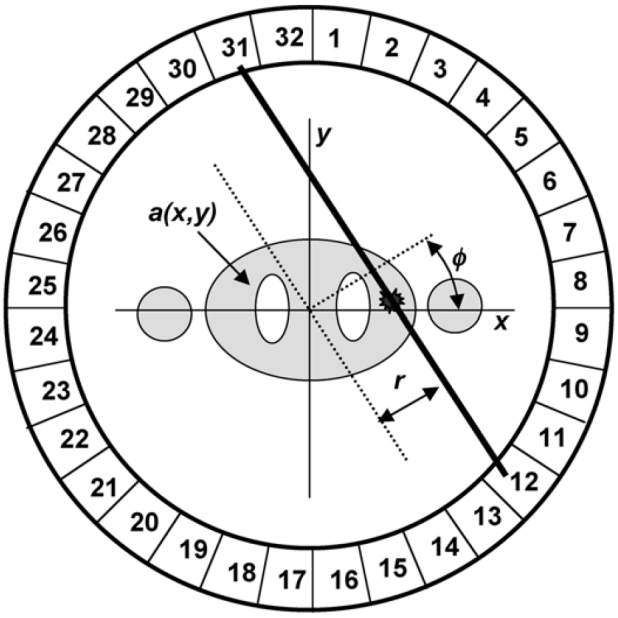

Figure 12: A simple 2D detector system with numbered detectors. (5)

The raw data, which consists of the detection of annihilation photon pairs, usually is histogrammed into a 2-D matrix, where each element in the matrix corresponds to the number of events recorded by a particular pair of detectors (or along a specific line of response). The matrix is arranged such that each row represents parallel line integrals or a

projection of the activity at a particular angle ϕ. Each column represents the radial offset from the center of the scanner, r. The relationship that relates which elements in this matrix (r,ϕ) record data from radioactivity in the object at location (x,y) is given by:

$$r = x\cos\phi + y\sin\phi$$

This 2-D matrix s(r,ϕ) (see Figure 13) is known as a sinogram because a point source located at a location (x,y) traces a sinusoidal path in the matrix as given by the above equation." (5)

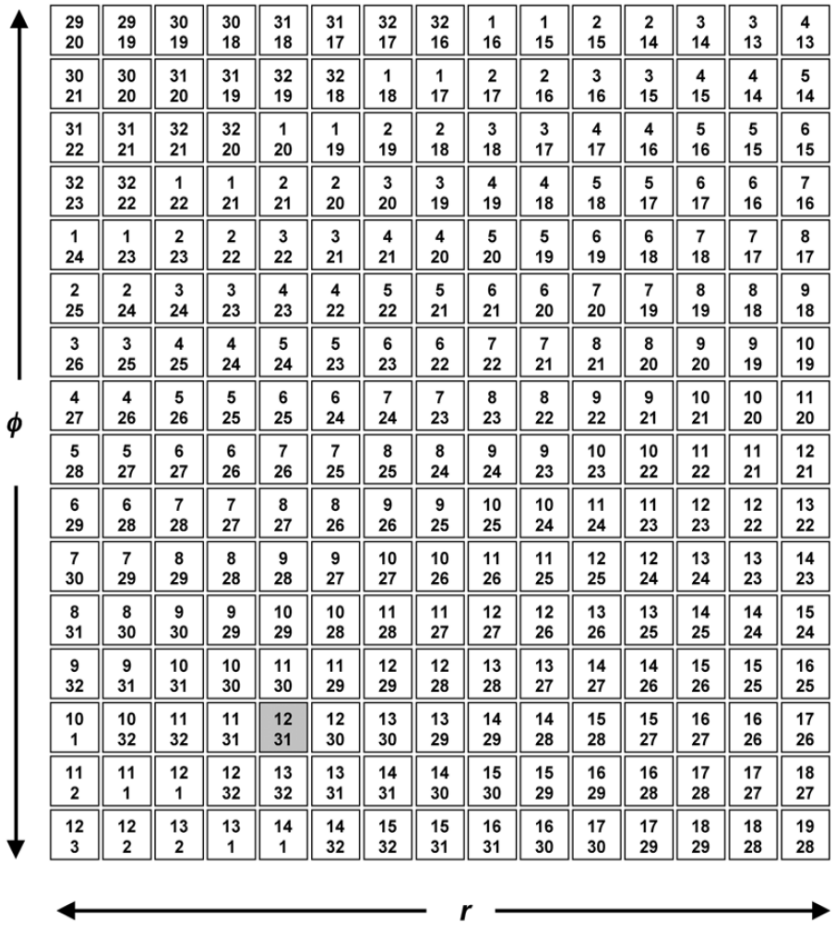

Figure 13: The sinogram, each entry represent a detector pair and the events in that pair will be recorded in that entry. (5)

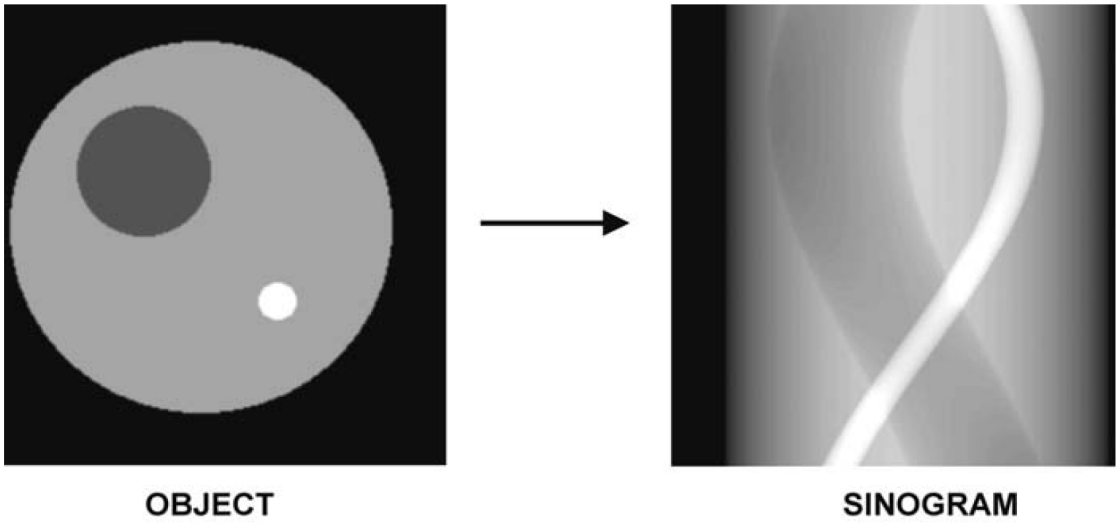

Figure 14: Illustration of how an object will appear in the sinogram. (5)

2.3.7 Image reconstruction

Image reconstruction is needed in order to obtain an image that looks like the object imaged. One of the techniques is iterative reconstruction. A flowchart of this method is shown in Figure 15. An estimate of the original object will be made and then forward projected in order to obtain a sinogram. This sinogram is then compared to the sinogram recorded from the PET assay. If the likeness is not good enough, it will be rejected and try again until it converge.

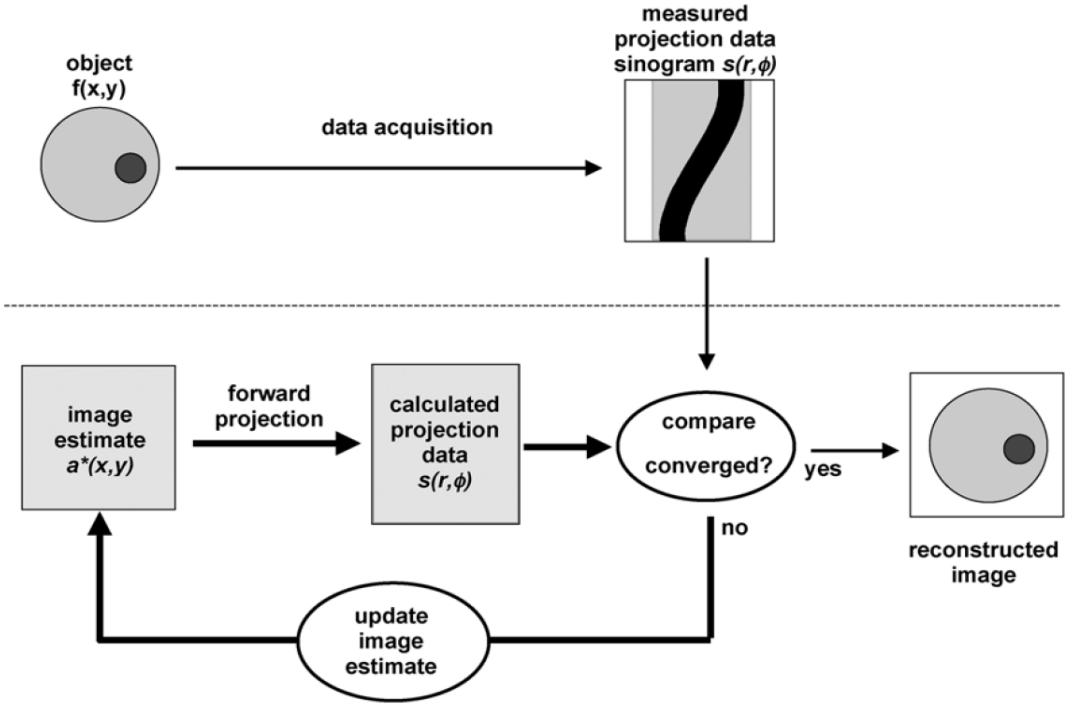

Figure 15: Flowchart of the iterative image reconstruction technique. (5)

2.3.8 Radiation dose to patients

If one are concerned about the radiation damage to the patient from this kind of survey, the effective dose for a PET survey (using FDG) have been calculated to 0.027mSv/MBq [ICRP]. The activity used in surveys range from 100-370 MBq. Others work with a bit larger number, 0.0299 mSv/MBq and using 370MBq, giving a total effective dose of about 11mSv. These dose values are close to the ones obtained from a CT scan. There is also worth mentioning that as the FDG is not evenly distributed some organs (like the bladder) will receive larger doses. (12) As for how the radioactivity leaves the body; 20% is excreted through the renal system while the rest stays to decay. The patient will therefore emit a heightened level of photons for about 12-24 hours after a survey. (13)

2.4 Pharmacokinetics

After acquiring PET data, we will try to put it into a model to describe the system; this is called tracer kinetic modeling. These models are very similar to pharmacokinetic models, the main difference is that the doses used are smaller (a tracer). Instead of introducing a drug that is supposed to affect the system, the tracer should ideally pass through without making any disturbance. There are three different kinds of tracer kinetic models; noncompartmental, compartmental and distributive. For PET analysis, the compartmental model is preferred by most. This is because “they are simpler to implement and often prove adequate parameter estimates”. Another trait of these models is that they “look” like what we are studying; different compartments for the different states of the tracer. One thing to note about the term compartment in this context is that it isn’t necessary a physical defined volume. Shown below is the system used for this study, as you see we have one compartment for FDG in tissue and one for FDG 6-P (metabolized FDG) in tissue, where both molecules are within the same cells.

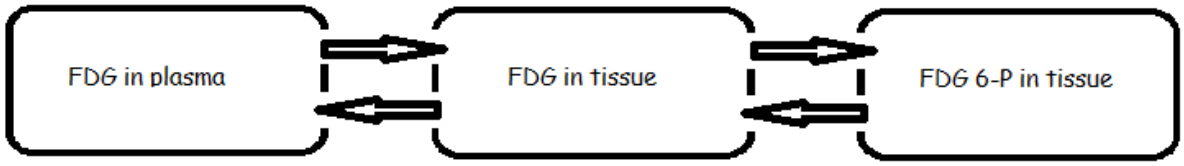

Figure 16: Three Compartment model for FDG *in vivo.*

The arrows in the model represent the movement of tracer between the compartments. These movements are decided by the interconnections across the compartments. These interconnections are linear if they are not dependant on tracer mass or

time, but they can vary across the tissue itself. Even though the biological processes we look at are in general non-linear, a linear model can in some cases still be used. In several studies you can obtain data by applying a small trace dose and observing the dynamics. "Such test signals give rise to very small perturbations about the operation point, so the dynamic equations describing experimental perturbations are linear even though the intrinsic dynamics of such a system may be nonlinear" (14). The main reason for this is that the mass of the trace dose is much less than the mass of molecules it resembles. Specifically, it has been shown (15) that when glucose metabolism is in steady state, the tracer system is linear. An important physical property of the tracer kinetic model is the mass balance. This means that the measured change of mass in a compartment must result from the amount of tracer coming into the compartment, minus the amount leaving it. In a dynamic PET series we can measure these variables over time, and find the rate of mass exchange. In this study, our equations consider the mass balance of the compartments, rather then the concentration of tracer. A complete set of equations like these are often called state equations.

2.4.1 Two-tissue compartment model

In this section a model that is commonly used to describe the uptake and retention of FDG is presented. (16) We define the following:

C_P (pmol/ml) is the molar concentration of tracer in the plasma

C_F (pmol/ml) is the molar concentration of unbound tracer

C_B (pmol/ml) is the molar concentration of metabolized or bound tracer.

The kinetic parameters k1, k2, k3, and k4 give the rate of tracer exchange between the compartments. k3 is an apparent first-order rate constant, while the rest is true first-order rate constants.

Cp(t) is assumed to be known and identical for all voxels. The other parameters will vary for each voxel location, s. Considering mass balance and blood fraction (bf) we want to solve for the following equations;

$$C_T(s,t) = C_F(s,t) + C_B(s,t) + C_F(s,t) \times bf$$

Where C_T is the activity measured in the voxel.

$$\frac{dC_F(s,t)}{dt} = k_{1s}C_P(t) - k_{2s}C_F(s,t) + k_{4s}C_B(s,t) - k_{3s}C_F(s,t)$$

$$\frac{dC_B(s,t)}{dt} = k_{3s}C_F(t) - k_{4s}C_B(t)$$

The solution to these is shown below

$$C_F(s,t) = \left\{ \frac{k_{1s}}{\alpha_2 - \alpha_1} \left[(k_4 s - \alpha_1) e^{-\alpha_1 t} + (\alpha_2 - k_4 s) e^{-\alpha_2 t} \right] \right\} \otimes C_P(t)$$

$$C_B(s,t) = \left\{ \frac{k_{1s} k_{3s}}{\alpha_2 - \alpha_1} \left[e^{-\alpha_1 t} - e^{-\alpha_2 t} \right] u(t) \right\} \otimes C_P(t)$$

where

$$\alpha_{1,2} = \frac{(k_2 + k_3 + k_4) \mp \sqrt{(k_2 + k_3 + k_4)^2 - 4k_2 k_4}}{2}$$

3 Experimental setup and procedures

3.1 The use of mice for this project

Mice have been used for this project. They have all received implants of human tumor xenografts. Ten mice with CWR22, six with MAS 98.12 and five with MAS 98.06. A brief description of these tumors is given in chapter 3.2. Half of the mice with CWR22 received radiotherapy. Later PET assays were done on all mice, comparing treated against controlled mice with CWR22 and MAS 98.12 against MAS98.06. A detailed description of the mice and their habitat is found in the appendix.

3.1.1 On the use of animals and the animal model

Once the decision of using animals for an experiment has been made, several aspects must be addressed. Concerning animal welfare, a rule of thumb called “the three R’s” has been constructed

*Reduction – Reduce the number of animals used

*Refinement - Refine the methods, models and environment

*Replacement - Replace in vivo research with in vitro research where this is possible

In general, animal experiments are used to answer questions in biology and medicine related to human or animal health. It has been shown that several biological processes in the body are similar across different species. In this study, mice have been utilized to gain knowledge about human cancers. In most cases, a specific drug or treatment will have the same effect on all species. The differences that do exist however can in some cases be used to an advantage in specialized research. One must also keep in mind that the dose given will not have the same effect on different sized animals. For instance, small rodents can endure more radiation than humans. For our PET study, we are mostly concerned about the metabolic processes. These processes are very much the same in most life forms wherever they are on the ladder of evolution. There are also differences between animals of the same species. So in order to get reproducible results and results that can be properly compared to other work, one should make sure to choose a specific strain of a specific species of animals.

After considering all the things concerning the animals used, we must now consider the effects of the environment they are kept in. Everything from the temperature to the bedding can cause differences so all animals should be treated equal. Most importantly, one must ensure that the animals are treated properly. Having stressed animals is ethically unacceptable and it will also affect the experiment. To ensure that the work done can later be

compared to other work, as much information about the above points should be recorded and presented with the work. (17)

3.1.2 Implantation of tumors

Prior to the tumor implantation, the mice were anesthetised by subcutaneous injections of “Zoletil Mix”. This mixture is made of 2.4 mg/ml tiletamine and 2.4 mg/ml zolazepam (Zoletil vet, Virbac Laboratories, Carros, France), 3.8 mg/ml xylazine (Narcoxyl vet, Roche, Basel, Switzerland), and 0.1 mg/ml butorphanol (Torbugesic, Fort Dodge Laboratories, Fort Dodge IA), diluted 1:5 in sterile water. The dose given was 50 µl/10 g of body weight. While waiting for the mice to fall asleep, tumors (human androgen-sensitive CWR22 xenografts) extracted from other mice were prepared. These tumors were cut into small cubes with sides of approx 1.3 mm length. Before operating, an area of skin was cleaned using alcohol. A one cm long cut was made on the back of the mice, and then tweezers were used to make small pockets under the skin. The tumors were then inserted into these pockets near the flanks. The wound was then glued together with histoacryl. Finally, a salve was applied to the eyes of the mice to prevent damage. This is because mice can’t close their eyelids when knocked out. The last remaining thing to do was to mark the mice. This was done using scissors and a special pincer to make triangular or circular cuts in their ears. When this procedure was complete for a group of mice, they were put back in the cage. They were here placed huddled together and covered with some of the bedding to prevent severe heat loss. Then the cages were labelled with a project nr and a note telling which mice are inside before being returned to their housing unit. A humane endpoint for the mice has been established. If the tumors grow to a size that will hinder the animal’s movement, they will be euthanized. As will all the animals in the end of this experiment.

3.1.3 Irradiation

One day before the PET assay, all cages were brought down to the irradiation lab. This was for two reasons; first to ensure that all mice receive a handling that is as similar as possible. Secondly, there were some mice to be irradiated from each cage. Each cage contained some mice from both groups. This is because the micro environment within each cage can be different, and we don’t want it to affect only one group. In correspondence to what was stated above, all mice were anesthetized. The mice were anesthetized cage by cage with the same method used as when implanting tumors. When the mice were knocked out, groups of four would be irradiated at the same time. They were placed upon a sheet with a 10 by 10 cm square drawn upon it, (the same size as the radiation field). The tumors were placed at

the corners of this square and the rest of the body located as far from the centre as possible (see Figure 17). After making sure the sheet was placed correctly under the beam, a 5 mm thick layer of polystyrene was laid on top of the mice. This layer was supported by small pieces of cardboard to ensure the mice wouldn't be crushed. The function of this layer was to create a dose buildup for greater effect in the tumor, as the millimeter of mouse skin is not enough to provide this. The source of radiation used was ^{60}Co (Mobaltron 80, TEM Instruments, Crawley, UK) with a dose rate of 0.8 Gy/min. This source gives off radiation in the form of gamma rays in the megavolt range. The dose given was 7.5 Gy. After irradiation, the mice were placed back into their respective cages. They were again placed huddled together for warmth. Then the cages were taken back to the animal stall.

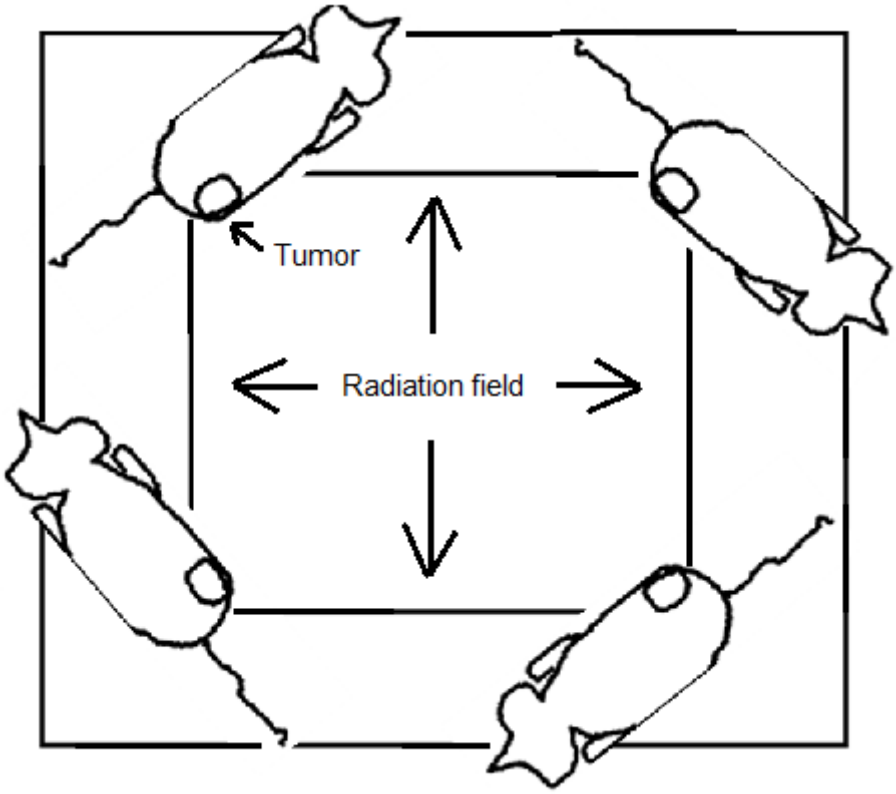

Figure 17: Setup for mice in the radiation field.

3.1.4 PET assay

The following day, the mice were transported to Rikshospitalet where the small PET scanner is located. This scanner is a microPET Focus 120, (Siemens Medical Solutions, Erlangen, Germany). A performance test of this device has been done by other scientists (18). Again the work began by administrating the anesthetic, but this time only on two mice at a time. The knocked out mice were placed in the PET scanner atop a cushion, with a heat lamp directed towards them. As they were about to be subjected to an hour long PET assay they

needed this to conserve sufficient body heat. Then a 10min transmission scan with a 68Ge point source was performed to obtain data for attenuation and scatter correction. Activity of the tracer was measured, and doses of 10-15 MBq 18F-labelled FDG (GE Healthcare AS, Oslo, Norway) in heparinized saline were prepared. These were carefully administrated into the venous vein of the tail. This was done on the first mouse in the same instant as the data acquisition began. Both mice had a needle already in place to make sure the dose for the second mouse could follow quickly. When the first pair had been in for some time, the second pair was anesthetized and prepared.

To ensure good FDG uptake, the mice have been denied food for 10 hours. The hungry and awake companions in the cage are prone to nibble on knocked out and defenseless mice. Therefore the pairs finished with the assay were not immediately placed back into their cage. Instead they were placed on top of surgical gloves filled with heated water. When they eventually showed signs of restored vitality they were put back in the cage. This process was repeated until the end of the day and continued on the next day.

Later 4D emission data were reconstructed using OSEM-MAP (2 OSEM iterations, 18 MAP iterations, b_0.5, matrix size_128_128_95 (19), (20), producing images with a voxel size of 0.87_0.87_0.80 mm3. The reconstructed time frames were 10 s during the initial 5 minutes, and the following time frames were 30 s.

3.2 The tumors used

3.2.1 CWR22

This tumor is an androgen-dependent xenograft model that is made from a primary human prostatic carcinoma (PCA). It was done by Pretlow TG et. al. (21) and several of these researchers have investigated the tumor line. They describe CWR22 as “having characteristics that suggest that it is exceptional among the currently available models for the study of human PCA. We believe that the general availability of this xenograft will offer a unique opportunity for the investigation of experimental therapy and the control of growth in PCA” (22).

3.2.2 MAS 98.12 and MAS 98.06

These are two different breast cancer xenografts with quite different properties. The luminal-like MAS 98.06 showed positive staining for estrogen receptor (ER). This is a protein which is a favorable prognostic marker. The basal-like MAS 98.12 however, did not show signs of ER.

The MAS 98.06 got more proliferation genes than the MAS 98.12 line (23). It might then be possible to identify them by looking at the metabolic rate of glucose, as this can be a sign of proliferation.

3.3 Non-linear curve fitting

The first curve fitted is the plasma function. For use in the pharmakokinetic modeling it is handy if the plasma function is expressed as a exponential function on the form described belov.

$$C_P = a \times e^{-bt} + c \times e^{-dt}$$

where t is the time, and the others are parameters that will be fitted to the curve. To fit the function to the data, a non-linear regression algorithm has been used. The IDL algorithm for this was developed by Craig Markwardt (24). It is based upon the Levenberg-Marquardt techniqe where a least squares regression is done. In order to adapt the model to fit the measurements, the parameters are regulated by minimalizing the sum of of the squares of the deviation between the measured time activity curve of plasma (TAC_P) and the fitted model. This sum is given by

$$s = \sum_{i=1}^{n} W_i (TAC_P(t_i) - C_P(t_i, par))^2$$

where $C_P(t_i,par)$ is the value estimated from the model, par is the vector containg the estimated parameters and W_i is the weight of each residiual. Each residual is weighted with the inverse of the standrad deviation of the corresponding datapoint in the measured TAC_P (25). The initial value of the parameters a,b,c,d had to be manually chosen, and if they are way of target, the algorithm might fail. Constrains for the parameters could be set aswell, but was not used for the plasma function. The models t=0 was set to when the TAC_P reach its peak. The final plasmafunction was therefore a combination of the fitted model, and erly TAC_P values.

The tumor model described in chapter 2.4.1;

$$C_T(s,t) = C_F(s,t) + C_B(s,t) + C_P(s,t) * bf$$

was fitted with the same algorigthm. Here the parameters was limited to positive values.

3.4 Image and data handling by the use of IDL

This section is about IDL sequences (program) that have been developed to get useful information out of PET-images. When this program is run from the beginning to the end, it should have collected all data needed from one tumor. The plasma function, the tumor region, the free and bound functions and the k-parameters. This data is saved both in graphic for your eyes and in IDL save files for later use.

It starts with reading image information from Dicom files and go all the way to usable output. All this is done without changing the source code in between sets of images. By prompting the user to answer questions, enter settings in the command line and using while-loops that don't stop before you got what you want, this has been more or less achieved.

Starting with something simple, a method for just looking at the pictures in order was developed. For example how one slice would change in time, or go through the entire animal, slice by slice, at a given time. For the moment these two types of visualization is available for coronal slices only. Displayed below in Figure 18 is a time dependant series, the image scaling have been optimized to look for the tumor in this mouse.

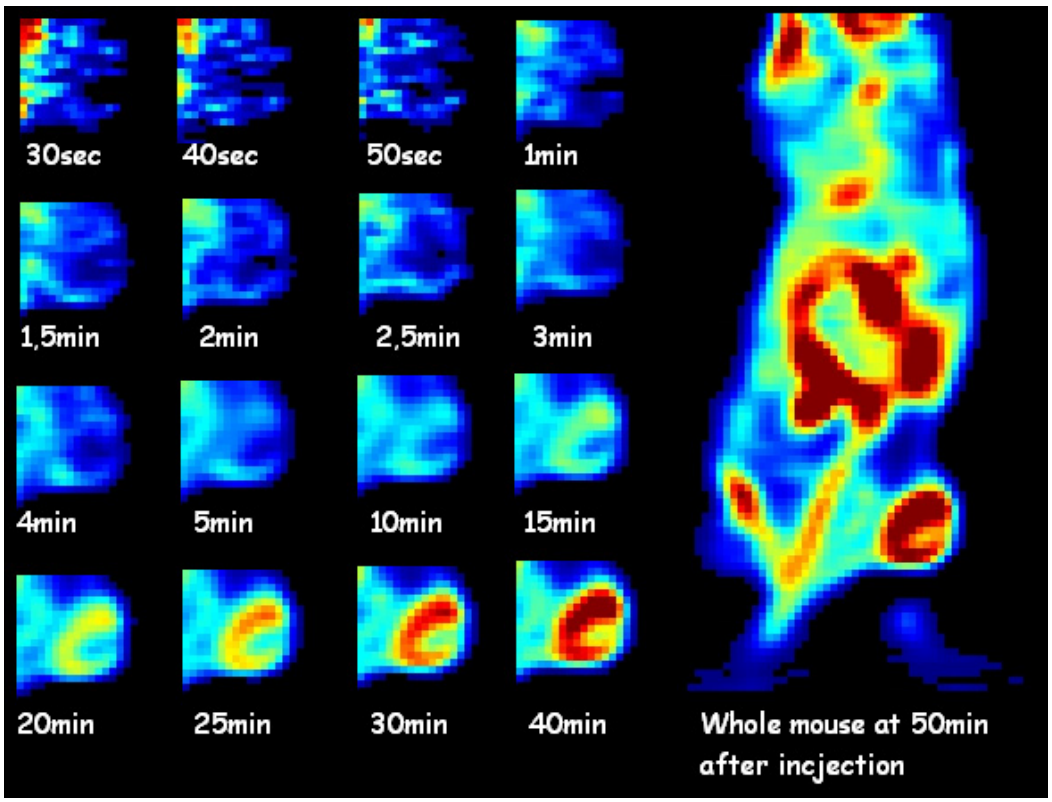

Figure 18: Coronal slice of tumor section and whole mouse. The time after injection of FDG is shown. Note that this picture has been rotated 180 degrees relative to the original.

As you can see the tumor is growing more and more visible as the time increases, as it accumulates more and more FDG. Heterogeneity within the tumor is also clearly visible in these images and you can see that the region in the middle of the tumor is getting its FDG last. It is very nice that it is possible to visualize this, as it is important to know about the different parts of the tumor and not just the average. But it is not enough to just see these images with the eyes, we need to collect data from each voxel within the tumor and analyze this more thoroughly. This can for example be done by looking at histograms and percentile values. Methods for doing this are described later.

The first thing you will have to do when starting the program is to choose which mouse you want to collect data from. A full image is displayed, showing all mice in the scanner. Imagine a small box containing just one mouse (see Figure 19). By clicking the bottom left corner and then the upper right corner of this box, this selection will be mapped onto a new array that fits it size, while the rest of the data will be rejected. By doing this, two things have been accomplished. First, the storage space required and RAM usage has been reduced to about 10%. Secondly, now only one mouse will be displayed, and therefore the scaling of images will be individual for that mouse.

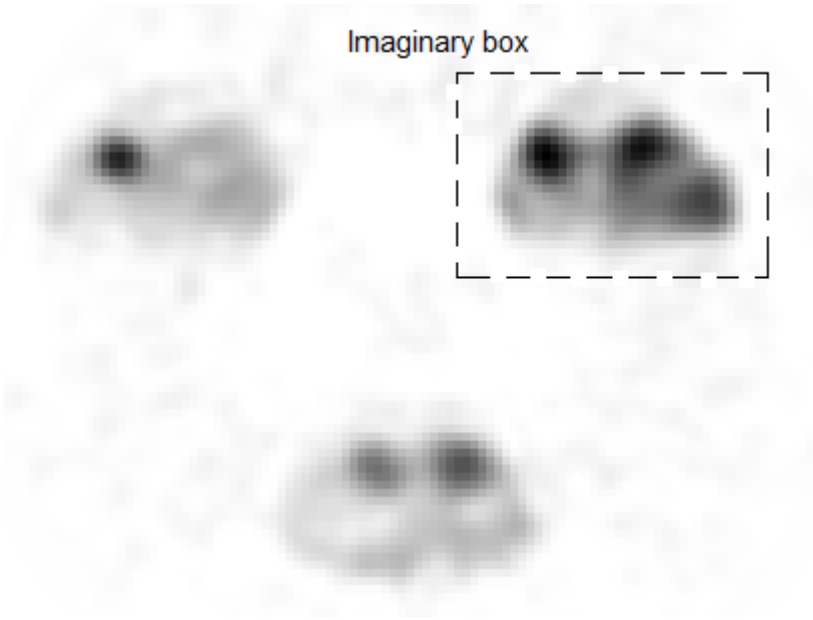

Figure 19: To choose which mouse to work on.

The first thing we need for our model is to determine the arterial input function, i.e. information about the FDG concentration in blood. As it can be quite difficult to look for an artery in small animals like mice, we rather try to find the left heart chamber where we can extract this information. This procedure in the program would also be able to collect data from any chosen voxel in the image (for example arteries in larger animals). Now, to do this we need to find the heart, which is not always an easy task. Sometimes you will get images that look like the left part of Figure 20. By clicking a random voxel, and then rejecting this as

your wanted voxel when the program prompts you, you will be able to choose new ways of displaying the image (you should get a message about the default scaling used). Image scaling and time interval is therefore adjustable. By trying and failing it will sometimes be possible to get an image like the one shown at the right hand side of Figure 20.

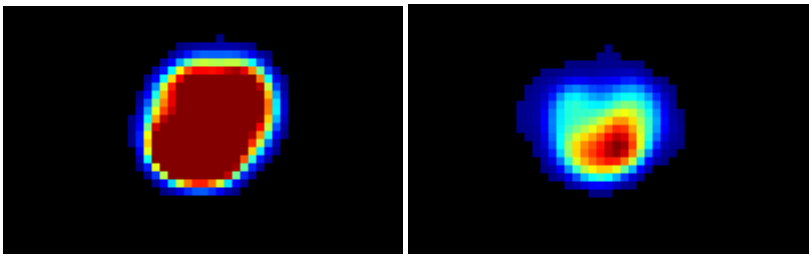

Figure 20: Heart slice with bad scaling on the left and optimized scaling on the right (both from the same mouse)

It is not always possible to get as nice images like this, but by making some educated guesses at the location of the heart one can still find voxels that might do. From these voxels reasonable functions can still be found.

When finally accepting the chosen voxel / location, the program runs on an autopilot if you use the default settings. In the end it should give you a few sample intensity functions from some voxels, and the averaged result that will be used in the end. Unfortunately it is not before this point you can be absolutely sure you got a reasonable function, and as it is now, you would have to force the program to stop and start over in order to look for a better function.

The next thing to do is find the tumor and then draw a region around it to define the location for the program. Again the program will start with showing you some pictures, helping you to pin point two of the tumor edges (in the z-plane). Be sure to click below the centre of the tumor when choosing its bottom edge, as these coordinates are later used to display k-maps of the tumor region. If the image is badly scaled, you should select a negative z-range to quickly be able to define new settings. When you've chosen the z-range, a series of x-y images will be shown, and all you got to do is delineate the tumor by tracing a region of interest (ROI) around the tumor. A nice image of this will look something like that displayed in Figure 21 below.

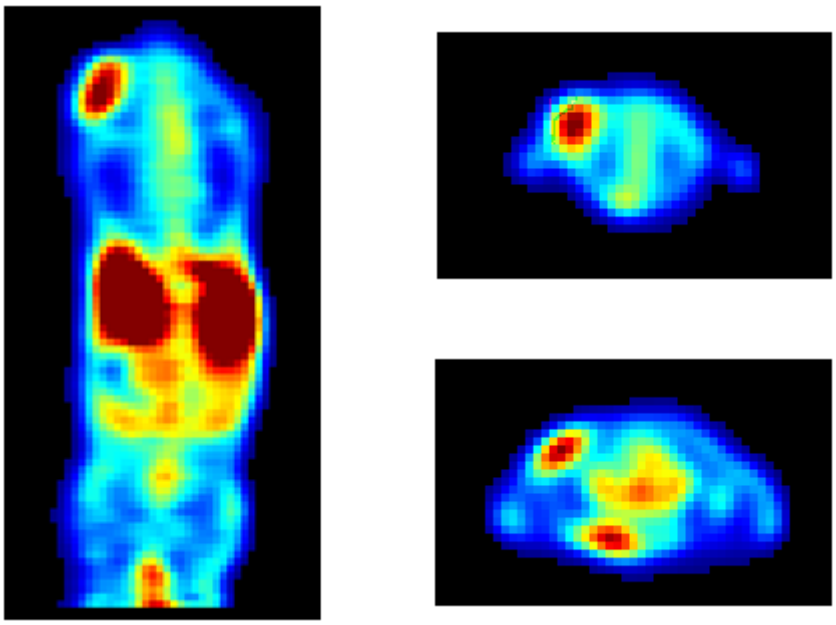

Figure 21: On the left, image to select the z range from. On the right, images to draw tumor ROIs in. The tumors seen here is the CWR22 xenografts.

When you have finished drawing all the ROIs you will be prompted to answer whether you are satisfied or not. Are you not satisfied with the regions you drew, or maybe the scaling was too bad to do so in the first place, you will get some new options. You can rescale the images and you can also watch a little movie that goes through all xz-images (coronal) in the mouse. Watching this movie might be helpful if you're having trouble finding the tumor. The y-value for each image will also be shown, and you can use a y-value from a good image to define the lower and upper values for z (also called z-range). Now we are back at the beginning and you can continue to try better scaling and drawing better ROIs until you are satisfied.

Now you got both a heart function (arterial function) and the tumor region plugged into the program. This is all it needs to do the pharmacokinetic modelling and produce data. The code for this was handed down from my supervisor Eirik Malinen. After a series of iterations the best fit for the model is presented. Functions called "free" and "bound" is displayed and represent the amount of free FDG among the cells and the bound or metabolized FDG. See Figure 22 below for a sample tumor function.

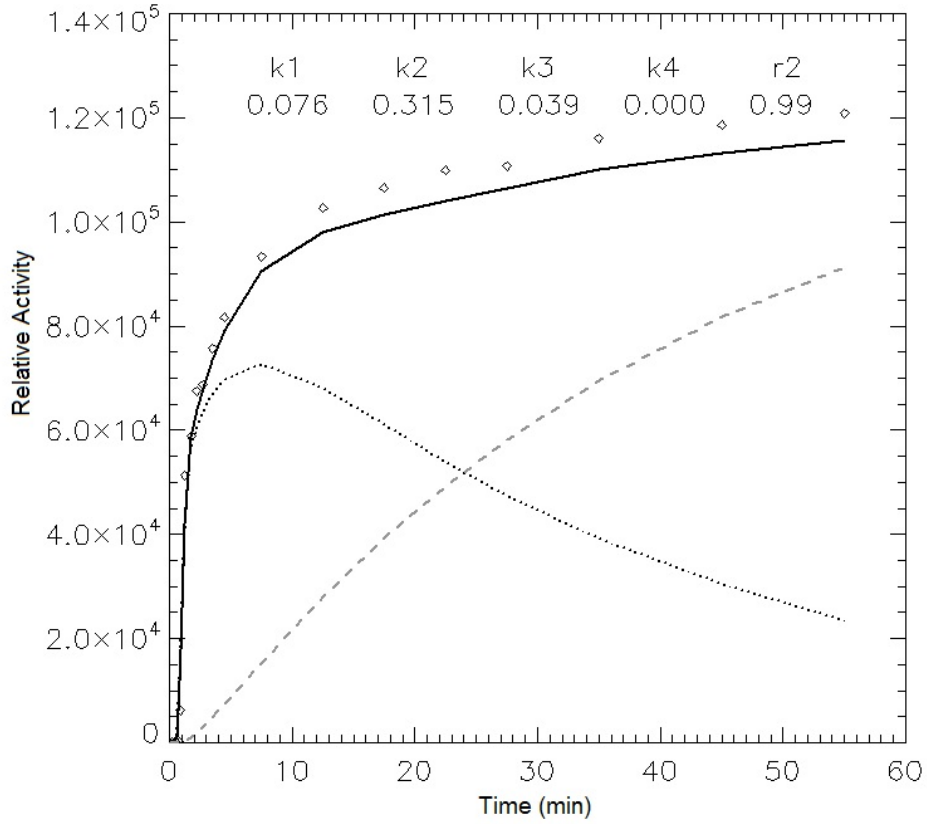

Figure 22: Median Intensity functions of FDG in tumor. Solid line is total. Bound is striped, and Free is Dotted. The median k-parameters for this treated CWR22 tumor are shown.

More importantly the program gives you “k-parameters” which represent the rate of physiological processes such as FDG uptake and metabolism in the tumor. And it is the distribution of these k-parameters within the tumor that we want to analyze later. Therefore at the end of this program, histograms of k-value distribution will be shown on the screen and then saved to disk. It is also interesting to see “k-value maps” of the tumor, basically a picture of the tumor with regard to k-value and not radioactive intensity. With a few more lines added to the program, a sort of 3D representation of this is displayed on a 2D computer screen. In fact, it’s just a lot of 2D images next to each other, but you can imagine them on top of each other. No colour bar to match the specific values is present, but the max and min values are displayed (as well as the mean value). Shown in Figure 23 is an example of these images.

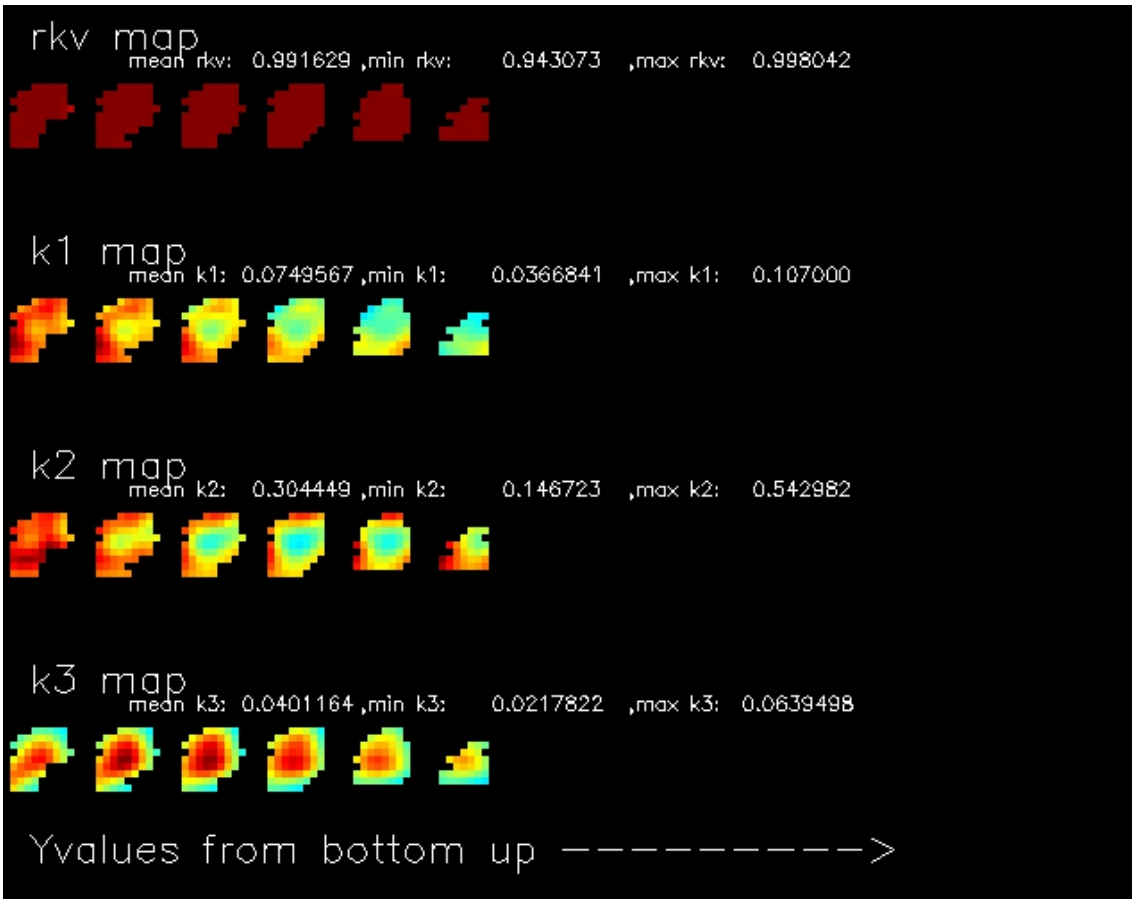

To sum up, when this program is run from the beginning to the end, it should have collected all data needed from one tumor. The plasma function, the tumor region, the free and bound functions and the k-parameters. This data is saved both in graphic for your eyes and in IDL save files for later use.

3.5 Metabolic rate of glucose and the Patlak plot

Assuming that the system will eventually enter a steady state it is possible to find a measure of the metabolic rate of glucose (MRglc). Using the principles of competitive kinetics, a lumped constant (LC) is introduced to relate the behavior of the tracer FDG to glucose in order to obtain.

$$MRglc = \left(\frac{K_1^* k_3^*}{k_2^* + k_3^*} \right) \frac{C_P}{LC}$$

Where C_P is the plasma concentration of glucose and assumed to be in steady state. The k* 's is the parameters found be pharmacokinetic modeling. (5)

The equation for the lumped constant is

$$LC = \frac{\lambda V_m^* K_m}{\phi V_m K_m^*}$$

Where ø is the fraction (1-r) of glucose that is metabolized after phosphorlyation. V_m^* and V_m are the maximum velocities and K_m^* and K_m are the apparent Michaelis-Menten constants. And λ is the ratio between the factors of FDG and glucose. (26)

The Patlak plot (see Figure 24 below) is obtained by plotting

$$\frac{\int_0^t C_P^*(s)ds}{C_P^*(t)}(x-axis, unitsoftime) vs. \frac{C_T^*(t)}{C_P^*(t)}(y-axis, unitless)$$

$$where$$

$$C_T^*(t) = C_E^*(t) + C_M^*(t)$$

and C_E is free FDG and C_M is bound FDG. (5)

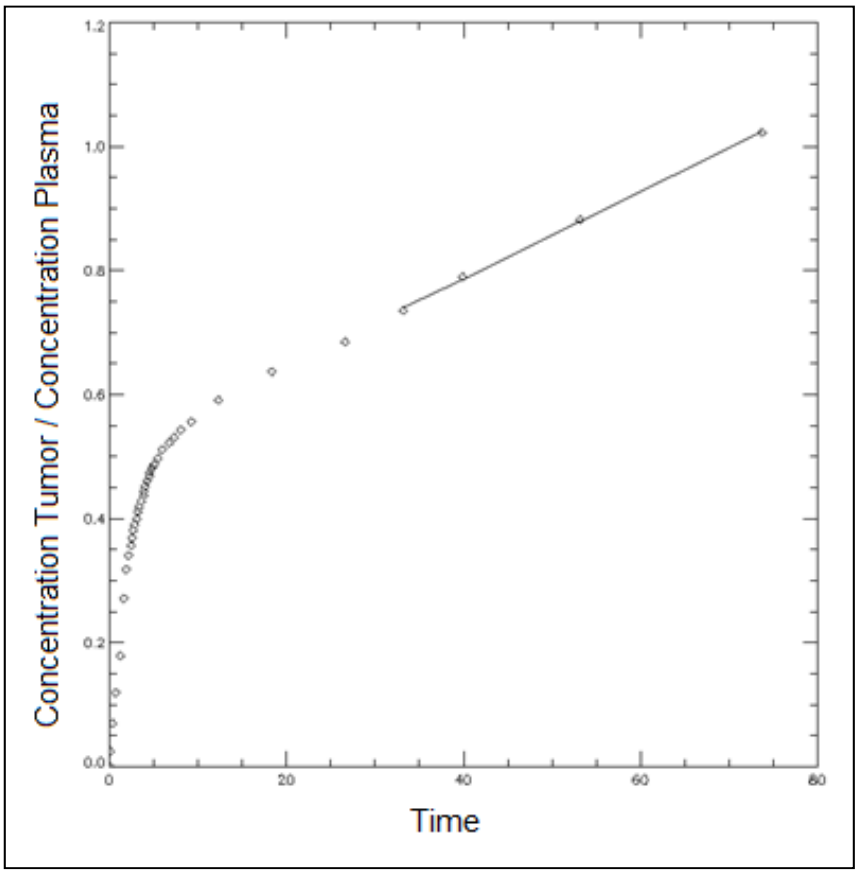

Figure 24: Patlak plot.

The slope of the end of the line should equal $\left(\frac{K_1^* k_3^*}{k_2^* + k_3^*}\right)$ and thus be linearly related to the metabolic rate of glucose. (5) This constant will be referred to as the MRglc for the remainder of the work, as the lumped constant is in most cases close to a constant (27), and that our C_P is incomparable. The absolute values will not be correct, but the comparison between the groups will not suffer.

3.6 Statistical methods

3.6.1 Hypothesis testing and the students t-test.

In statistics there is a way of assessing uncertainty through so-called p-values. If it is of interest to ascertain whether something is true (a), then a hypothesis expressing the opposite (b) is put forward. Then the chance for this hypothesis to be true is calculated, and if the chance for (b) is less than 5%, it seems highly probable that our initial assumption (a) is correct. (28).

In this work, the students t-test implemented in Interactive Data Language (IDL) has been used. In this work it is important to be sure if two groups show different properties, and this test fits the description. For this test, two arrays of data are compared. The hypothesis is that the data of both arrays are drawn from the same distribution. The following is the description of the function given in the IDL help file.

“The TM_TEST function computes the Student's T-statistic and the probability that two sample populations X and Y have significantly different means. X and Y may be of different lengths. The result is a two-element vector containing the T-statistic and its significance. The significance is a value in the interval [0.0, 1.0]; a small value (0.05 or 0.01) indicates that X and Y have significantly different means. The default assumption is that the data is drawn from populations with the same true variance. This type of test is often referred to as the t-means test. The T-statistic for sample populations x and y with means ` x and ` y is defined as:”

$$T = \frac{\bar{x} - \bar{y}}{\sqrt{\frac{\sum_{i=0}^{N-1} (x_i - \bar{x})^2 + \sum_{i=0}^{M-1} (y_i - \bar{y})^2}{(N + M - 2)} \left(\frac{1}{N} + \frac{1}{M}\right)}} \quad (29)$$

The function returns the t-value and the p-value.

4 Results

4.1 General investigations

4.1.1 Illustrations of dynamic series

For the MAS 98.12 set, a presentation of the PET images is shown in figure 25, depicting a time series for a whole mouse. A few samples of the total of 37 time frames have been selected.

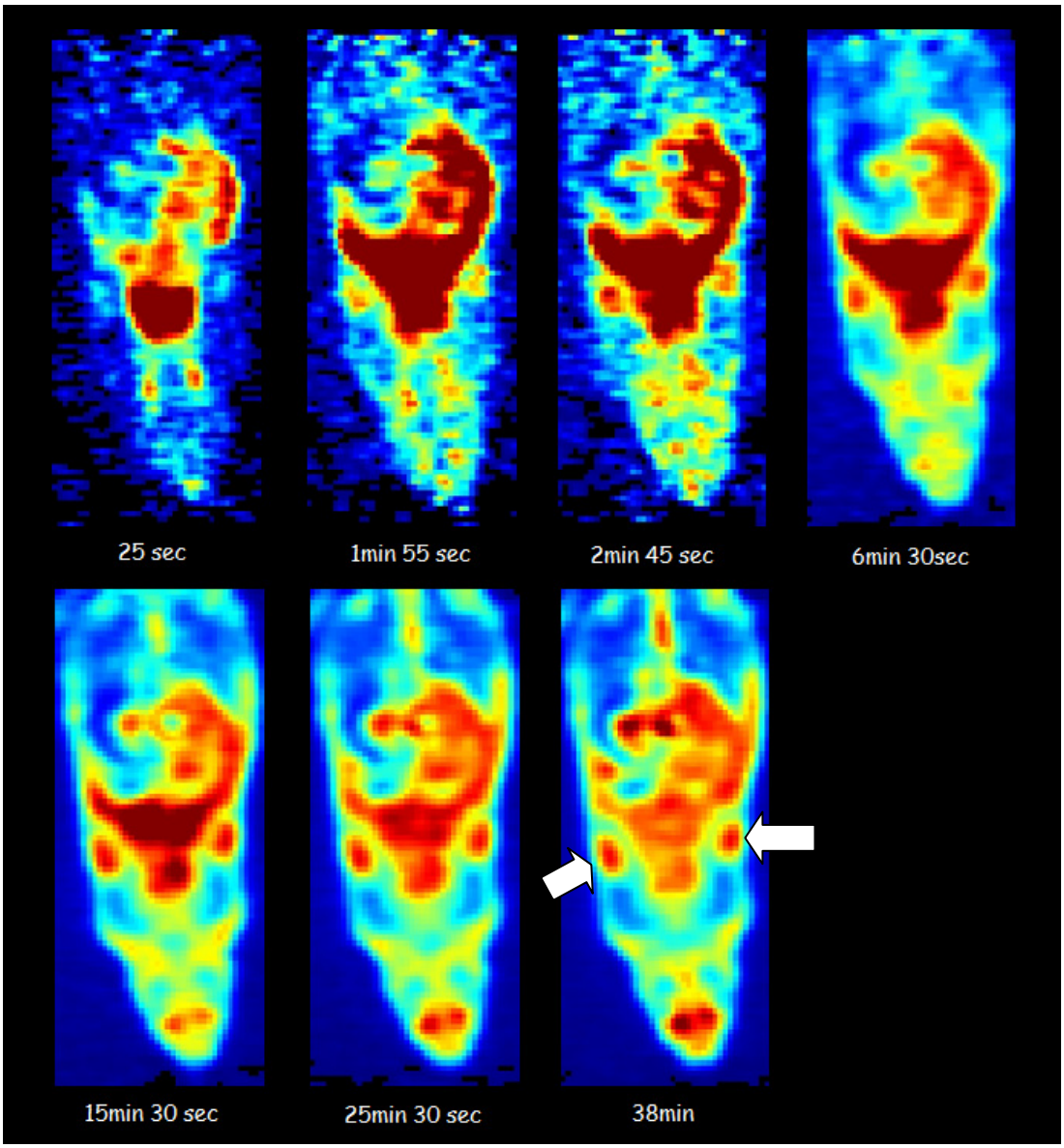

Figure 25: Illustration of a dynamic PET series of mouse with MAS 98.12 xenograft. The arrows indicates the location of the implanted tumors.

These images show high activity in the heart and then in the intestine at an early stage but the activity in these areas fade over time. Activity in the tumors can be seen across the entire series and does not fade significantly. It can also be seen that the brain and bladder accumulates more and more FDG over time. The early images are noisier because of the high temporal resolution.

The full dynamic series of the heart (of 20 time points for this mouse) is shown in Figure 26. The image series shows a rapid uptake that quickly decline as the bolus of FDG passes the heart.

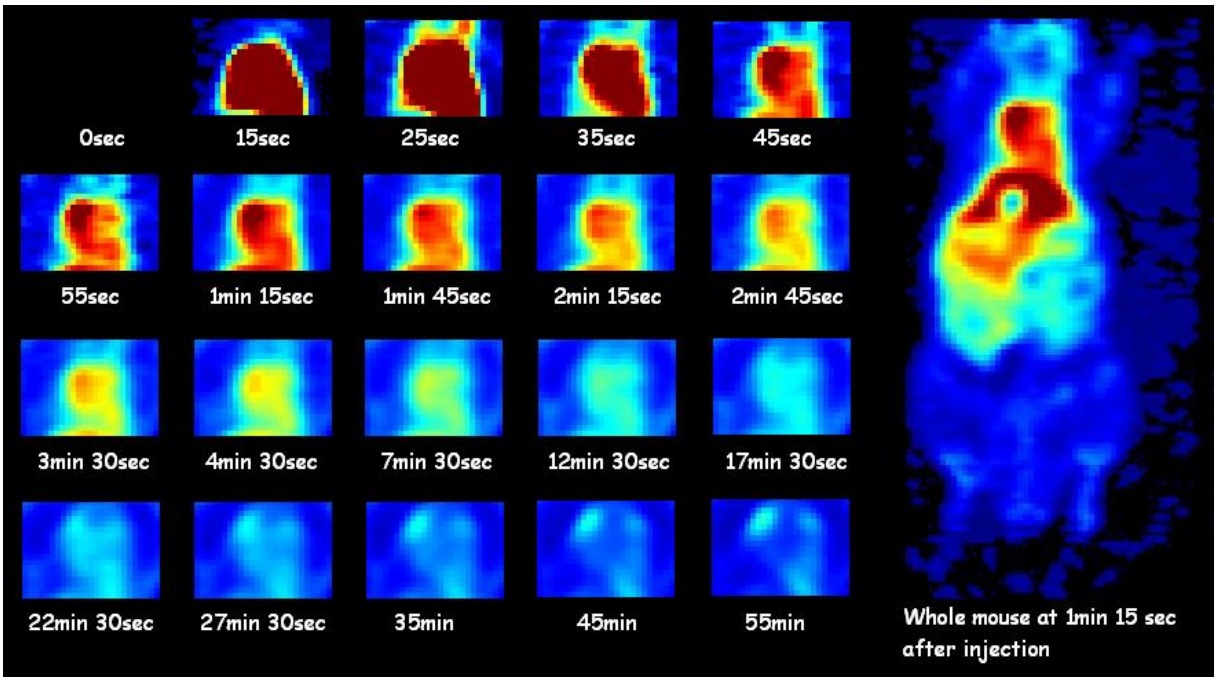

Figure 26: A dynamic FDG-PET series of the heart of CWR22 mouse.

4.1.2 Plasma function

The plasma function itself might be useful to investigate. Some plasma functions from different mice are shown in Figure 27. Although some differences can be seen, mostly due to differences in injected activity, these functions describe the same course as depicted in the images in Figure 26.

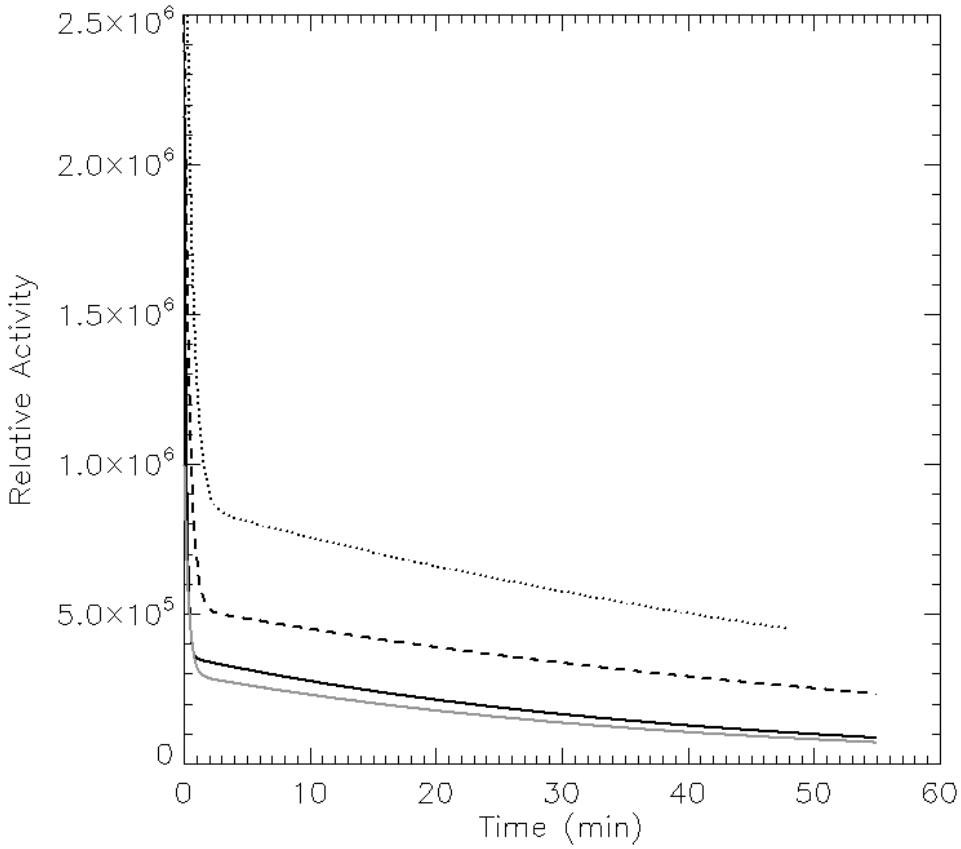

Figure 27: Plasma functions. The solid line is from a CWR22 Control, the Gray line is from a treated CWR22, the dotted line is MAS 98.12 and the dashed line is MAS 98.06. Note that these are from individual mice.

4.1.3 Tumor curves

In Figure 28, curves describing the uptake in a single tumor voxels of a CWR22 mouse is shown. As seen, FDG is rapidly accumulated before a plateau is reached. The k-parameters are displayed along with r-squared and the blood fraction. Here we can see how the measured tumor activity can be divided into three parts; free FDG, bound FDG and FDG in blood. The underlying characteristics of the free and bound component show that the plateau is a consequence of a decreasing free component and an increasing bound one. Also, there is a considerable heterogeneity in the uptake characteristics voxel-to-voxel. In Figure 29, curves for a full tumor are depicted. As can be seen, the tumor is not much different from the random voxel. The function is entirely different from the what is found in the heart though.

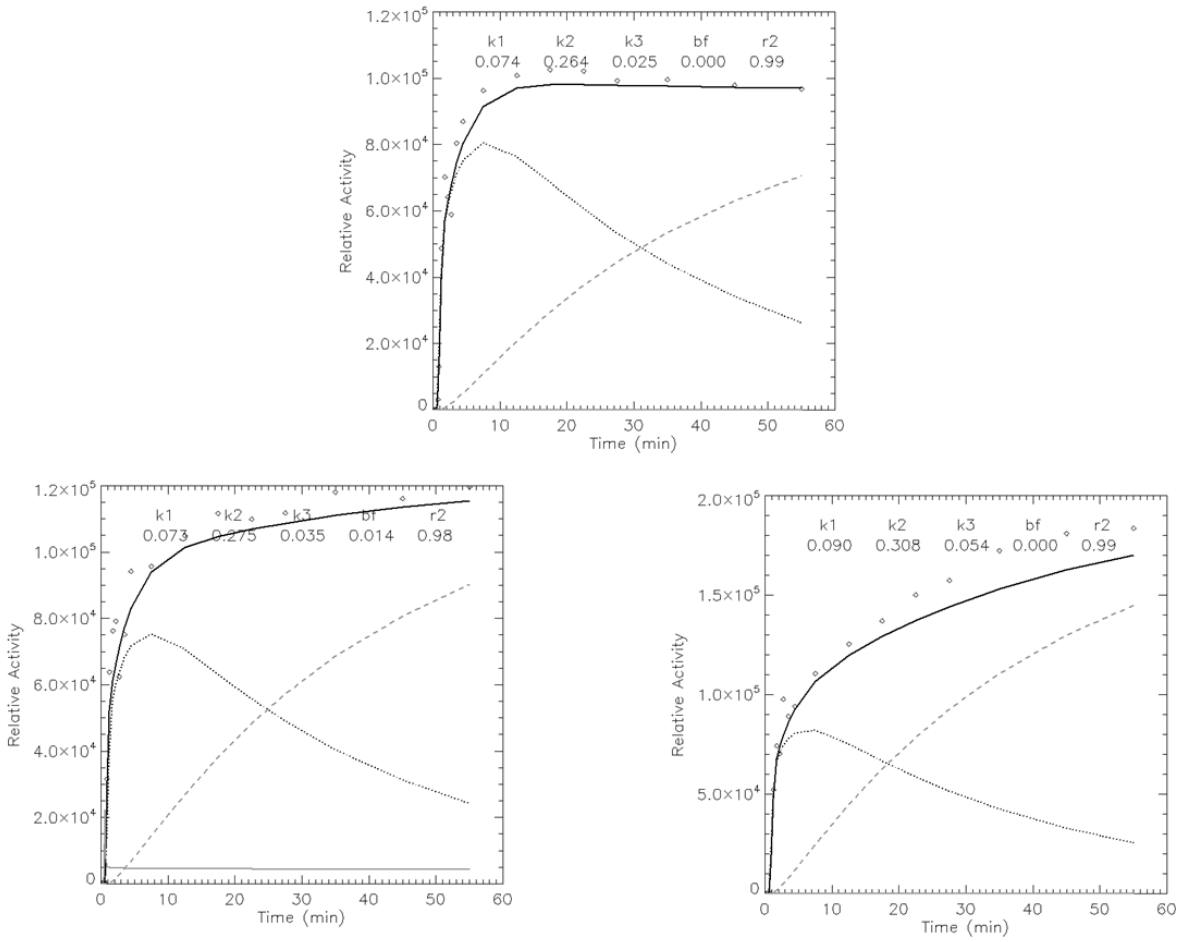

Figure 28: Tumor voxel uptake curves. The solid line represents the total fitted uptake curve. The dotted line represents free FDG and the dashed line bound FDG. The solid grey line at the bottom is activity from blood within the tumor. The diamonds are the raw data.

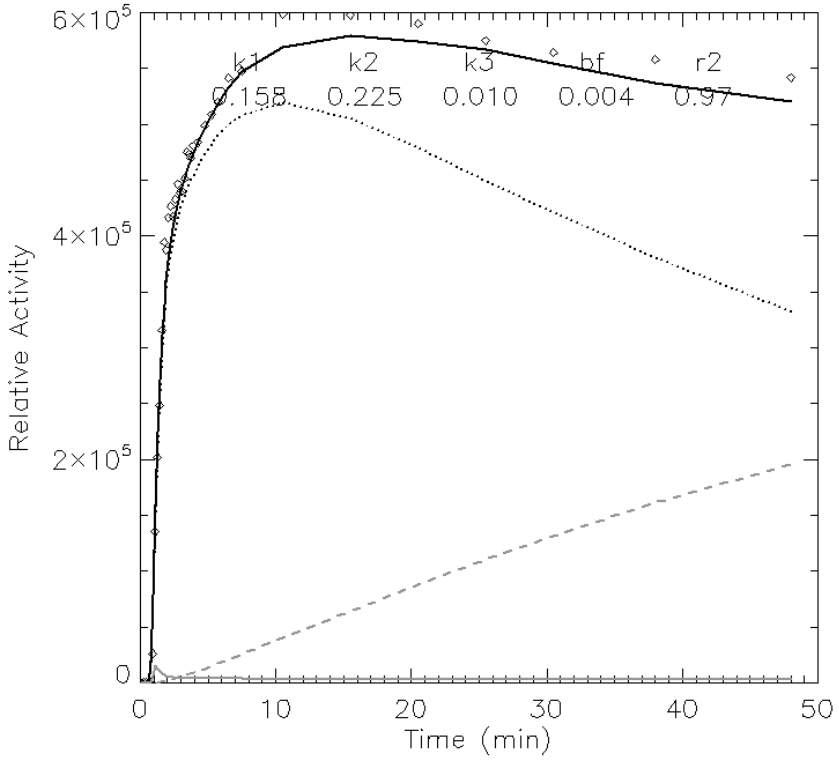

Figure 29: Full tumor uptake functions. The solid line represents the total uptake function. Dotted line represents free FDG and dashed line bound FDG. The solid grey line at the bottom is activity from blood within the tumor. The diamonds are the raw data.

4.1.4 Distribution of pharmacokinetic parameters

To illustrate tumor heterogeneity, the range of k-parameters across the voxels can visualized in histograms (figures 30-32). In the histograms the diversity within the tumor is displayed. The distribution seems fairly Gaussian but somewhat left-skewed for k3 in this tumor.

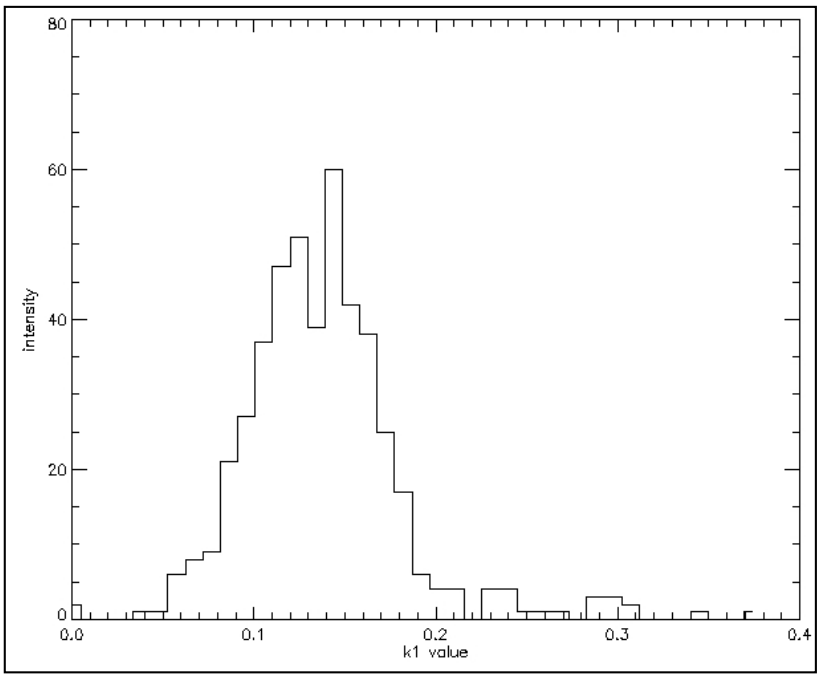

Figure 30: Histogram of k1 values for a CWR22 control tumor

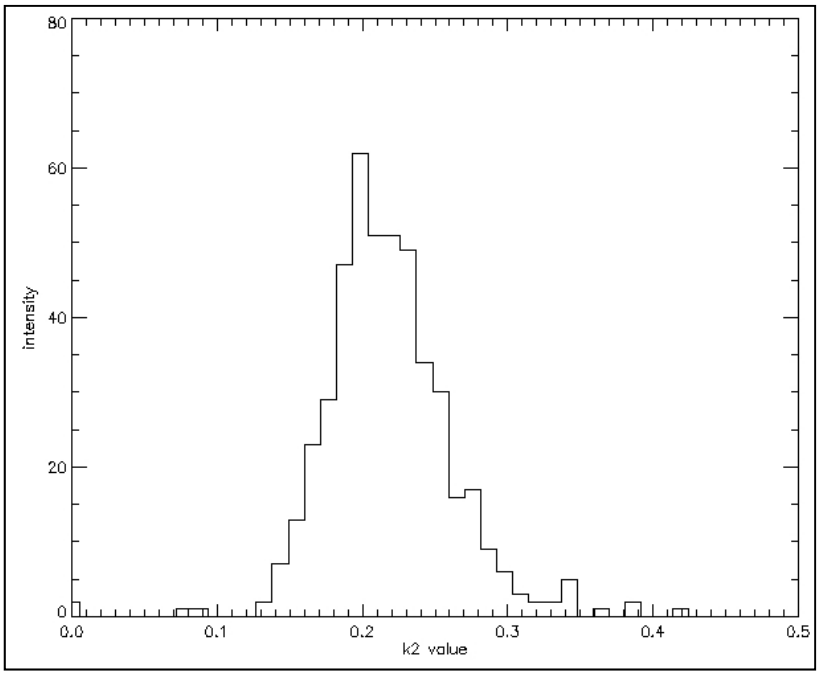

Figure 31: Histogram of the k2 values for a CWR22 control tumor.

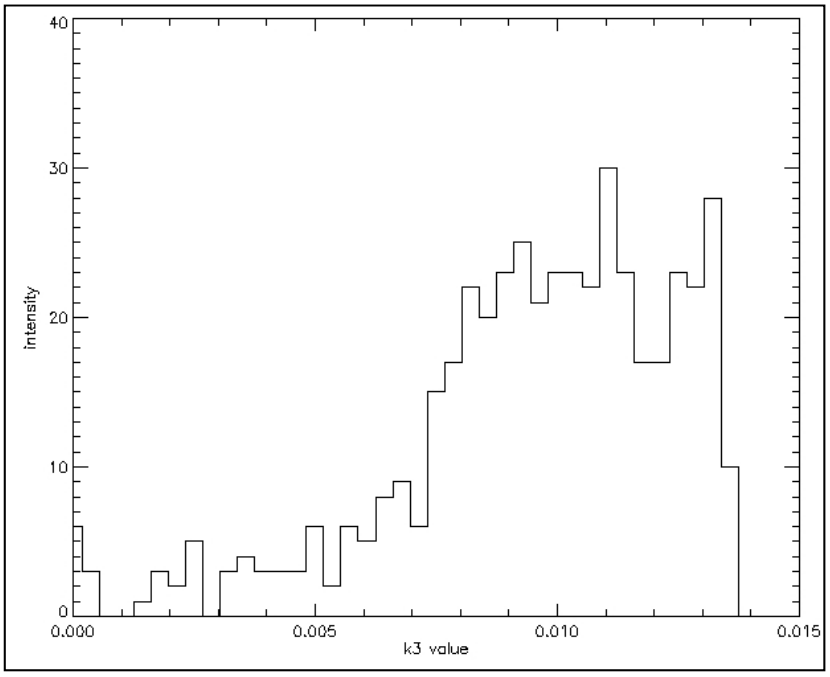

Figure 32: Histogram of the k3 values for a CWR22 control tumor.

In Figure 33, an area of tumor with high uptake has been compared to an area of low uptake. The difference between these curves is clear, and it seems like it is the bound FDG that makes the difference. In Figure 34, a map of the k-parameters of a tumor is presented. Here we can see that the tumor seems to be fairly symmetric out from the centre, but in both the k1 and k2 maps there is something interfering with this pattern.

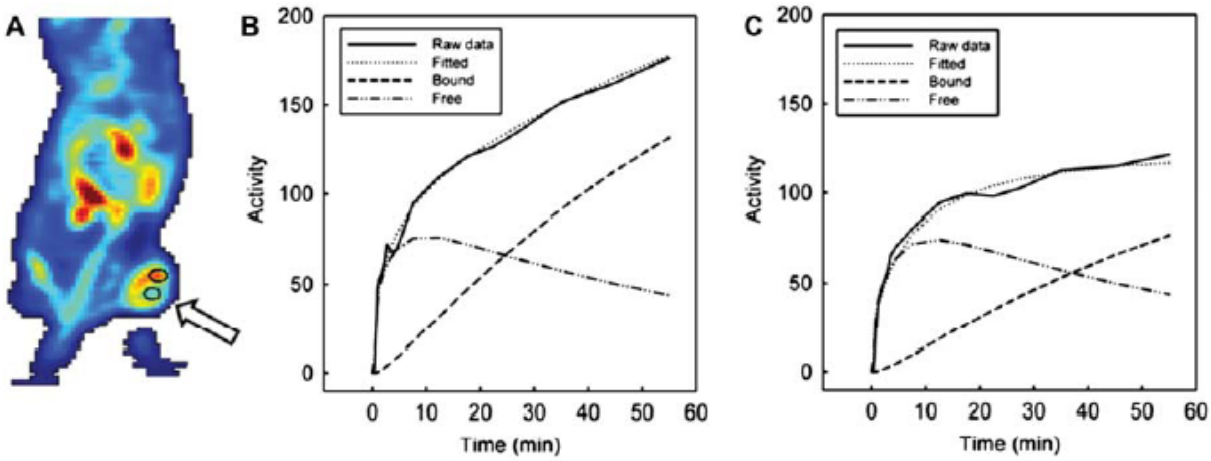

Figure 33: Area of high activity against area of less activity for an untreated CWR22 tumor.

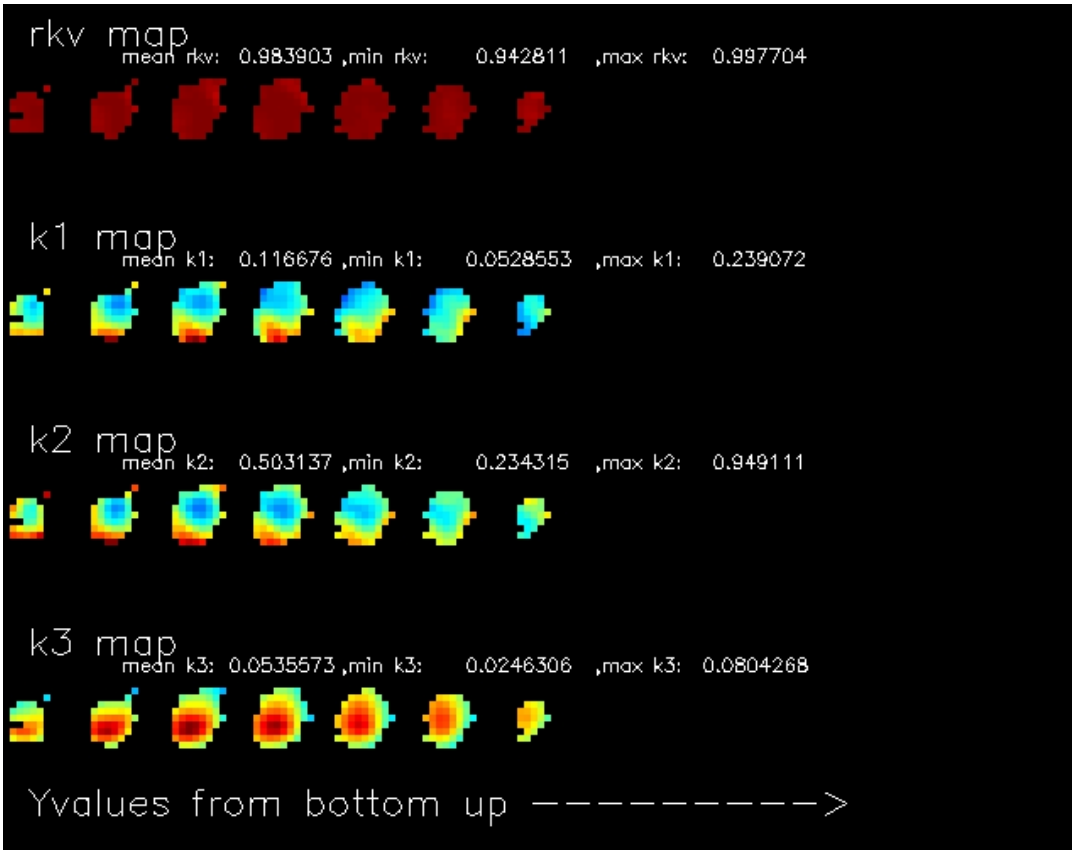

Figure 34: Maps of the k-parameters in the xz-plane of tumors or the sagital/transverse plane. From left to right the index of the coronal value increases. This is a CWR22 tumor that received 7.5 Gy.

4.1.5 Investigation of the input parameters of the model

The non-linear regression model used demands initial estimates of the various parameters to be calculated. Several different initial “guesses” of the k-parameters into the model was used to investigate whether this affected the results. In Table 1 the results of changing the initial k1 value (normally set to 0.3 min^{-1}) is displayed.

	Test mouse 1			Test mouse 2			Test mouse 3		
	k1	k2	k3	k1	k2	k3	k1	K2	k3
K1=0	2,78E-06	0,5	0,1	2,68E-06	0,5	0,1	3,29E-06	0,5	0,1
K1=0,05	0,075014	0,249436	0,025316	0,081373	0,33766	0,040026	0,127239	0,558205	0,052117
k1=0,1	0,074996	0,249428	0,025371	0,081367	0,337625	0,040021	0,127359	0,559442	0,05206
k1=0,2	0,075186	0,250828	0,025431	0,081361	0,337633	0,040025	0,127354	0,55917	0,052116
k1 = 0,3	0,07509	0,250305	0,025428	0,081365	0,337555	0,040026	0,127356	0,559216	0,052099
K1=0,4	0,075054	0,250286	0,025427	0,081361	0,337646	0,04002	0,127359	0,559178	0,052095
K1=0,5	0,075204	0,250258	0,025427	0,08135	0,33764	0,040027	0,127356	0,559332	0,052084
K1=0,6	0,075097	0,250831	0,025431	0,081359	0,337656	0,040022	0,127348	0,559205	0,052073
K1=0,7	0,075054	0,250147	0,025431	0,081368	0,337663	0,040022	0,12737	0,559233	0,05209
K1=0,8	0,075099	0,250294	0,02543	0,081375	0,337691	0,040024	0,127365	0,559141	0,052106
K1=0,9	0,075094	0,250232	0,025428	0,081356	0,337674	0,040022	0,127369	0,559049	0,052101
K1=1	0,075041	0,250097	0,025429	0,081367	0,337742	0,040017	0,127342	0,559352	0,052099
K1=10	0,075003	0,249429	0,025433	0,081372	0,337561	0,040022	0,127379	0,559361	0,052093

Table 1: Results of changing the initial k1-value (in bold).

There are only minor changes to be seen here except when k1 is set to zero. This testing was done extensively, still the additional data showed no different results.

4.1.6 Adding a blood fraction parameter to the model

We also wanted to se how the resulting tumor functions would look like if we assumed that a part of the voxel contained blood. First a randomly selected voxel from each tumor was scrutinized. One of the voxel had a relative large increase in r^2 following the introduction of the blood fraction and was worth a closer look, see Figure 35. For most voxels there wasn't a great difference, but for 6 out of 16 voxels the r^2 was more or less increased. See Table 2.

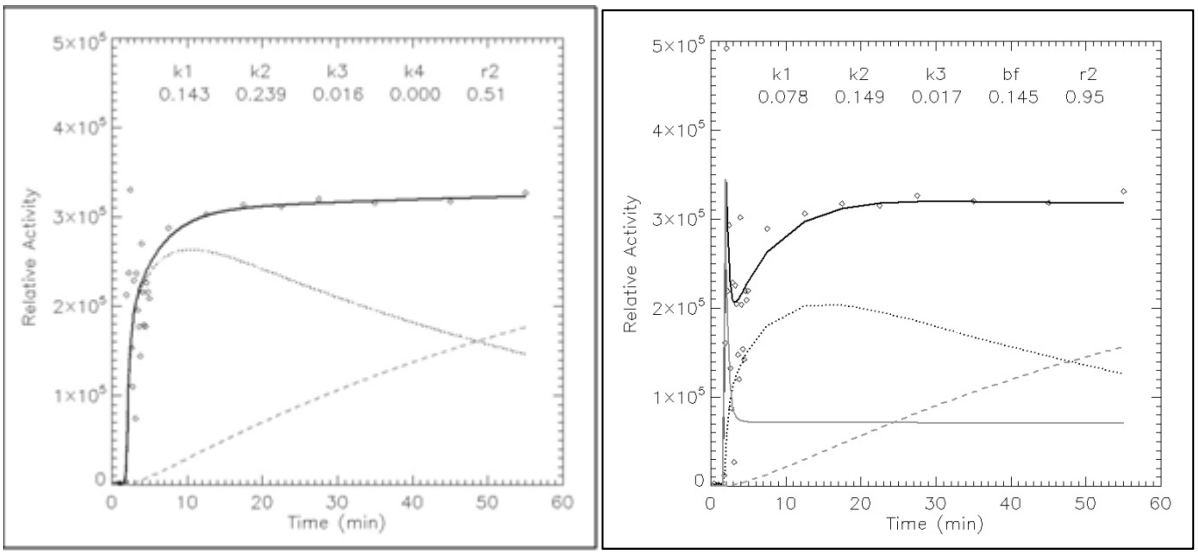

Figure 35: On the left; old uptake and free/bound functions for a MAS 98.06 tumor. On the right; the functions after introducing the blood fraction parameter.

For the specific voxel in Figure 35 there is a significant difference between the k1 and k2 parameters as well as the r^2. The initial spike coming from the activity in blood vessels inside this voxel can be clearly seen. For the entire tumors however the r^2 doesn't change much, but there is still some variation in the mean values (see Table 3).

	k1			k2			k3			rkv		
Number	Old	New	%	Old	New	%	Old	New	%	Old	New	%
3v	0,208	0,205	98,56	0,438	0,435	99,32	0,014	0,014	100	0,95	0,95	100
3h	0,2	0,184	92	0,414	0,391	94,44	0,015	0,016	106,7	0,97	0,97	100
1h	0,079	0,078	98,73	0,159	0,157	98,74	0,013	0,013	100	0,96	0,96	100
1v	0,141	0,138	97,87	0,211	0,209	99,05	0,008	0,008	100	0,98	0,98	100
2h	0,198	0,172	86,87	0,266	0,24	90,23	0,009	0,009	100	0,96	0,97	101,04
2v	0,203	0,159	78,33	0,312	0,264	84,62	0,005	0,005	100	0,94	0,98	104,26
5h	0,176	0,156	88,64	0,31	0,283	91,29	0,015	0,015	100	0,94	0,94	100
5v	0,155	0,137	88,39	0,345	0,317	91,88	0,014	0,015	107,1	0,95	0,96	101,05
6h	0,209	0,209	100	0,467	0,467	100	0,016	0,016	100	0,98	0,98	100
6v	0,183	0,14	76,5	0,389	0,32	82,26	0,019	0,021	110,5	0,92	0,97	105,43
6v2	0,137	0,137	100	0,34	0,34	100	0,069	0,069	100	0,94	0,94	100
6h2	0,087	0,087	100	0,354	0,353	99,72	0,107	0,107	100	0,97	0,97	100
1v2	0,208	0,113	54,33	0,513	0,312	60,82	0,035	0,041	117,1	0,84	0,92	109,52
1h2	0,172	0,169	98,26	0,374	0,37	98,93	0,039	0,039	100	0,96	0,96	100
2v2	0,143	0,078	54,55	0,239	0,149	62,34	0,016	0,017	106,3	0,51	0,81	158,82
2h2	0,069	0,069	100	0,133	0,133	100	0,027	0,027	100	0,98	0,98	100

Table 2: Results of adding blood fraction when looking at individual voxels. The percentage is that of the new value compared to the old. The first set of rows is from MAS 98.12 tumors, and the second for MAS 98.06 tumors.

Control

	k1			k2			k3			rkv
Number	Old	New	%	Old	New	%	Old	New	%	Median
5v_101209	0,076	0,073	96,053	0,507	0,588	116	0,039	0,068	174,36	0,97
5h_101209	0,05	0,05	100	0,234	0,29	123,9	0,035	0,066	188,57	0,98
1v2_130110	0,078	0,074	94,872	0,276	0,266	96,38	0,025	0,025	100	0,97
1h2_130110	0,075	0,074	98,667	0,25	0,247	98,8	0,025	0,025	100	0,97
4v_130110	0,081	0,076	93,827	0,337	0,315	93,47	0,04	0,039	97,5	0,99
4h_130110	0,076	0,071	93,421	0,286	0,264	92,31	0,029	0,029	100	0,99

7,5Gy

	k1			k2			k3			rkv
Number	Old	New	%	Old	New	%	Old	New	%	Median
11v_081209	0,125	0,124	99,2	1,163	1,161	99,83	0,047	0,048	102,13	0,91
15v_081209	0,021	0,021	100	1,533	1,437	93,74	0,662	0,69	104,23	0,94
15h_081209	0,095	0,095	100	1,015	1,013	99,8	0,308	0,329	106,82	0,97
5v2_130110	0,076	0,074	97,368	0,324	0,312	96,3	0,071	0,072	101,41	0,98
51v_130110	0,107	0,093	86,916	0,454	0,393	86,56	0,071	0,071	100	0,97
6v_130110	0,127	0,109	85,827	0,599	0,477	79,63	0,052	0,052	100	0,98
6h_130110	0,162	0,133	82,099	0,442	0,372	84,16	0,033	0,034	103,03	0,97

Table 3: Results of adding blood fraction when looking at whole tumor. The percentage is that of the new value compared to the old. These data are from the CWR22 tumors.

4.2 TAC

4.2.1 TAC for treated tumors against controls

The normalized time activity curve is a basic approach to investigate a tumor. As can be seen from Figure 36, there is clear distinction in normalized TAC between the treated and untreated CWR22 tumors. The irradiated tumors accumulate more FDG and have a greater internal variance than the control group. A graph displaying the p-values following T-testing for each time point is given in Figure 38 below.

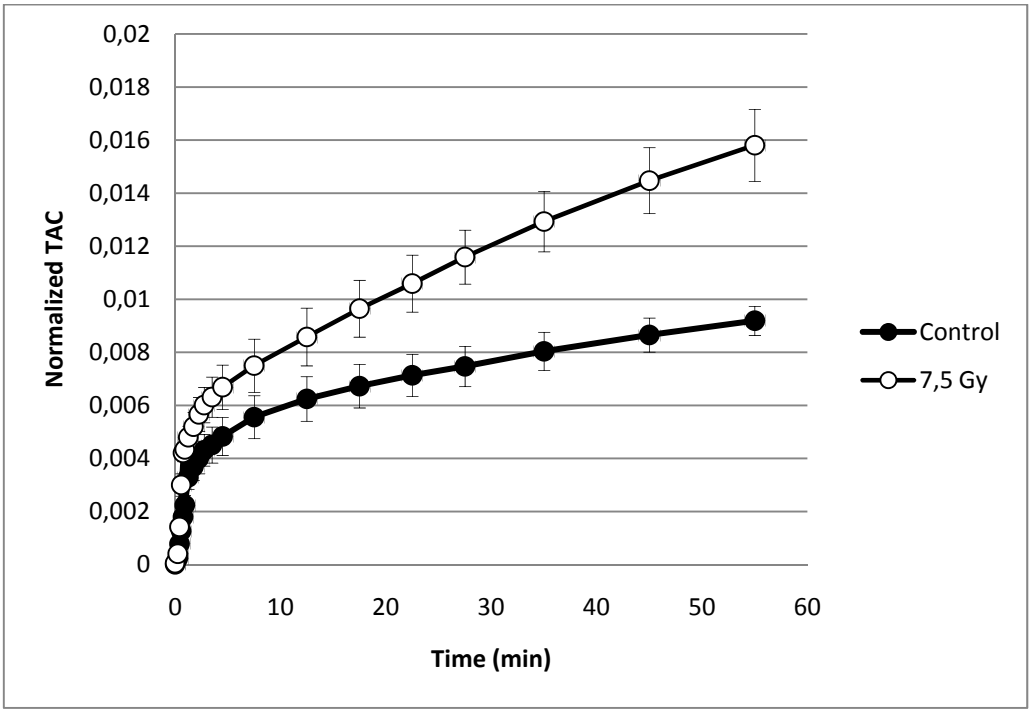

Figure 37: TAC for CWR22 xenografts with standard errors shown.

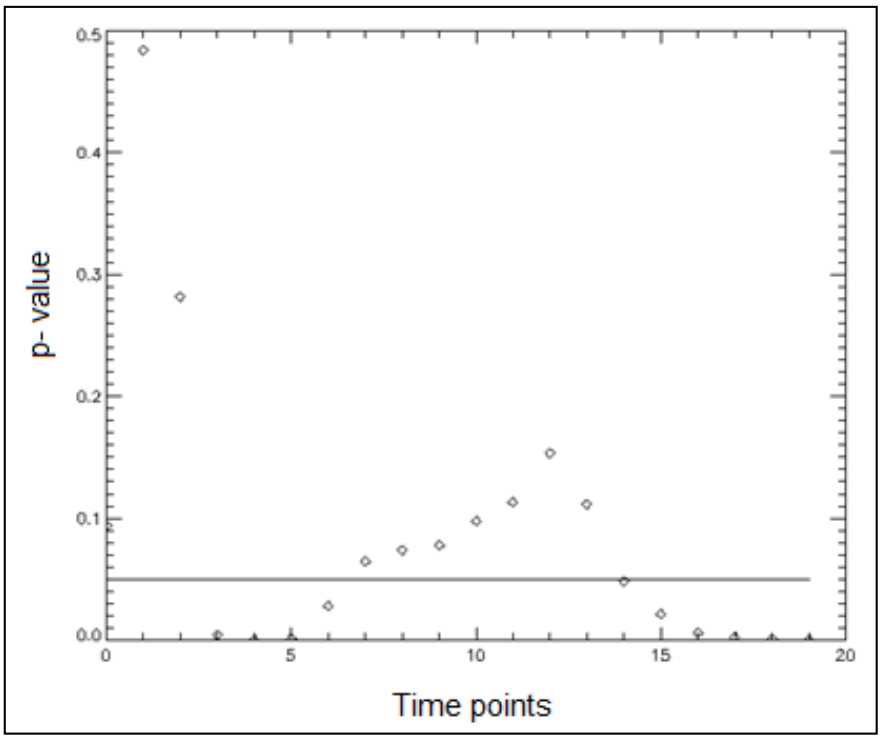

Figure 38: p-values for the CWR22 TAC curve (not real time on x axis)

For most time points there is a statistical significant difference, but it is more pronounced at the end of the time series.

4.2.2 TACs of the MAS 98.12 and MAS 98.06 tumors

As can be seen in Figure 39, the MAS 98.12 line seems to have a more rapid uptake than the MAS 98.06 line. But as the MAS 98.06 line does not reach its maximum during the assay its final value is greater than that of the MAS 98.12 line. The p-value following T-testing is shown in Figure 40. Except for the time points where the curves cross each other, there is a significant difference between the two groups.

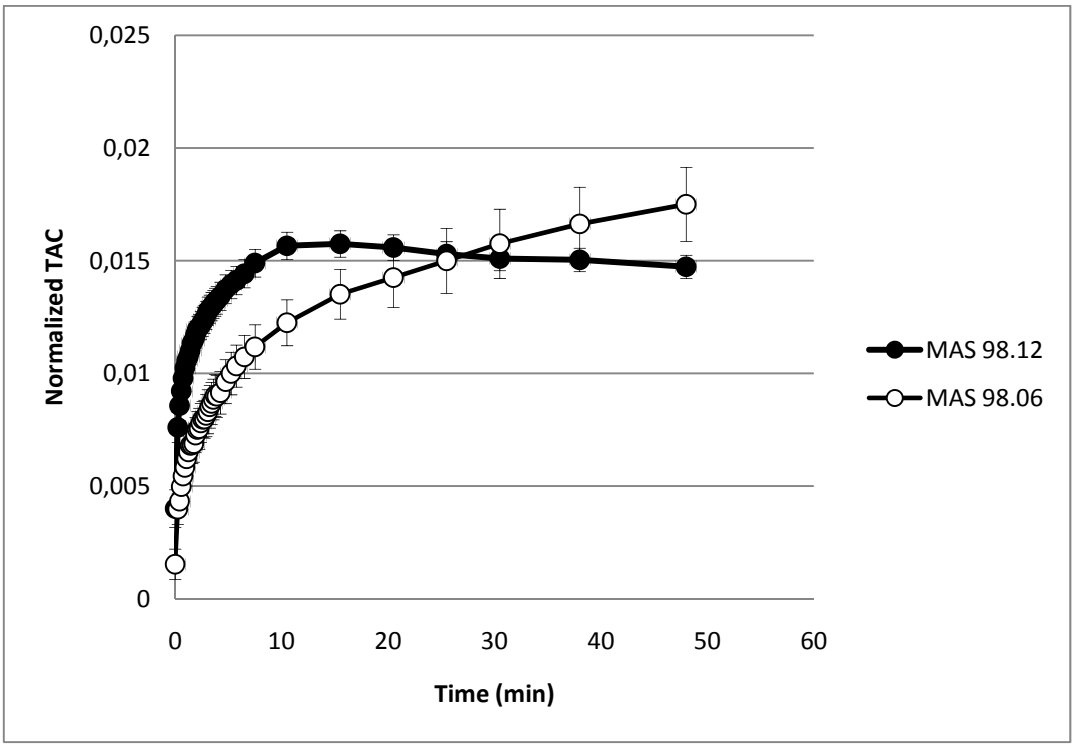

Figure 39: TAC for MAS 98.12 and MAS 98.06 tumor with standard errors shown

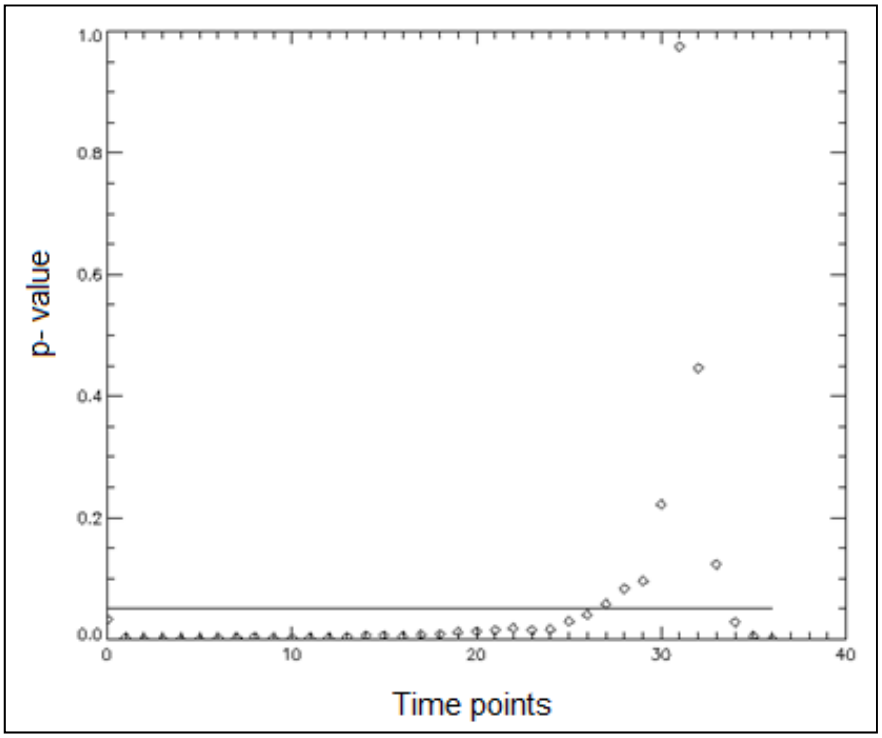

Figure 40: p-values for MAS 98.12 and MAS 98.06 TAC (not real time on x-axis).

4.3 Pharmacokinetic parameters

4.3.1 Median parameters of the CWR22

By investigating the pharmacokinetic parameters calculated, more information about the tumors might be obtained. The median values of the k-parameters for the different groups of CWR22 xenografts are shown in Figure 41 below. There is borderline statistical significance for k1 and k2, but not for k3.

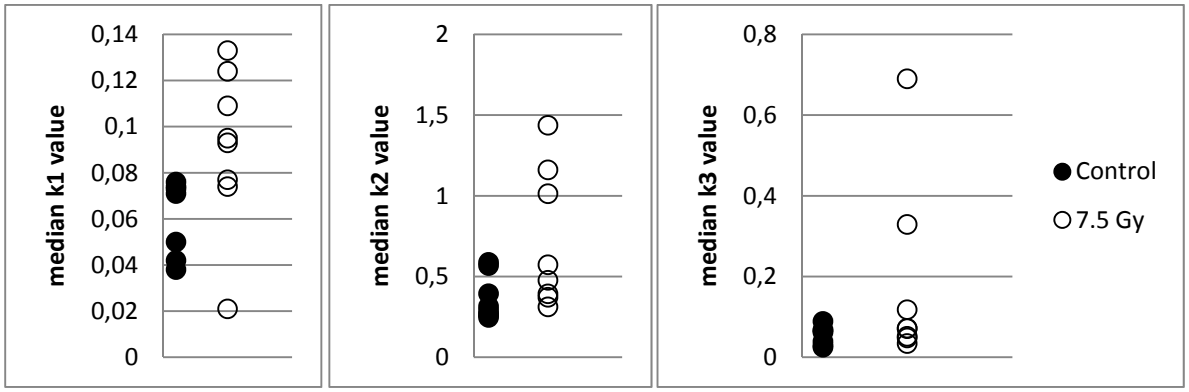

Figure 41: Median k-parameters for each CWR22 tumor in the different groups. The statistical test gives the following p-values; for k1 the p-value 0.06, for k2 the p-value 0.04, for k3 the p-value 0.14.

4.3.2 Median parameters of the MAS 98.12 and MAS 98.06

In figure 42, median k1-k3 values are shown for of the MAS 98.12 and MAS 98.06 tumors. Comparing the two groups, the p-value for k1 and k2 indicates no significance, but k3 was highly different.

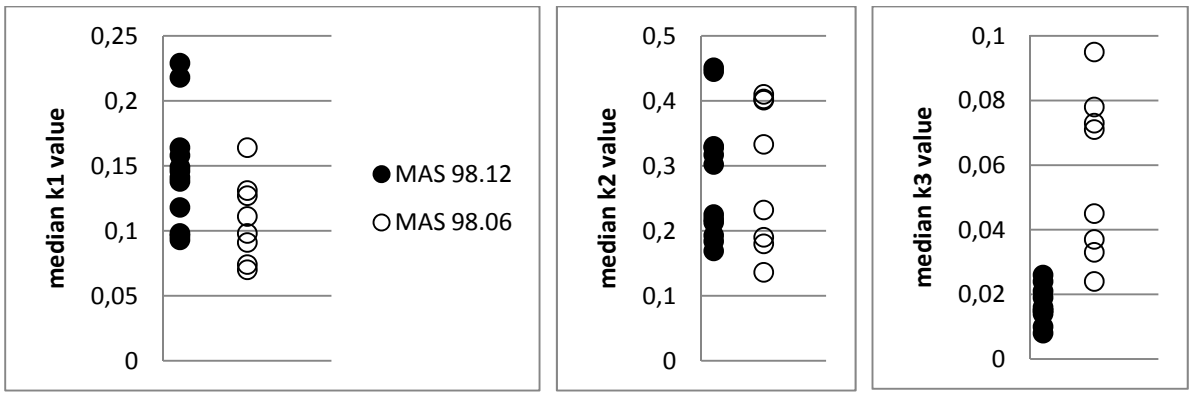

Figure 42: Median k-parameters for each MAS 98.12 and MAS 98.06 tumor. For k1 the p-value is 0.06, for k2 the p-value is 0.92 for k3 the p-value is << 0.01.

4.3.3 Histograms and percentile charts of CWR22

In the following, investigations of the tumor heterogeneity will be presented. In Figure 43, the mean histogram of k1 values across all voxels in treated and untreated tumors is shown. Note that the histogram will not represent the distribution of any one tumor, but the distribution of the entire group of collected voxels.

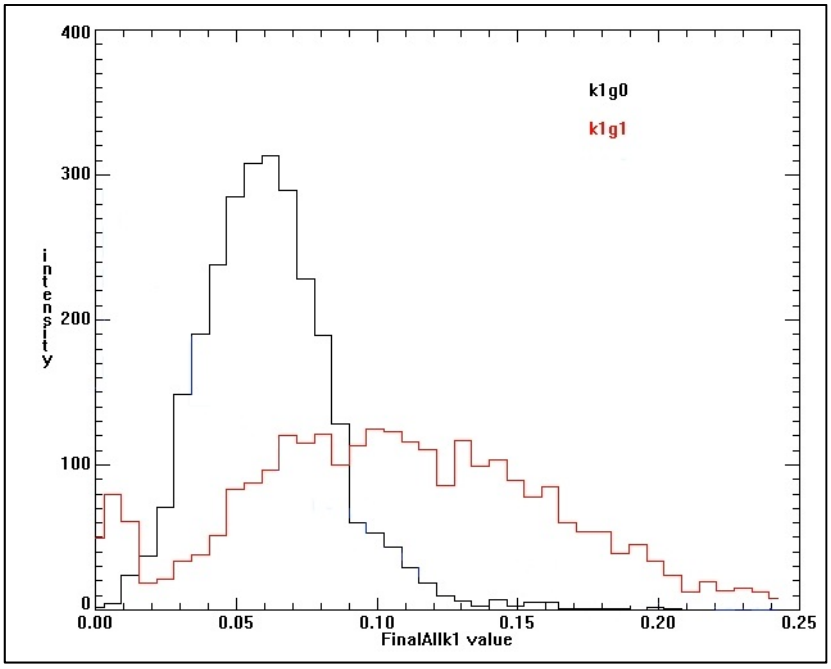

Figure 43: Histogram of k1 values for CWR22 xenografts. G0 is the control group and g1 is the one that got a dose of 7.5Gy.

The two histograms in Figure 43 are clearly dififferent. It is therefore useful to look at the percentile values for these histograms and the p-values for each percentile. The median is the 50 percentile, where 50% of the data is below this value. The percentile value for all the 1-99 percentiles is calculated in the same way.

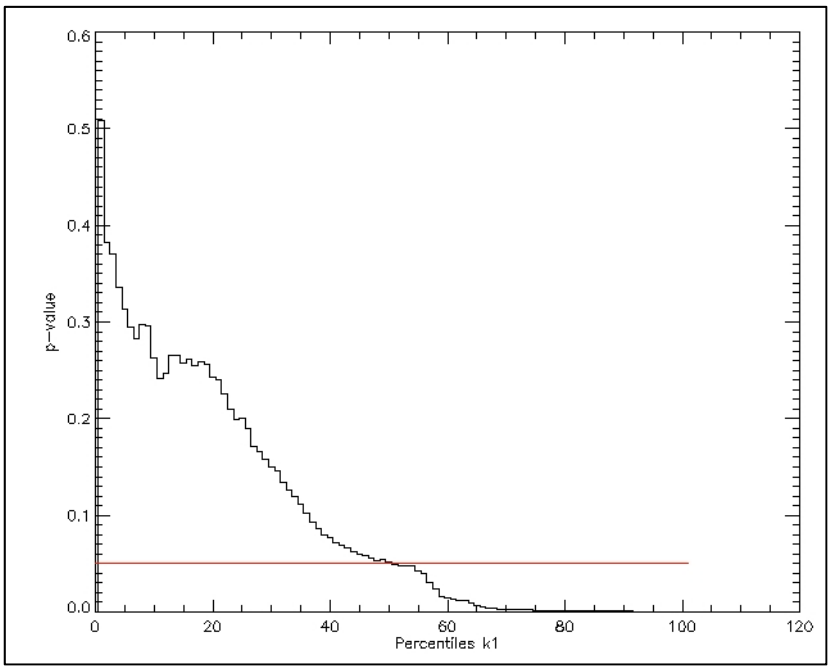

Figure 44: p-values for the percentiles of the k1 for CWR22 tumors. The solid line corresponds to a p-value of 0.05.

In Figure 44 it is shown that by looking at k1 values larger than the median significant difference between the groups can be found. The histograms in Figure 45 show that there is a difference in the k2 values as well. Figure 46 indicates significant differences around the median value of k2.

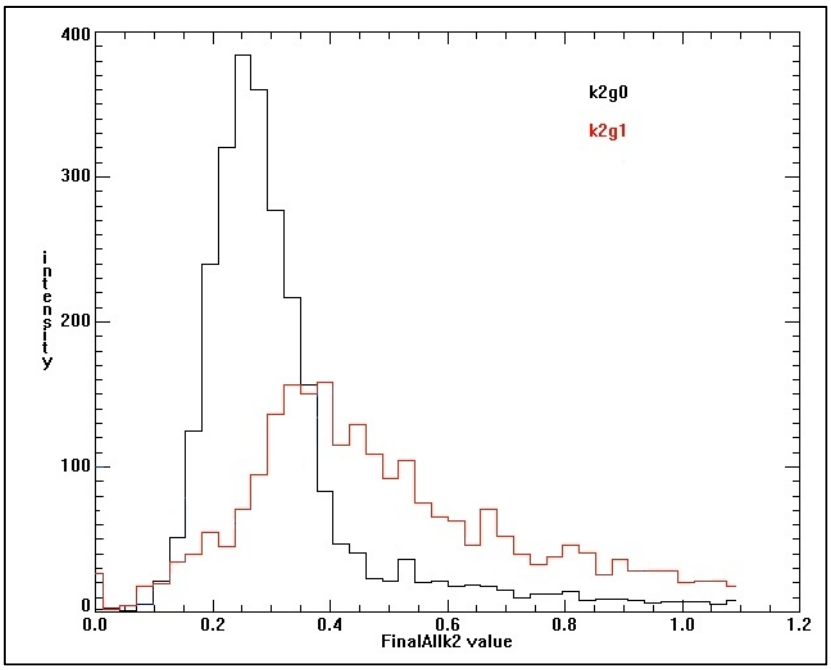

Figure 45: Histogram of k2 values for CWR22 xenografts. G0 is the control group and g1 is the one that got a dose of 7.5Gy.

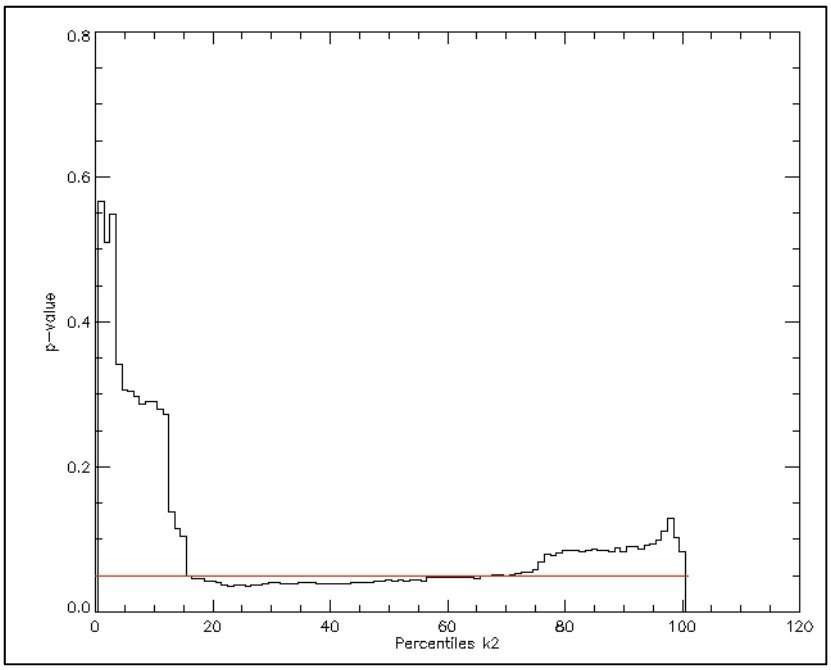

Figure 46: p-values for the percentiles of the k2 for CWR22 tumors. The solid line corresponds to a p-value of 0.05.

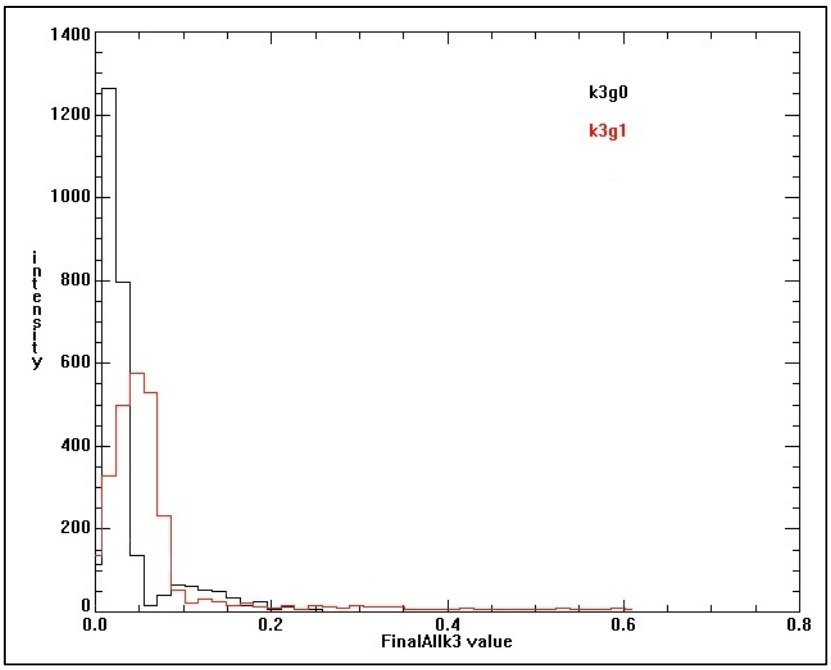

Figure 47: Histogram of k3 values for CWR22 xenografts. G0 is the control group and g1 is the one that got a dose of 7.5Gy.

The histograms for k3 are not as distinctive as before, and the p-values reveal that there is no way to distinguish the groups by looking at the k3 percentiles.

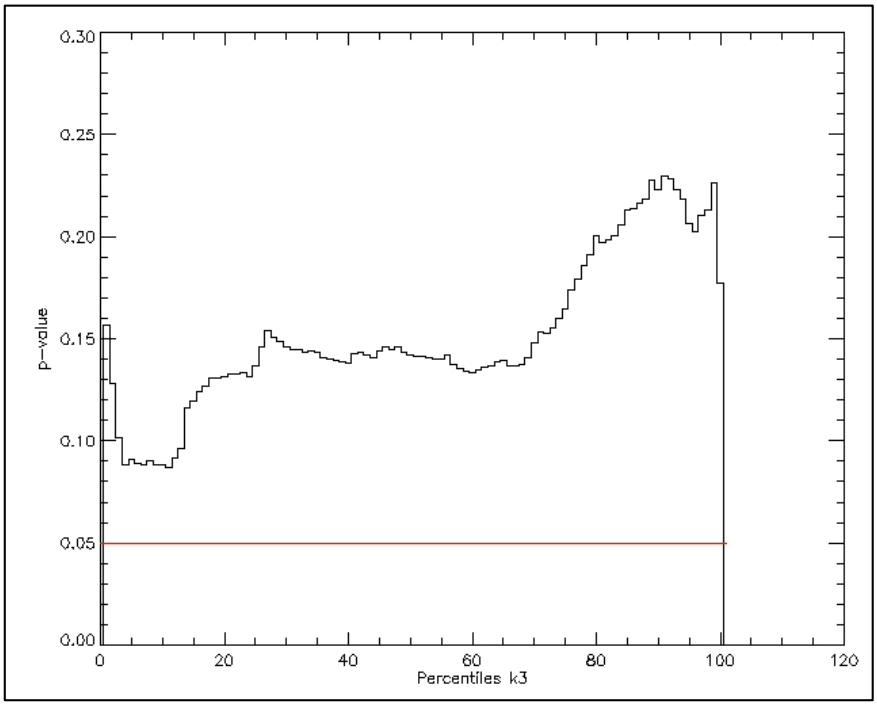

Figure 48: p-values for the percentiles of the k3 for CWR22 tumors. The solid line corresponds to a p-value of 0.05.

4.3.4 Histograms and percentile charts of MAS tumors.

Histograms of MAS 98.12 and MAS 98.06 tumors were also compared using T-tests. For k1, Gaussian-looking histograms appear (Figure 49).. No statistical significance was found for the median values of k1, but according to the chart in Figure 50 it seems that there is significance for lover percentile values.

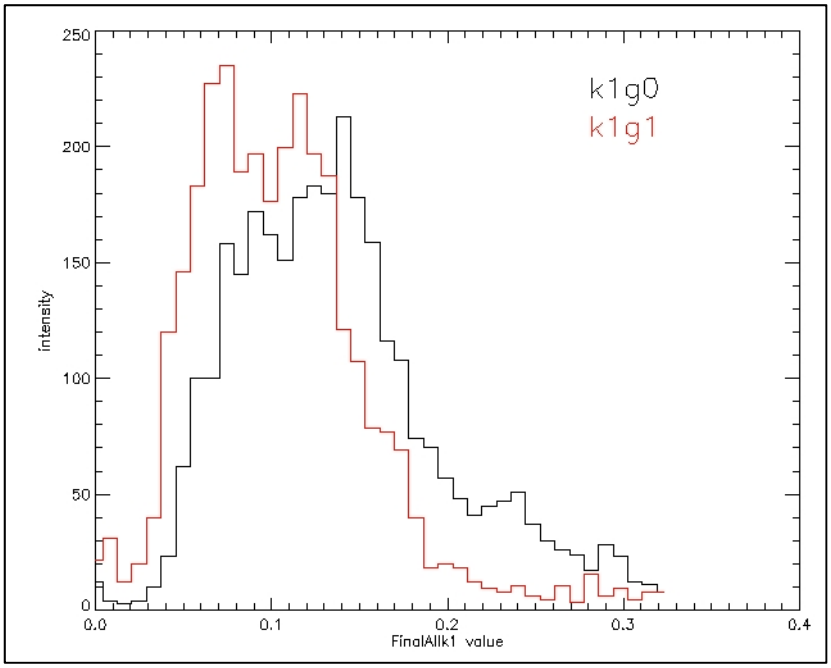

Figure 49: Histogram of k1 values for the other xenografts. G0 is MAS 98.12 group and g1 is the MAS 98.06 group.

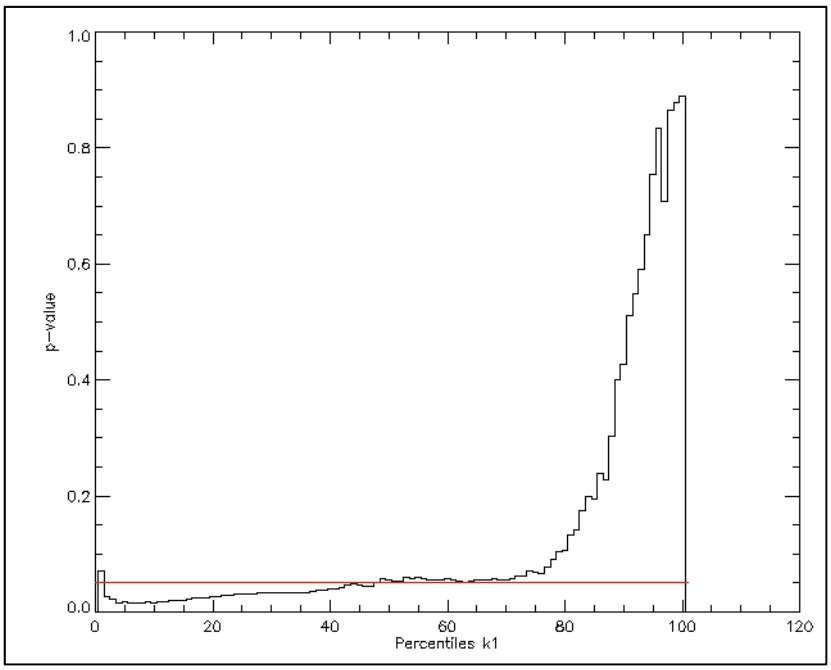

Figure 50: p-values for the percentiles of the k1 for MAS 98.12 and MAS 98.06 tumors. The solid line corresponds to a p-value of 0.05.

For k2, the distributions in Figure 51 are highly overlapping. Figure 52 show that no significant differences were found.

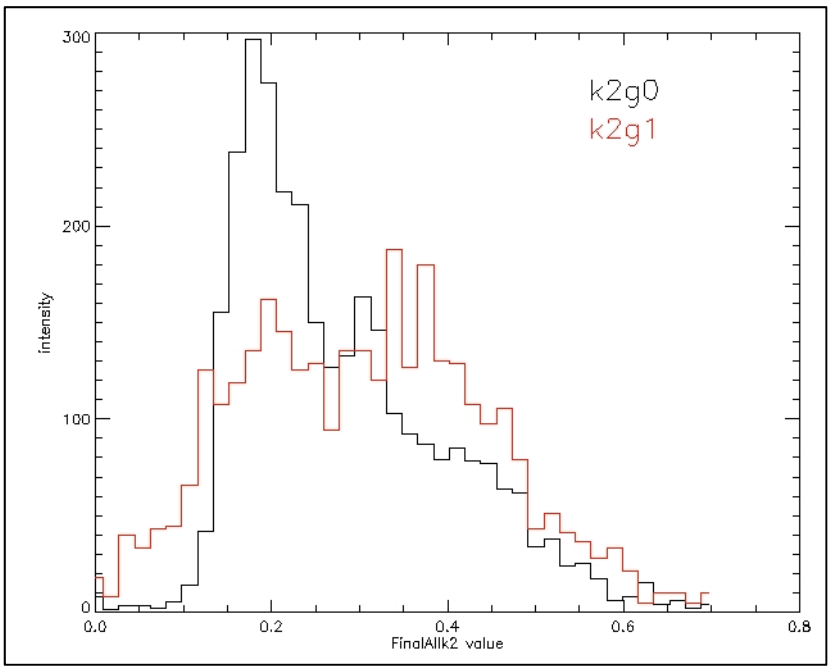

Figure 51: Histogram of k2 values for the other xenografts. G0 is MAS 98.12 group and g1 is the MAS 98.06 group.

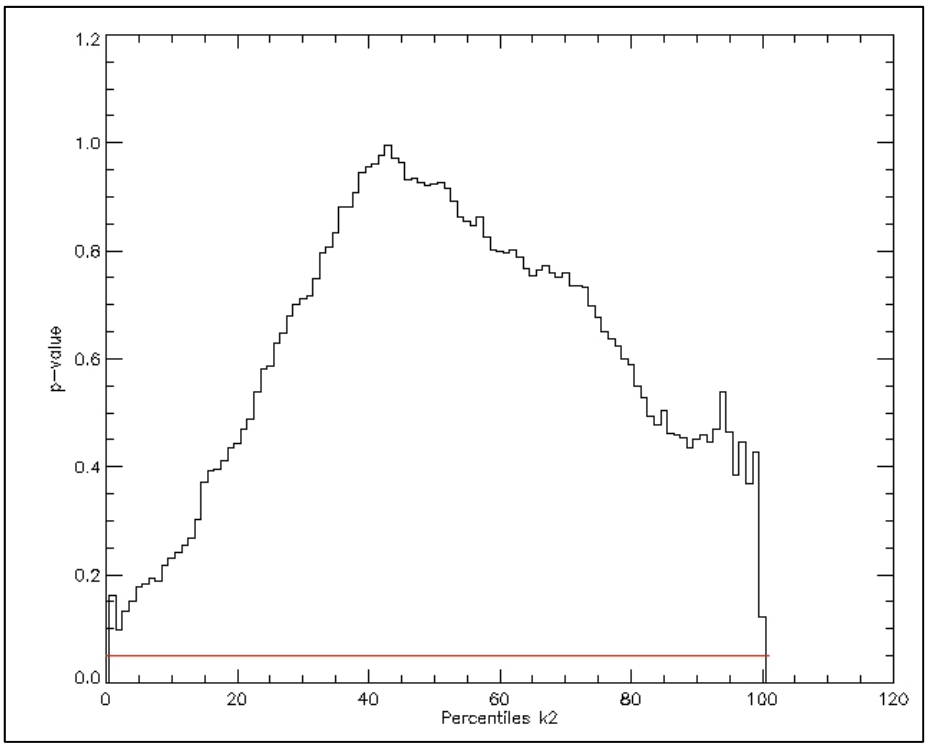

Figure 52: p-values for the percentiles of the k2 for MAS 98.12 and MAS 98.06 tumors. The solid line corresponds to a p-value of 0.05.

For k3, Figure 54 seems display the clearest distinction between the groups so far. The p-value chart shows highly significant p-values (Figure 53).

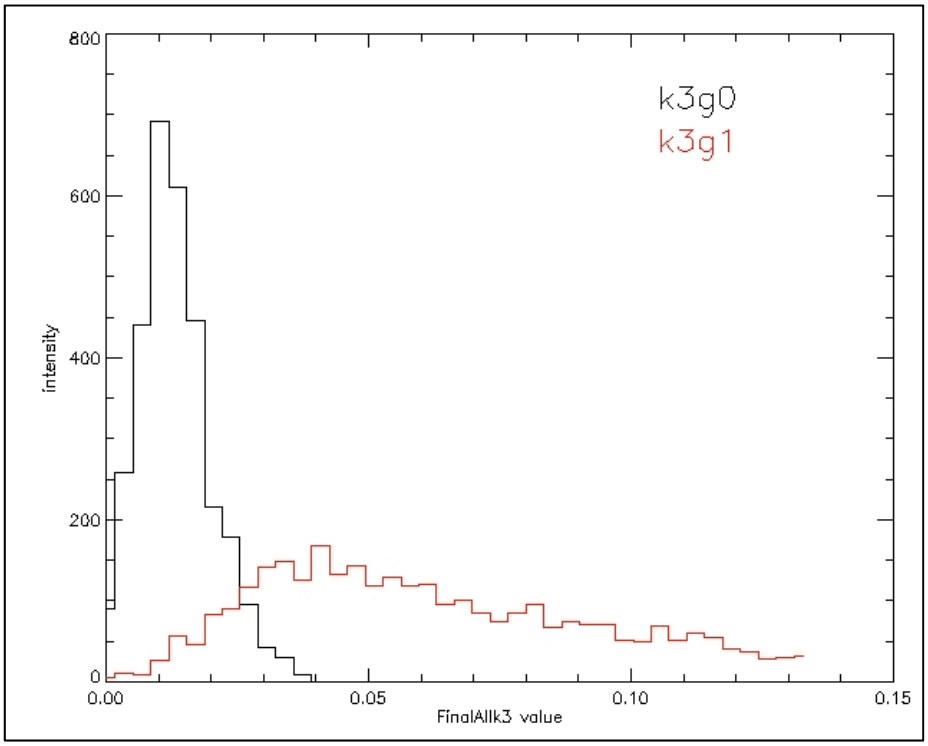

Figure 54: Histogram of k3 values for the other xenografts. G0 is MAS 98.12group and g1 is the MAS 98.06 group.

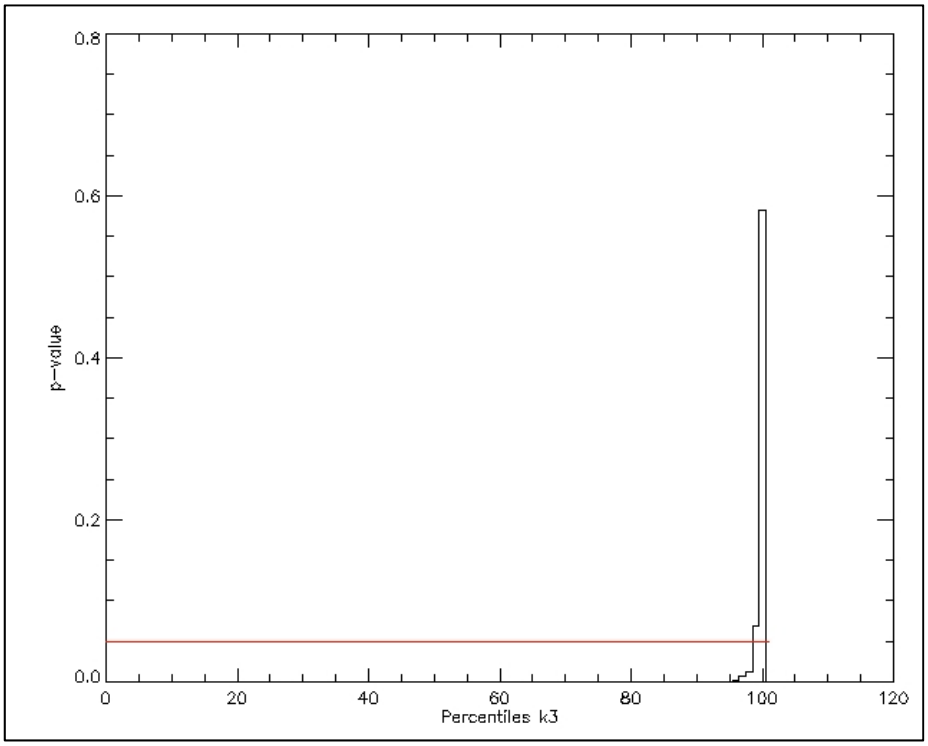

Figure 55: p-values for the percentiles of the k3 for MAS 98.12 and MAS 98.06 tumors. The solid line corresponds to a p-value of 0.05.

4.4 The Patlak plot and calculation of MRglc

Using Patlak analysis, the slope of the line shown in Figure 56 is linearly related to the observed value for metabolic rate of glucose. By doing this for each tumor, there is a new way of finding differences between the groups.

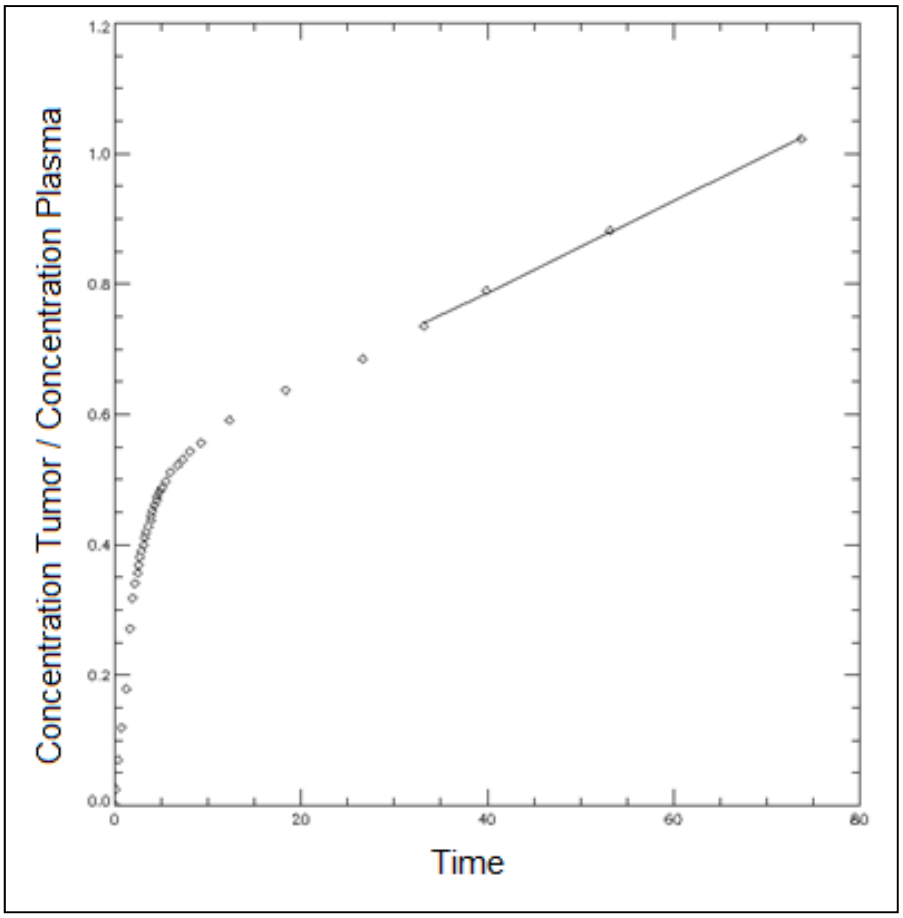

Figure 56: A typical Patlak plot. The slope of the regressed line shown is proportional to the MRglc of the tumor.

4.4.1 Patlak and MRglc for CWR22 tumors.

In Figure 57 the results of both methods for calculating the MRglc (via pharmacokinetic and Patlak analysis, respectively) is shown. For the first data set this evaluation yield a p-value << 0.01 for both the Patlak and pharmacokinetic analysis, respectively. However, it can be seen from the plots in Figure 57 that the MRglc estimate for the treated group by using k-parameters show a wider spread.

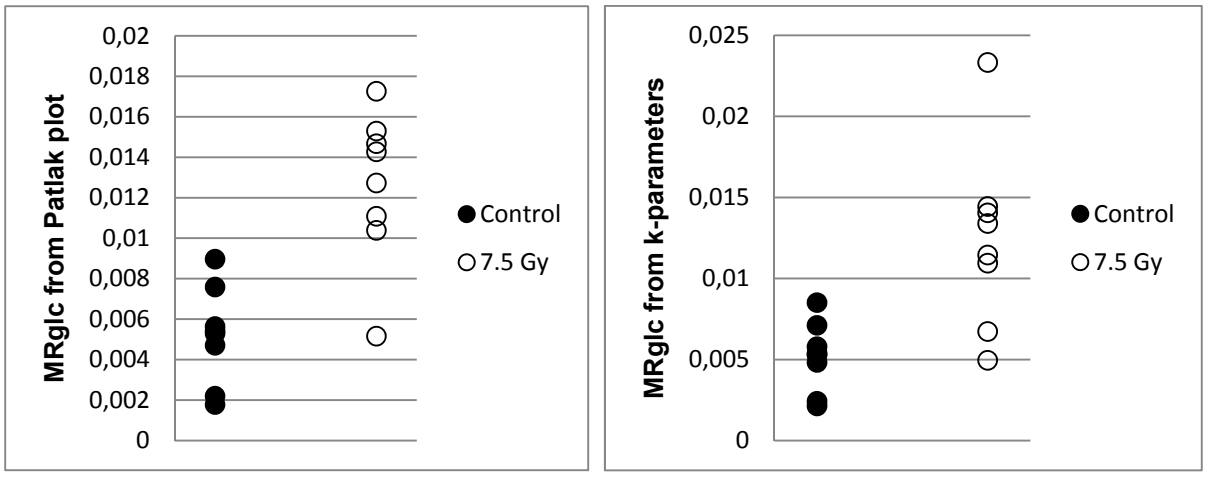

Figure 57: MRglc estimate on the CWR22 data, from Patlak plot on the left and from k-parameters on the right.

4.4.2 Patlak and MRglc for MAS 98.12 and MAS 98.06

For the MAS 98.12 and MAS 98.06 data, the two methods of analysis both gives highly signicant results (Figure 58).

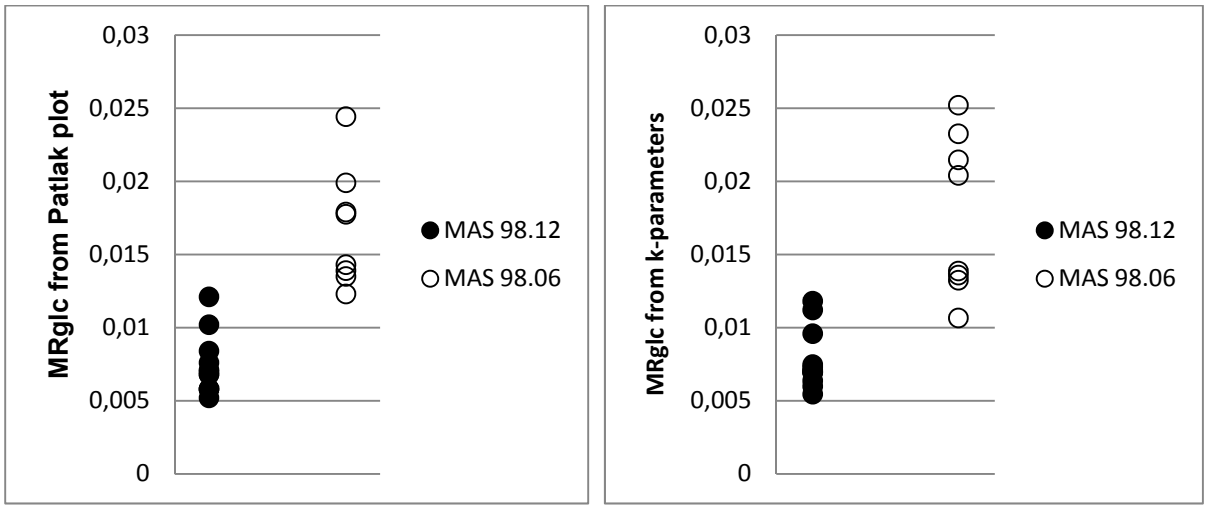

Figure 59: MRglc estimate on the MAS 98.12 and MAS 98.06 data, from Patlak plot on the left and from k-parameters on the right.

4.5 Other investigations

In the end of this chapter other and maybe more unusual surveys have been conducted.

4.5.1 Blood fraction of the tumors

It was previously investigated if adding the blood fraction parameter would improve the model. This later led to testing if the blood fraction would be different between groups of tumors (see Figure 60). There doesn't seem to be huge differences between the groups unless one counts the larger spread of the irradiated tumors. The Student's t-test did not show statistic significance between the groups.

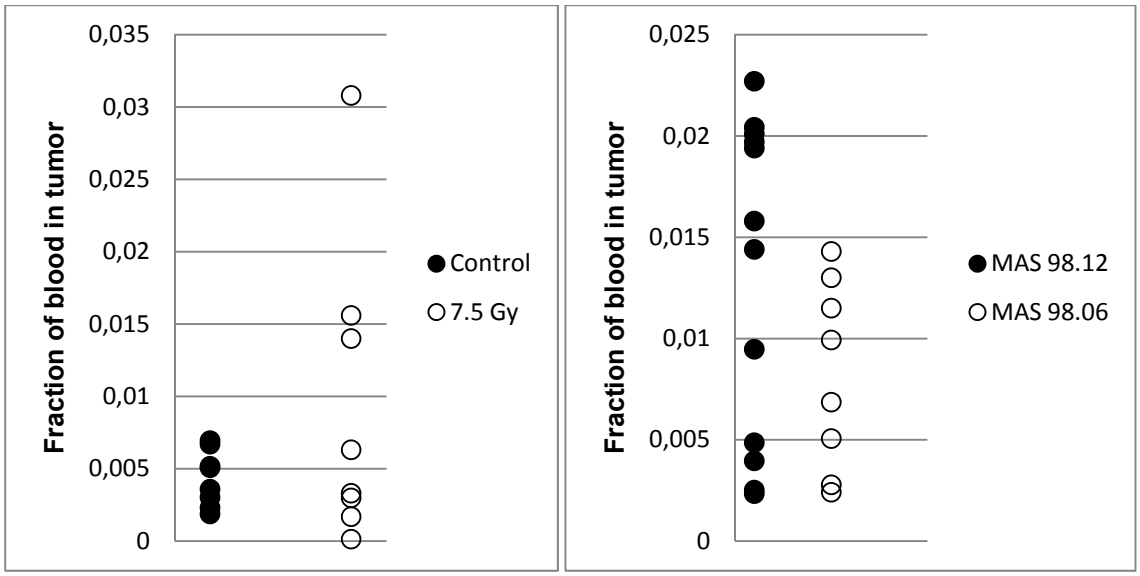

Figure 60: The median blood fraction for the different tumors.

4.5.2 Time dependant k-parameter histograms

To investigate the way FDG distribution in the tumor varies over time, several histograms have been created. See Figure 61 and Figure 62.

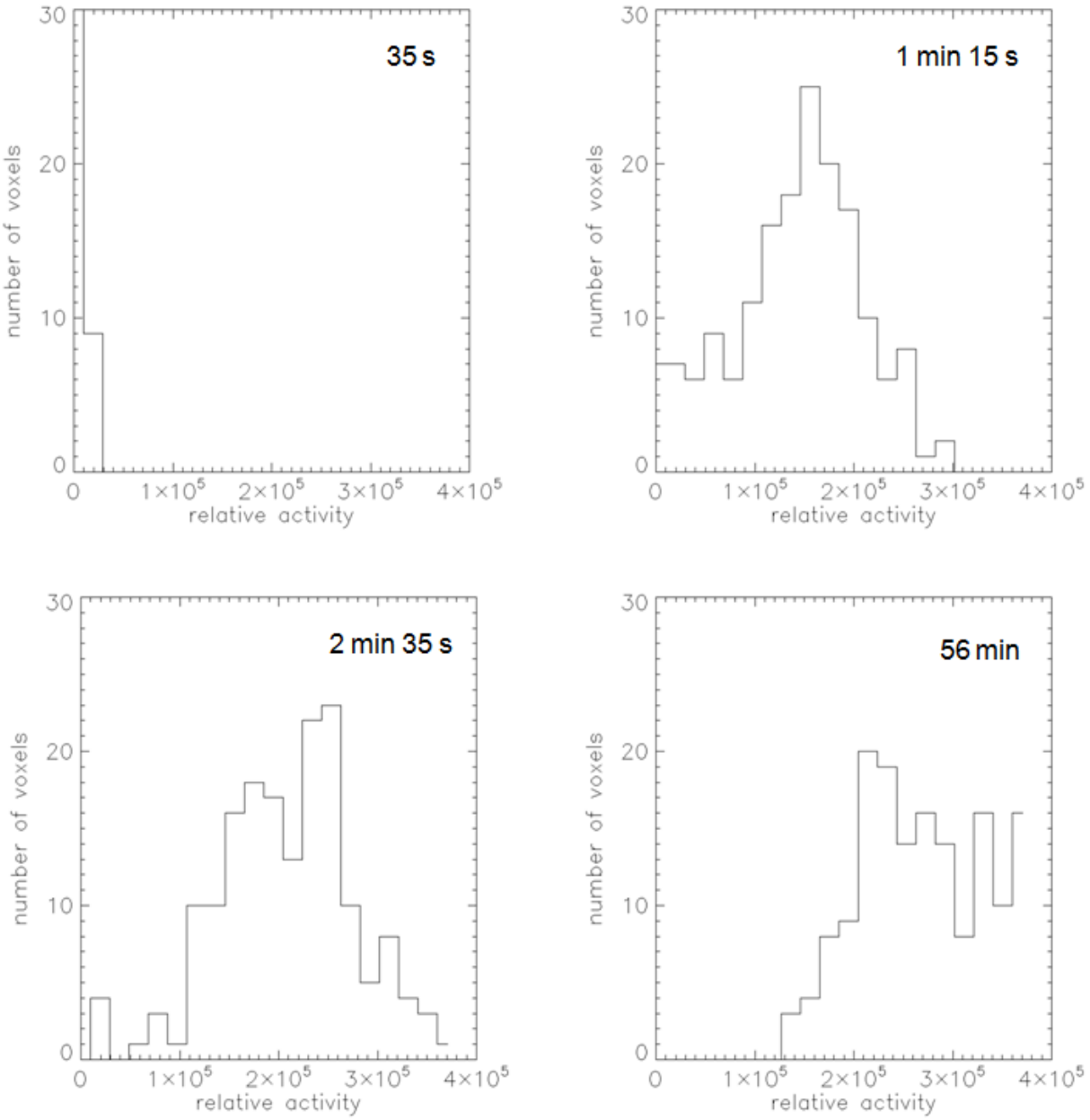

Figure 61: Histograms of voxel activity as a function of time for one tumor. Not that the y-axis is limited to 30.

These histograms is just for some of the time points, a full 2D histogram of all time points is shown as well in Figure 62.

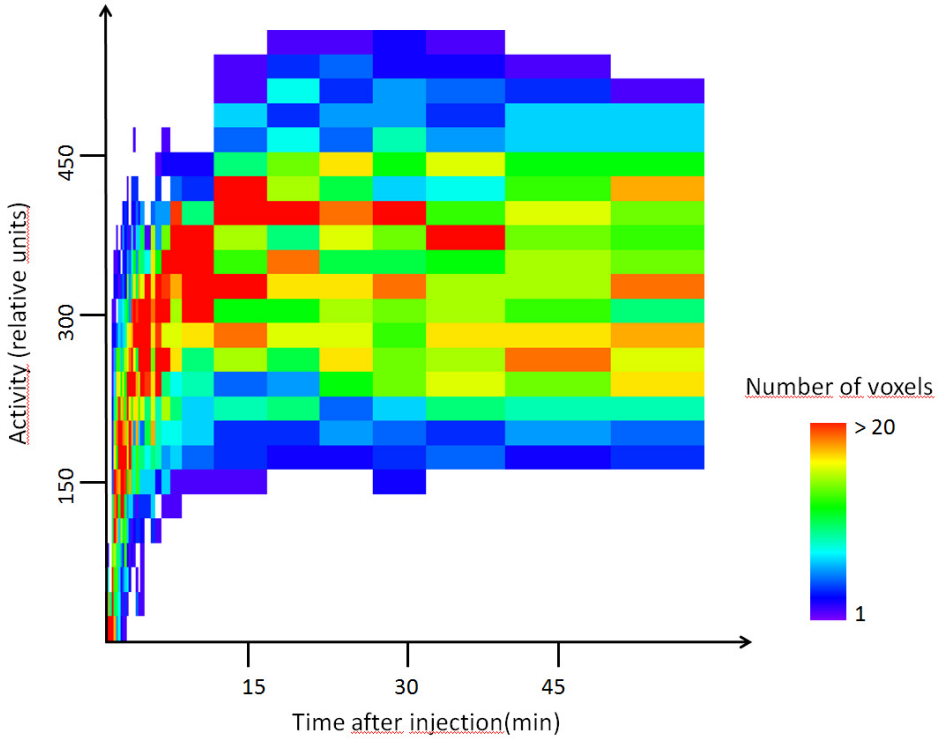

Figure 62: 2D histogram of voxel activity as a function of time for one tumor. The color scale represents height of the bins, red is high.

4.5.3 Dependence on distance from centre of tumor

In this part, the dependence on distance from centre of tumor for the various parameters was investigated . A linear relationship between the metabolic rate of glucose and distance from center of tumor is apparent, and Figure 63 shows this for one tumor. No large differences in the radial dependence could be found, although the data may indicate a higher metabolic rate in the center of tumor and that some tumors have a greater dependency of the distance from the center of the tumor than others.

correlation to distance from center of tumor							
k1g0	-0,0638	k2g0	0,258	k3g0	-0,219	MRg0	-0,585
k1g1	0,258	k2g1	0,309	k3g1	-0,229	MrRg1	-0,414
p-value	0,569	p-value	0,978	p-value	0,973	p-value	0,27

Table 4: k value and MR dependency on distance from center of tumor for CWR22. G0 is control group and g1 got a dose of 7.5 Gy.

correlation to distance from center of tumor							
k1g0	-0,0732	k2g0	0,0577	k3g0	-0,273	MRg0	-0,678
k1g1	0,086	k2g1	0,226	k3g1	-0,405	MRg1	-0,756
p-value	0,167	p-value	0,501	p-value	0,456	p-value	0,578

Table 5: k value and MR dependency on distance from center of tumor for breast cancer. G0 is MAS 98.12 and g1 is MAS 98.06.

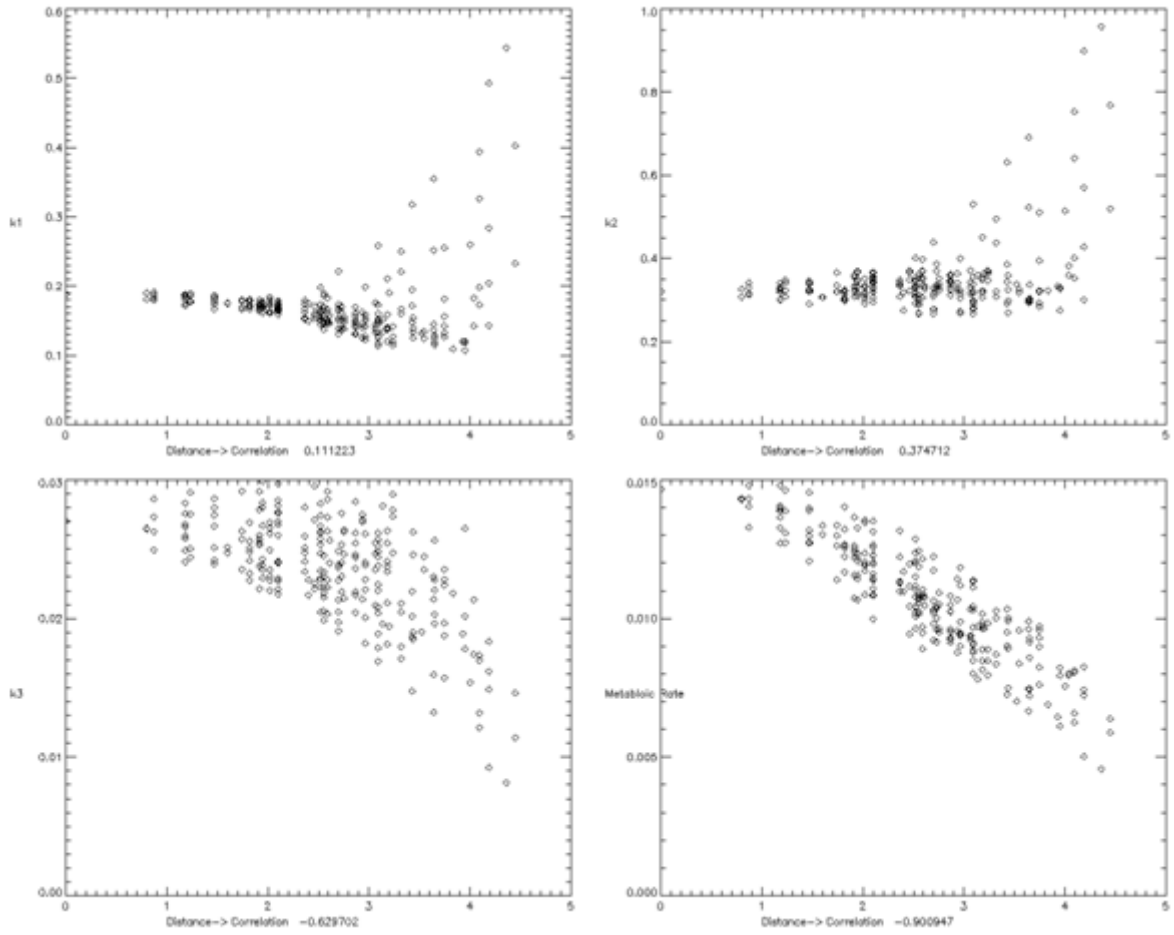

Figure 63: Top left; k1 versus distance from center of tumor, correlation 0,11. Top right; k2 versus distance, correlation 0,37. Bottom left k3 versus distance, correlation -0,63. Bottom right; Metabolic rate of glucose versus distance, correlation -0.901.

5 Discussion

5.1 General issues of diagnostic imaging

In the field of imaging there are several restrictions and sources of error. Let's start with the ultimate challenge; to choose between noise, resolution, dose and acquisition time. In most imaging modalities, especially for CT, you usually can't change one variable for the better unless another variable is changed for the worse. For example better resolution indicates smaller voxels, which will reduce the signal to noise ratio (SNR). To keep the SNR constant the tube current can then be increased. However, there are no side effects from building a better detector, and the problem is not impossible.

These issues exist for PET as well, but there are some differences that make the choices easier. For a dynamic PET scan it is more or less the biology of the system that is investigated that decides the acquisition time needed. The time resolution can be variable across the time series. A good time resolution is chosen where the activity measured is assumed to change rapidly. For this study the highest time resolution used was 10 seconds. As already mentioned, better resolution (in any of the four dimensions) will reduce the SNR.

The SNR is a coefficient that tells us how much of the displayed changes are due to noise and how much is due to actual differences in the underlying biology. If we are looking at very small changes in tissue a high SNR is needed. By increasing the voxel size a better SNR can be obtained. But the problem with large voxels is the partial volume effect; the same voxel can contain various types of tissue and only the mean across the voxel will be shown.

For this specific study we try to investigate the heterogeneity of the tumor and would therefore like to reduce the voxel size as much as possible. In PET the voxel size is restricted by the machinery itself and in general new machines improve the resolution. The small PET scanner used in this study for example got much better resolution than a normal scanner used in the clinics. An other problem with PET is that only in the center of the scanner is the data correctly recorded, I think they get skewed or something away from the center. (I will check up on this / explain properly later).

5.2 Specific issues for this study

5.2.1 Tumor delineation

The tumor delineation has been done by an untrained hand and not properly looked over by a radiologist. The delineation was done as similar as possible on all tumors. The goal was to trace the edges of the tumors but has most likely resulted in both clipping away pieces of the tumor and including some outlying tissue.

5.2.2 The arterial input function

The model used for pharmacokinetics and the time activity curve both depend on the arterial input function. The arterial input function is a measure of the FDG availability in blood plasma close to the cells. The general assumption is that each voxel lie next to a blood vessel and interchange FDG with this blood vessel only.

In this study small mammals (mice) are the subject of the PET assay and their arteries is too small to identify in PET images. The artery function could technically have been found by measuring blood samples from the mice. But taking blood samples from three mice every 10 seconds is not possible, and a total of 37 samples (same number of time points used in one assay) would probably drain the mouse dry. Therefore a procedure for determining the “arterial” input function by looking at the heart was derived. The resulting function was found viable for use as an arterial input function. We had to assume that the measured activity of the heart would mainly resemble the activity in the outlying blood vessels. A new model with an added time delay of the input function (assuming a transition time from heart to outlying blood vessels) showed no improvement of the model. This parameter was therefore removed from the final model used.

There is another problem with measuring FDG activity in the blood as compared to other tracers. As FDG resembles and can be used by cells as normal glucose, the blood cells themselves can absorb some of the FDG. The activity measured in the heart will therefore include FDG trapped inside blood cells. Therefore not all the FDG assumed to be present are actually available for the tumor cells. (5). A way to measure the ratio between FDG inside blood cells and free in plasma has not been found. But as this is a problem that is similar for all mice involved the effect should be minimal.

The final problem as so far found about the heart function is that the initial spike when the bolus pass the heart is quicker than we can correctly measure. As a result the peak is somewhat smeared out. Again, this affects all mice in a similar fashion.

5.2.3 The CWR22 dataset

There were some problems concerning this dataset. The tumor delineation was not always easy. Worse, for two of the mice (11 and 15 in same image) finding an arterial input function was very difficult and a compromise had to be made. The data was recorded partly in december 2009 and partly in January 2010. This may have caused some variation in the reconstruction and scaling used. But as som mice from each group was imaged each time, this should not cause an effect that separate the groups.

5.2.4 The MAS 98.12 and MAS 98.06 dataset

As opposed to the other dataset, the delineation of tumors and extraction of the arterial input function was not a problem. Nevertheless, there were other problems.

The first problem is that three different time resolutions were used. To solve this problem some steps had to be taken. In the part of the IDL program where the TACs were compared the time array for the first image that went through the routine was saved. All other time arrays and TAC data were then changed to fit the first time array by interpolation.

The second problem with this dataset is that in most of the images we now had three mice at a time inside the scanner. This led to a larger time difference in between the mice as to when the FDG was administrated. To work around this problem, the time at which the heart function reached its peak was recorded for each tumor. All the TAC data recorded before this point was rejected and the time array was updated to fit this change. Then the data was subject to the same steps taken above in order to fit it into the time array used by other mice. This had to be done in order to produce correct pharmacokinetic parameters as well.

Finally one mouse received a bad injection of FDG and the data acquired had to be discarded for this study.

The steps taken should hopefully be enough to eliminate most of the effects these unwanted differences could cause.

5.3 Investigations of the CWR22 data

For this test we were trying to determine signs of early tumor response using FDG PET. Several different tactics were employed to deal with this problem. The first thing looked at was the uptake function itself, the normalized time activity curve (TAC).

5.3.1 The time activity curve

From the graph presented (see Figure 37 on page 44) a stronger and stronger difference between the curves as time goes on was observed. The graph indicates that the irradiated tumors accumulate more FDG. At first this increased activity in treated tumors seems contra intuitive as we are expecting the tumor cells to die. Many different effect can cause variations of FDG uptake, among them is blood flow, oxygen availability and GLUT transporters. However there might be an other explanation; a common phenomenon referred to as “metabolic flare”. This is described as an increased metabolic rate or increased standard uptake value (SUV) of FDG following various treatments like radiotherapy, hormonal therapy and somewhat in chemotherapy. An article written by Basu Sandip and Nair Naendra has this to say about the matter; “The increase in FDG uptake accompanying radiotherapy during the initial 2–3 weeks following therapy is prominent in epithelial surfaces and is related to inflammatory infiltrate of neutrophils, lymphocytes, and macrophages.” “In general, at least an interval of 4 weeks (preferably 6–8 weeks) following radiotherapy is suggested to circumvent the misinterpretation. The minimum interval for re-evaluation after starting therapy, according to RECIST, is 4 weeks, where again, FDG PET can be comfortably applied.” (30) It appears like the suggestion is that we should have waited quite a lot longer before doing a PET assay on the mice. But we are actually trying to use FDG-PET to find early response qualities. Others have also done these kinds of studies. The following article is not about RT but for hormonal therapy. In the article by F Dehdashti et. al. they have investigated whether this “metabolic flare” is a sign of a hormonally responsive breast cancer. “There were seven responders and four nonresponders based on clinical follow-up. None of the responders had a clinical flare reaction, but all demonstrated metabolic flare, with a mean +/- standard deviation increase in tumor standardized uptake value (SUV) for FDG of 1.4+/-0. 7. No evidence for flare was noted in the nonresponders (change in SUV for FDG -0.1+/-0.4; P = 0.008 vs. responders).”” The findings of a metabolic flare by FDG-PET and the degree of ER blockade by FES-PET early after institution of tamoxifen treatment appear to predict responsiveness to antiestrogen therapy in patients with ER+ metastatic breast cancer” (31). Considering the findings in that study it still seems viable to do PET studies shortly after radiotherapy. Okay, back to the results.

The p-value chart given off the TAC gives a slightly different picture than the TAC itself. It suggests a significant difference at the very beginning of the uptake. But after some consideration this result has been neglected. It would be dependant on how fast the FDG was administrated and the time resolution might not be good enough to capture the true curve. After 20minuntes there is already a statistical significance (p-value slightly below 0.05) but if we wait 10 more minutes it is reduced to about 0.01. So for this very specific assay,

monitoring the mouse for maybe 5 minutes, 30 minutes after administration of FDG, will be enough to determine the response.

There was a group of mice that got 15 Gy but that was only 4 tumors in a total of 3 mice, and the data are very variable. They go all across the chart and may suggest a change from the control values in either direction. Therefore these results have not been further discussed.

One of the tumors (11v) receiving a dose of 7.5 Gy had TAC end values similar to the control group. There is several ways to interpret this. First, something might have gone wrong. For example that the tumor somehow was outside the field or the tumor delineation was faulty. The second and more optimistic explanation is that we might have singled out a radio resistant tumor. It could also just be a case of statistic fluctuations of the data. For the moment the answer to this question goes unanswered.

5.3.2 Pharmacokinetic model

By looking at the pharmacokinetic modeling more information about the tumors might be obtained. On a first glance increased values for all the estimated k-parameters can be seen for treated tumors. By looking at the whole tumor, statistic significance is reached for the k2 parameter only. Next thing on the schedule is the k histograms. We can here easily see that the distribution of treated tumor voxels differ from that of untreated tumors. A recently applied test also gives the impression that the heterogeneity of the tumor itself might increase for treated tumors, although statistical significance was not reached. The closest was p-value of 0.1 for k2. The table for this test will be added in the results or appendix. Another way to look at the k-parameters of the tumors is the percentile chart. Here we can find in what part of the tumor histogram that the differences between the groups is greatest. Again the data suggest stronger values for treated tumors and there is an area of the histograms for both k1 and k2 that has statistical significance. There is still no statistic significance to be found for the k3 parameter though. Still, the method of looking at each percentile of the tumor seems more robust than taking an average over the entire tumor. On a final note, the tumor mentioned above (11v) is shown as a treated tumor by looking at the k1 and k2 parameters, as it should be. However, now another treated tumor (5v2) got k1 and k2 values similar to the control group.

5.3.3 Looking at the metabolic rate of glucose

We can also look at the metabolic rate of the tumors using two different techniques. From using the Patlak plots an increased metabolic activity in the treated tumors with very good p

value is shown. The k-parameters found can also be combined to produce the same variable found in the Patlak plots. Even though these two methods should return the same variable, differences occur. These differences have been calculated to about 0-25%. It should then be mentioned that the Patlak plots give better results than the combined k-parameters. Again all the signs tell of more metabolic active tumors after treatment. Interestingly enough, the 5v2 tumor look like a control tumor if we only look at the individual k parameters, but if we combine the parameters to obtain metabolic rate of glucose it shines through as a treated tumor. The 11v tumor however got a MRglc similar to the control group. It should be mentioned that the k3 parameter tips the scales in this calculation.

5.3.4 TAC versus pharmacokinetics

Now that the results from TACs and pharmacokinetics has been discusses, it is time to choose which method to use. The p-values obtained from the TAC are better than the p-values from the pharmacokinetic modeling. The internal group variations are also larger for the various k parameters than that of the TAC values, if we consider the last time points of the TAC. From these observations, the TAC or even a single measurement of tumor activity gives stronger results than the pharmacokinetic modeling.

The tumors in the control group are defined as controls in all the different tests done on them. In other words, none of the untreated tumors show signs of treatment response. Most of the treated tumors show response, but not all. The different tests might place the same tumor in different categories. Because of this, a full analysis including all the tests mentioned above might be useful to determine the true response of the tumor.

5.4 Investigations of the MAS 98 xx data

5.4.1 The time activity curve

As can be seen from the TACs themselves and the following p-value chart, there is differences between the groups here. Here complete different shapes of the TAC curves can be seen as well. The curve from the MAS 98.12 data shows rapid uptake and then fading while the MAS 98.06 got slower uptake and doesn't reach maximum intensity during the assay. This means that we can for example again use a one frame shot at about 40 minutes after administration of FDG (for mice) to see the difference between the groups. However there might be trouble getting an exact quantification of what the TAC at this point should be for a given group. Then one can turn to the entire series and see the actual shape of the

curve. By doing so it will be possible to discern a MAS 98.12 tumor from a MAS 98.06 by investigating the shape of the curve even if it is not proper normalized. For this reason, a full dynamic PET scan will be useful. A dynamic PET scan will also make it possible to obtain more useful data, like the k parameters from pharmacokinetic modeling.

5.4.2 Pharmacokinetic modeling

From the results it is apparent that the MAS 98.12 line got higher values of k1 than that of MAS 98.06 and that there is significant difference between the groups. For the k2 parameter however, the data are much too similar. The k3 parameter got the best statistical significance, where the values for MAS 98.06 are greater than that of MAS 98.12. For this dataset the k-parameters also seem to be a good measure on what group the selected tumor belongs in. Again it can be useful to have a look at the distribution of the k-parameters. In the first histogram it seems that the k1 values for both groups follow a similar skewed Gaussian distribution with the one for MAS 98.12 is shifted to higher values. The p-value chart for each percentile in the tumors show good statistical difference for most of the tumor, proving that k1 is a good parameter to distinguish these groups. As expected the k2 histogram and p-value chart does not show a big difference between the groups. The shape of the histograms is different, but that might just be because of the way they are created. Again we see good differences when looking at the k3 values. The p-value across percentiles is exceptionally good, and the histograms shows two completely different distributions. This shows that the k parameters both by looking at the entire tumor and by looking at the percentiles may very well be used to characterize tumors along with the TAC.

5.4.3 Metabolic rate of glucose

The calculated MRglc using both Patlak plots and combination of the k parameters yield a good p-value and the result that the MAS 98.06 line is more metabolic active than the MAS 98.12. The developers of these lines found similar results (23). Again the more simple method applied in the Patlak plot trumps the more difficult pharmacokinetic model.

5.4.4 TAC versus pharmacokinetics

For this dataset both the TACs and the k-parameters could alone distinguish the different tumors. That is not so surprising, as this dataset was a lot more homogenous than the previous. It does seem however that it would be enough with one or more measurements of the tumor activity to correctly classify the tumor. Then again, this is for the when assuming

that we already know that it is either MAS 98.12 or MAS 98.06 that we are looking at. If in the future there will be more tumor types and characteristics to choose between, a full exploration of the pharmacokinetic variables might prove useful as well.

5.5 Radial dependency

In this study it has been investigated if there is a relationship between the parameter values and the distance from the centre of the tumor. For the various k parameters there have been no clear signs of such a relationship. The charts in Figure 63 for k1 and k2 increase at the end of the tumors. This is most likely because these voxels have better blood availability and therefore higher rate constants for FDG exchange with blood plasma. For the metabolic rate of glucose however, there is a slight indication that the MRglc is higher in the middle of the tumor. This is quite contra-intuitive if we look at two aspects of tumor biology. The blood network inside a tumor is usually not structured as it is in normal tissue (2). Tumor cells far from blood vessels should therefore receive less oxygen, and many large tumors have necrotic areas in the middle. From the data collected however it doesn't seem to be much signs of necrosis in the midst of the tumor. So all right, there is activity and live tumor cells in the middle of the tumor. Still they should receive less blood, therefore less oxygen and therefore have less to work with in order to metabolize glucose.

The other thing most cells need to grow is growth factors. The xenografts in the first data set are androgen dependant, and should therefore behave in a way that shows the tumor cells close to blood vessels grow and metabolize faster than the rest. It is therefore established that a tumor normally grows from the rims and out. There is no sign of this in any of the data collected. There can however be some imaging reasons for this. First we must consider the partial volume effect. If this outer layer of fast growing tumor cells are thinner than the width of the voxels (0,87mm) there is a good chance that some of the voxel will contain cells that are outside the tumor, and thus lower the activity level of the entire voxel. The other reason that might cause higher activity in the center of tumors is the reconstruction algorithms. In particular the filters that have to be used to subdue "false data". These filters might be prone to favor centers of activity more than the edges. A good filter should be able to correctly display a homogenous cylinder, but this might not always be the case. In the article by (32) they have done some investigations on this subject using phantoms. They were mainly interested in small tumors and resulting partial volume effect, but from the picture presented in the article even the 12mm "tumor" showed higher activity in the middle of the tumor. Their results also showed that the signal obtained is dependant on the smoothing filters used. Both these effects can explain why the tumor looks more active in the

center than at the edges. As we have not been able to confirm the data with histology one can only speculate in what is the true answer. If these mechanisms have a significant effect in perturbing the data, one must make sure works that shall be compared use the same algorithms.

As we can still see significant difference between groups in the dataset presented, we might assume that doing the same error for all data is more or less ok when comparing the data in a qualitative study. Either way, there were little differences to be found in between the groups in this aspect. Both groups have more or less the same radial dependence for MRglc. It can be noted that the relationship is stronger for the MAS 98 xx tumors than the CWR22 tumors.

5.6 Conclusions

After completing various tests it seems like the simple TACs and the Patlak plots are the best parameters in order to characterize tumors and response.

When looking at the k-parameters of the CWR22 tumors, the median values are not always the best to distinguish the groups. It should therefore be considered investigating all the percentiles. It follows that choosing a random subset of voxels (or cells like in biopsy) might not be sufficient in order to characterize the tumor.

5.7 Further work

As mentioned for the CWR22 data, some tests show treatment response in some tumors and not in other tumors. It would have been interesting to investigate the response of these select tumors in other ways, say by histology or measure size over a long period of time. This should be done in order to know what actually happened to these tumors, are they responders or not.

Monitoring the same tumor before treatment and after treatment as was originally intended for this project might also provide valuable results.

If the method for determining differences between tumors lines is desired for the clinic, a lot of work is ahead. Then characterization data of many more tumors must be recorded, and by doing so maybe more common traits of aggressive tumors can be found.

Index

FDG, 7
IDL, 2
MRglc, 31
Patlak plot, 31
ROI, 28
SNR, 53

Bibliography

1. **Statistisk sentralbyrå - Statistics Norway.** Dødsårsaker 2008. *ssb.no.* February 19, 2010. [Cited: November 14, 2010.] http://www.ssb.no/dodsarsak/.

2. **Eric J. Hall, Amato J. Giaccia.** *Radiobiology for the Radiologist, Sixth Edition.* Philadelphia : Lippincott Williams & Wilkins, 2006.

3. **Wikipedia.** [Cited: November 11, 2010.] http://en.wikipedia.org/wiki/Radiotherapy#History_of_radiation_therapy.

4. **Petsenteret.** [Cited: October 20, 2010.] http://www.petsenteret.no/2pet_fdg.shtm.

5. **Phelps, Michael E.** *PET Molecular Imaging and Its Biological Applications.* New York : Springer-Verlag New York, Inc, 2004.

6. **Attix, Frank H.** *Introduction to radiological physics and radiation dosimetry.* New York : John Wiley and Sons, Inc, 1986.

7. **Philip Mayles, Alan Nahum, Jean-Claude Rosenwald.** *Handbook of radiotherapy physics.* Boca Raton : Taylor & Francis Group, 2007.

8. *Initial and Subsequent Approach for the Synthesis of 18FDG.* **Joanna S. Fowler, Tatsuo Ido.** 2002, Seminars in nuclear medicine, Volume 32, pp. 6-12.

9. **Wikipedia.** [Cited: October 20, 2010.] http://en.wikipedia.org/wiki/Fludeoxyglucose_(18F).

10. *A simulation study of a method to reduce positron annihilation spread distributions using a strong magnetic field in positron emission tomography* . **Iida H, Kanno I, Miura S, Murakami M, Takahashi K, Uemura K.** 1986, IEEE Transactions on Nuclear Science, Volume 33, pp. 597-600.

11. *A multicrystal two dimensional BGO block detector using circular photomultipliers.* **Casey ME, Nutt R.** 1995, IEEE Transactions on Nuclear Science, Volume 42 , pp. 1095-1101.

12. **Miles N. Wernick, John N. Aarsvold.** *Emission tomography: the fundamentals of PET and SPECT.* London : Elsevier Academic Press, 2004.

13. **Drug information Online .** [Cited: October 20, 2010.] http://www.drugs.com/mmx/fludeoxyglucose-f-18.html.

14. *Modeling and identification of metabolic systems.* **E. R. Carson, C. Cobelli and L. Finkelstein.** 1981, The American Journal of Physiology - Regulatory, Integrative and Comparative Physiology. 240 9, pp. 120-129.

15. *Basic studies on metabolic steady state. Linearity of a metabolic tracer system.* **K. H. Norwich, G. Hetenyi.** 1971, Radiation and Environmental Biophysics Volume 7 Number 3, pp. 169-180.

16. *Direct reconstruction of kinetic parameter images from dynamic PET data.* **M. Kamasak, C.A. Bouman, E.D. Morris, K. Sauer.** 2003. Conference Record of the Thirty-Seventh Asilomar Conference on Signals, Systems and Computers. . p. 1919:1923.

17. **Engh, Annelise Hem & Espen.** Laboratory Animal Science in a nutshell. s.l. : Norwegian School of Veterinary Science, 2001.

18. *Performance Measurement of the microPET Focus 120 Scanner.* **Jin Su Kim, Jae Sung Lee, Ki Chun Im, Su Jin Kim, Seog-Young Kim, Dong Soo Lee, Dae Hyuk Moon.** 2007, Journal of Nuclear Medicine, Volume 48 No. 9 , pp. 1527-1535.

19. *Resolution and noise properties of MAP reconstruction for fully 3-D PET.* **Qi J, Leahy RM.** 2000, IEE Transactions on Medical Imaging, Volume 19, pp. 493-506.

20. *High-resolution 3D Bayesian image reconstruction using the microPET smal-animal scanner.* . **Qi J, Leahy RM. Cherry SR, Chatziioannou A, Farquhar TH.** 1998, Physics in Medicine and Biology, Volume 43, pp. 1001-13.

21. *Xenografts of primary human prostatic carcinoma.* **Pretlow TG, Wolman SR, Micale MA, Pelley RJ, Kursh ED, Resnick MI, Bodner DR, Jacobberger JW, Delmoro CM, Giaconia JM, et al.** 1993, Journal of the National Cancer Institute, pp. 394-8.

22. *CWR22: Androgen-dependent Xenograft Model Derived from a Primary Human Prostatic Carcinoma.* **Mark A. Wainstein, Feng He, Daniel Robinson, Hsing-Jien Kung, Stuart Schwartz, Joseph M. Giaconia, Nancy L. Edgehouse, Theresa P. Pretlow, Donald R. Bodner, Elroy D. Kursh, Martin I. Resnick, Allen Seftel, Thomas G. Pretlow.** 1994, Cancer Research, Volume 54, pp. 6049-6052.

23. *Molecular profiling and characterization of luminal-like and basal-like in vivo breast cancer xenograft models.* **Anna Bergamaschi, Geir Olav Hjortland, Tiziana Triulzi, Therese Sørlie, Hilde Johnsen, Anne Hansen Ree, Hege Gierckskу Russnes, Sigurd Tronnes, Gunhild M. Mælandsmo, Oystein Fodstad, Anne-Lise Borresen-Dale, Olav Engebraaten.** 2009, Molecular Oncology, Volume 3, pp. 469-482.

24. **Markwardt, C.B.** Non-linear least squares fitting in IDL with MPFIT. . *Astronomical Data Analysis Software and Systems XVII.* Quebec : s.n., 2008.

25. **Sollien, Thea.** *Stokastikse indikatorer ved dynamisk kontrastforsterket CT av pasienter med malignt lymfom.* Oslo : Universitetet i Oslo, 2010.

26. *Noninvasive determination of local cerebral metabolic rate of glucose in man.* **Huang SC, Phelps ME, Hoffman EJ, Sideris K, Selin CJ, Kuhl DE.** 1980, American Journal of Physiology - Endocrinology and Metabolism, pp. 238:E69-82.

27. *Metabolic brain imaging. Direct regional measurement of transfer coefficients and lumped constant.* **Gjedde A, Kuwabara H, Evans AC.** 1990, Acta radiologica. Supplementum, Volume 374, pp. 117-121.

28. **Erik Bølviken, Eva Skovlund.** *Lectures in Applied Statistics.* Oslo : Department of Mathematics, University of Oslo, 1994.

29. **IDL. help** [Cited: October 10, 2010.] http://www.astro.virginia.edu/class/oconnell/astr511/idl_5.1_html/idl1da.htm.

30. *Is it time to incorporate quantitative functional imaging data, FDG PET in particular, into the response evaluation criteria in solid tumours?* **Basu Sandip, Nair Narendra.** 2006, Nuclear Medicine Communications; Volume 27(5), pp. 413-416.

31. *Positron emission tomographic assessment of "metabolic flare" to predict response of metastatic breast cancer to antiestrogen therapy.* **Dehdashti F, Flanagan FL, Mortimer JE, Katzenellenbogen JA, Welch MJ, Siegel BA.** European Journal of Nuclear Medicine, volume 26(1), pp. 51-6.

32. *A phantom for investigation of tumour signal and noise in PET reconstruction with various smoothing filters: experiments and comparisons with simulated intensity diffusion.* **A. Skretting, O. Glomset, T.V. Bogsrud.** 2010, Radiation Protection Dosimetry, pp. 1-4.

Appendix

A.1 Paper published in Acta Oncologica

Acta Oncologica, 2010; 49: 914–921

ORIGINAL ARTICLE

Preclinical dynamic ^{18}F-FDG PET – tumor characterization and radiotherapy response assessment by kinetic compartment analysis

KATHRINE RØE[1,3], THOMAS B. ALEKSANDERSEN[3], ALEXANDR KRISTIAN[2], LINE B. NILSEN[1,3], THERESE SEIERSTAD[1,4], HONG QU[3], ANNE H. REE[1,3], DAG R. OLSEN[5] & EIRIK MALINEN[3,6]

[1]*Department of Radiation Biology, and* [2]*Department of Tumor Biology, Institute for Cancer Research, The Norwegian Radium Hospital, Oslo University Hospital, Oslo, Norway,* [3]*University of Oslo, Oslo, Norway,* [4]*Department of Health Sciences, Buskerud University College, Drammen, Norway,* [5]*University of Bergen, Bergen, Norway and* [6]*Department of Medical Physics, The Norwegian Radium Hospital, Oslo University Hospital, Oslo, Norway*

Abstract

Background. Non-invasive visualization of tumor biological and molecular processes of importance to diagnosis and treatment response is likely to be critical in individualized cancer therapy. Since conventional static ^{18}F-FDG PET with calculation of the semi-quantitative parameter standardized uptake value (SUV) may be subject to many sources of variability, we here present an approach of quantifying the ^{18}F-FDG uptake by analytic two-tissue compartment modeling, extracting kinetic tumor parameters from dynamic ^{18}F-FDG PET. Further, we evaluate the potential of such parameters in radiotherapy response assessment. *Material and methods.* Male, athymic mice with prostate carcinoma xenografts were subjected to dynamic PET either untreated (n=8) or 24 h post-irradiation (7.5 Gy single dose, n=8). After 10 h of fasting, intravenous bolus injections of 10–15 MBq ^{18}F-FDG were administered and a 1 h dynamic PET scan was performed. 4D emission data were reconstructed using OSEM-MAP, before remote post-processing. Individual arterial input functions were extracted from the image series. Subsequently, tumor ^{18}F-FDG uptake was fitted voxel-by-voxel to a compartment model, producing kinetic parameter maps. *Results.* The kinetic model separated the ^{18}F-FDG uptake into free and bound tracer and quantified three parameters; forward tracer diffusion (k_1), backward tracer diffusion (k_2), and rate of ^{18}F-FDG phosphorylation, i.e. the glucose metabolism (k_3). The fitted kinetic model gave a goodness of fit (r^2) to the observed data ranging from 0.91 to 0.99, and produced parametrical images of all tumors included in the study. Untreated tumors showed homogeneous intra-group median values of all three parameters (k_1, k_2 and k_3), whereas the parameters significantly increased in the tumors irradiated 24 h prior to ^{18}F-FDG PET. *Conclusions.* This study demonstrates the feasibility of a two-tissue compartment kinetic analysis of dynamic ^{18}F-FDG PET images. If validated, extracted parametrical maps might contribute to tumor biological characterization and radiotherapy response assessment.

Positron emission tomography (PET) using the glucose analogue fluorine-18 (^{18}F)- fluorodeoxyglucose (FDG) has for many years been utilized in oncology. The application of this non-invasive imaging modality is not confined to tumor detection and staging, but may also be applied for monitoring therapy responses [1,2], and as a corollary of this, the technique can provide prognostic stratification [3,4]. The development of ^{18}F-FDG PET has provided cancer medicine with a valuable non-invasive metabolism-visualization modality.

The application of ^{18}F-FDG in tumor imaging is based on a phenomenon called the Warburg effect or aerobic glycolysis, in which glucose is converted into lactic acid in the presence of oxygen, being a specific metabolic abnormality in cancer cells [5]. After intravenous injection, ^{18}F-FDG is transported into the cytosol by glucose transporters (GLUTs), where it is trapped as FDG phosphate. In malignant tumors, particularly one of the isoforms, GLUT1, is frequently overexpressed, but overexpression of GLUT3 and GLUT12 has also been reported [6]. Intracellularly, ^{18}F-FDG is enzymatically phosphorylated by the enzyme hexokinase (HK), whose mitochondrial form is substantially elevated in rapidly proliferating tumors. As a result of the Warburg effect, glucose-starved tumor cells will have increased blood flow and

Correspondence: Kathrine Røe, Department of Radiation Biology, Institute for Cancer Research, The Norwegian Radium Hospital, Oslo University Hospital, Montebello, 0310 OSLO. Tel: +47 22781236. Fax: +47 22781207. E-mail: Kathrine.Roe@rr-research.no

(Received 17 May 2010; accepted 30 May 2010)

ISSN 0284-186X print/ISSN 1651-226X online © 2010 Informa Healthcare
DOI: 10.3109/0284186X.2010.498831

glucose transport, increased glucose phosphorylation, and decreased rates of dephosphorylation [6,7].

Conventional static ^{18}F-FDG PET employs coincidence detection at a certain time period after ^{18}F-FDG injection and is not time resolved. This technique allows visual identification of regions presenting elevated ^{18}F-FDG uptake, and calculation of the semi-quantitative parameter standardized uptake value (SUV). Although SUV has been shown to correlate to cancer malignancy, SUV is subject to many sources of variability which are not controlled for, or not even taken into account. These include PET system quality control accuracy, image reconstruction algorithm and filtering, body composition, time interval between tracer injection and PET, length of uptake period, plasma glucose level and partial volume effects [8–10]. On the other hand, dynamic ^{18}F-FDG PET employs time resolved coincidence detection, and biologically relevant information from kinetic analysis of the ^{18}F-FDG uptake may subsequently be extracted. Such tracer kinetic characteristics may not be obtained by static acquisition.

Identification of the most malignant and aggressive regions of tumors are of outmost importance in radiotherapy planning and evaluation [11]. Kinetic analysis of dynamic image series may provide parametrical maps depicting tumor properties of relevance for treatment selection and guidance. For instance, concomitant radiosensitization and/or dose escalation strategies appear attractive. Many of these dose escalation strategies are based on SUV, but more biologically relevant target regions may be obtained from kinetic analysis.

New tracers for PET applications are constantly being developed [12,13]. Although these tracers, if validated, are targeting specific processes of high importance, they may at first be expensive and unavailable to most users. In contrast, the full potential of dynamic ^{18}F-FDG has not yet been realized. The feasibility of employing parameters extracted from kinetic modeling of dynamic image series is in our opinion under-investigated. Also, ^{18}F-FDG is often the only tracer being available at many PET centers today. Besides the practical advantages of this tracer, it benefits from the relatively long physical half-life and quite low positron range of ^{18}F, and has a lower cost than the more specific tracers.

The purpose of this work was to establish an analytic tool for extraction of kinetic parameters from dynamic ^{18}F-FDG PET series, and to explore the potential of such parameters in radiotherapy response assessment.

Material and methods

Animals, xenografts and anesthesia

Male, BALB/c nude mice (30–35 g, 6–8 weeks old) were used in this study. The Institutional and National Committee on Research on Animal Care approved the protocol, and the experiment was performed according to Interdisciplinary Principles and Guidelines for the Use of Animals in Research, Marketing and Education (New York Academy of Science, New York, NY).

Xenografts were generated by subcutaneous (s.c.) implantation of $(\sim 2\ \text{mm})^3$ tumor tissue from the human androgen-sensitive CWR22 xenograft into the animals flanks. Procedures for implantation, growth and harvesting of CWR22 xenografts in mice were followed according to previous reports [14,15]. Animals were included into the study when their shortest tumor diameter reached 8 mm.

Animals were anesthetized with s.c. injections of a mixture of 2.4 mg/ml tiletamine and 2.4 mg/ml zolazepam (Zoletil vet, Virbac Laboratories, Carros, France), 3.8 mg/ml xylazine (Narcoxyl vet, Roche, Basel, Switzerland), and 0.1 mg/ml butorphanol (Torbugesic, Fort Dodge Laboratories, Fort Dodge, IA), diluted 1:5 in sterile water. A dose of 50 µl/10 g of body weight was given prior to radiation (to both untreated and irradiated animals) and PET acquisitions.

Radiotherapy

Eight of the 16 tumors received a single radiation dose of 7.5 Gy 24 h prior to PET imaging. The radiation was delivered by a ^{60}Co source (Mobaltron 80, TEM Instruments, Crawley, UK) at a dose rate of 0.8 Gy/min. Groups of four mice were simultaneously irradiated by positioning their tumors in the four corners of a 10×10 cm radiation field, whilst keeping the rest of their bodies outside the radiation field. The cobalt source produces a megavolt beam that gives an initial dose buildup with depth, resulting in a maximum radiation dose at 4 mm depth. To achieve a homogeneous dose deposition within the tumor volume, a 5 mm thick polystyrene bolus was placed on top of the tumor.

PET imaging

Dynamic ^{18}F-FDG PET was performed at a small animal PET scanner (microPET Focus 120, Siemens Medical Solutions, Erlangen, Germany). After 10 h of fasting, the anesthetized animals received i.v. bolus injections of 10–15 MBq ^{18}F-labelled FDG (GE Healthcare AS, Oslo, Norway) in heparinized saline, before a 1 h dynamic PET scan was performed. Attenuation and scatter correction was obtained by a 10 min transmission scan with a ^{68}Ge point source. 4D emission data were reconstructed using OSEM-MAP (2 OSEM iterations, 18 MAP iterations, $\beta = 0.5$, matrix size$=128 \times 128 \times 95$) [16,17], producing images with a voxel size of $0.87 \times 0.87 \times 0.80\ \text{mm}^3$.

The reconstructed time frames were 10 s during the initial 5 minutes, whereas the following time frames were 30 s. Further post-processing was executed in Interactive Data Language (IDL) v6.2 (Research Systems Inc., Boulder, CO).

Arterial input functions

Both the xenograft and the heart were imaged simultaneously within the same field-of-view, and thus, the arterial input function (AIF) could be determined individually for each animal. First, a 3D image series representing mean ^{18}F-FDG concentration taken over the initial uptake phase (0–1 minute) was generated from the dynamic PET series. Second, a seed point was manually located centrally in the heart, before region growing was performed within a sphere of 3 mm radius. Third, the grow region was refined by automatically excluding voxels where the time-activity curves (TACs) had characteristics differing from those expected from standard AIFs, defined as when the peak intensity of the TAC was less than four times the plateau level intensity of the TAC. Fourth, the AIF was determined by fitting a biexponential function ($AIF=A\ exp(-Bt)+C\ exp(-Dt)$) to the mean TACs in the refined grow region by the use of Levenberg-Marquardt least squares minimization (MPFIT; http://purl.com/net/mpfit) [18].

Kinetic modeling

Region-of-interests (ROIs) were manually delineated around individual tumors in the reconstructed dynamic PET images. Before kinetic modeling, a semi-quantitative measure was calculated to compare intra-group TACs and particularly differences in TACs between untreated and irradiated animals. Differences in injected dose of ^{18}F-FDG were corrected for by calculating normalized tumor TACs, i.e. the tumor TAC divided by the area under the plasma activity curve (i.e. the AIF).

The TAC in each tumor voxel was subjected to a two-tissue compartment kinetic model to describe the distribution and uptake of ^{18}F-FDG in tissue. The model was adopted from the work by Kamasak et al. [19], who applied this model in direct reconstruction of kinetic parameters from PET sinogram data. This model is similar to that originally proposed by Phelps et al. in 1979 [20]. In the model, C_p (pmol/ml) is the concentration of ^{18}F-FDG in plasma, i.e. the AIF, and C_T (pmol/ml) is the ^{18}F-FDG concentration in tumor. The concentration of ^{18}F-FDG in tumor can be separated into two tissue compartments; the concentration of unbound or not metabolized ^{18}F-FDG (C_F (pmol/ml)), and the concentration of bound or metabolized ^{18}F-FDG (C_B (pmol/ml)). The kinetic parameters k_1 (min^{-1}), k_2 (min^{-1}), k_3 (min^{-1}) and k_4 (min^{-1}), describe the exchange rates of ^{18}F-FDG between these compartments. Whereas the parameters k_1, k_2, and k_4 are first order rate constants, k_3 is an apparent first-order constant describing the glucose metabolism in proportion to the concentration of ^{18}F-FDG, dependent on the number of binding sites not being rate-limited. Using this compartment model, kinetic parameters could be extracted from the TAC of each tumor voxel by applying the following first order differential equations:

$$\frac{dC_F(t)}{dt} = k_1 C_p(t) - (k_2 + k_3) C_F(t) + k_4 C_B(t) \quad (1)$$

$$\frac{dC_B(t)}{dt} = k_3 C_F(t) - k_4 C_B(t) \quad (2)$$

The solutions of these equations are:

$$C_F(t) = \left\{ \frac{k_1}{a_2 - a_1} [(k_4 - a_1)e^{-a_1 t} + (a_2 - k_4)e^{-a_2 t}] \right\} \otimes C_p(t) \quad (3)$$

$$C_B(t) = \left\{ \frac{k_1 k_3}{a_2 - a_1} [e^{-a_1 t} + e^{-a_2 t}] \right\} \otimes C_p(t) \quad (4)$$

where $\otimes$ is the convolution operator and a_1 and a_2 are real valued constants:

$$a_1, a_2 = \frac{(k_2 + k_3 + k_4)}{2} \mp \frac{\sqrt{(k_2 + k_3 + k_4)^2 - 4k_2 k_4}}{2} \quad (5)$$

Using IDL, $C_F(t)+C_B(t)=C_T(t)$ was fitted to the TACs using Levenberg-Marquardt least squares minimization. Signal intensity of individual tumor voxels was smoothed over the neighboring $3\times3\times3$ voxels before fitting. The goodness of fit between the raw data and the fitted function was evaluated by calculations of correlation coefficients (r^2) in each tumor voxel. Inter-tumor variability in goodness of fit was compared by calculation of median tumor r^2. Inter-tumor and intra-tumor variations in kinetic parameters were assessed by calculations of median values and range for untreated and irradiated tumors.

Statistics

Statistical analysis was performed in SigmaStat v3.5 (Systat software, Inc., Chicago, IL). Differences between groups were analyzed using two-sided Mann-Whitney *U*-tests and a significance level of 5%.

Results

Qualitative assessment of PET images

Rapid ^{18}F-FDG uptake was detected in the heart and liver, whereas ^{18}F-FDG accumulation in the tumor was slower. The static images obtained at the last part of dynamic PET acquisitions revealed heterogeneous cumulative ^{18}F-FDG uptake in the tumors. The dynamic PET scan lasted for 60 min, a duration that was found to be too short to assess the degradation of tracer in this xenograft model, and consequently, estimation of the k_4 parameter was not possible in this study.

Arterial input functions

The heart could be identified in the PET images of all animals, allowing determination of individual AIFs. Representative PET images of ^{18}F-FDG uptake in the cardiac ventricle of one animal as function of time after ^{18}F-FDG injection are shown in Figure 1A. In Figure 1B, the corresponding AIF can be seen.

Quantitative kinetic modeling and radiotherapy response assessment

After correcting for differences in injected dose of ^{18}F-FDG, substantially different shapes of the normalized TACs were detected in irradiated tumors compared to untreated tumors (Figure 2). Significant differences were detected both in the initial phase of the ^{18}F-FDG uptake (t=1 min, p=0.029; t=1 min 15 s, p=0.001; t=1 min 30 s, p=0.014) and at the end of the dynamic scan (t=27.5 min, p=0.029; t=35 min, p=0.009; t=45 min, p=0.009; t=55 min, p=0.009).

By applying kinetic modeling, ^{18}F-FDG uptake was separated into free (not metabolized) and bound (metabolized) tracer. Model fitting produced parametrical images of all tumors and allowed quantification of the three kinetic parameters k_1, k_2 and k_3 in all tumor voxels. In Figure 3A, two tumor ROIs with high and low ^{18}F-FDG uptake, respectively, are delineated. These visual differences corresponded to different TACs, unveiling also different free and bound components, as seen in Figure 3B and C. The kinetic parameters of the low uptake regions was k_1=0.098 min^{-1}, k_2=0.425 min^{-1}, and k_3=0.048 min^{-1}, whereas in the high uptake region the parameters were k_1=0.189 min^{-1}, k_2=0.616 min^{-1}, and k_3=0.072 min^{-1}. The goodness of fit (r^2) between raw data and fitted function ranged from 0.91 to 0.99 (median=0.97). Parametrical maps of k_1, k_2, k_3 and r^2 of six slices through an irradiated CWR22 xenograft are shown in Figure 4, together with median, minimum and maximum tumor values of each parameter.

Untreated tumors demonstrated homogeneous intra-group median values of all three kinetic parameters (k_1, k_2 and k_3). In contrast, the tumors exposed to a 7.5 Gy radiation dose 24 h prior to ^{18}F-FDG PET showed heterogeneous intra-group parameter variations (Figure 5A–C). Compared to the untreated tumors, the median values of all kinetic parameters were significantly increased in the irradiated tumors (k_1, p=0.028; k_2, p=0.010; k_3, p=0.028). There were no significant differences in r^2 between untreated and irradiated tumors (p=0.515).

Discussion

In this study we have implemented and evaluated the feasibility of a kinetic two-tissue compartment model for analysis of dynamic ^{18}F-FDG PET images. Perturbations in the tumor microenvironment were elicited by irradiating CWR22 xenografts, and subsequently reflected by elevated TACs and significantly increased k_1, k_2 and k_3 values, as compared to the untreated xenografts.

Before kinetic modeling, we performed a semi-quantitative calculation of tumor ^{18}F-FDG uptake, which may be comparable to the conventional SUV.

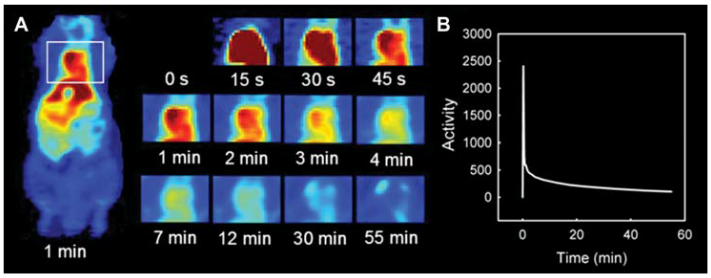

Figure 1. ^{18}F-FDG uptake in one animal's heart at different time points (A). The resulting AIF determined by fitting a biexponential function to the mean TAC of the identified 3D region of the heart (B).

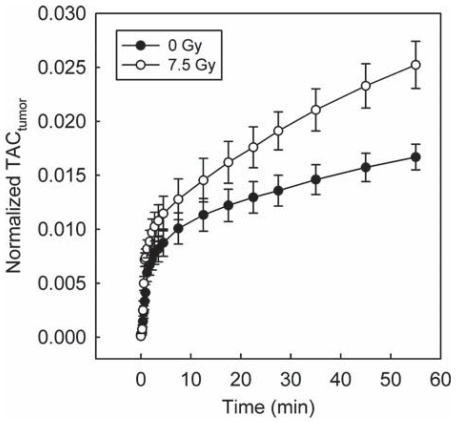

Figure 2. Mean and SEM TACs of eight untreated tumors and eight irradiated tumors, corrected for differences in injected dose of ^{18}F-FDG by normalizing the tumor TACs by the area under the AIF. Differences between the two groups were significant in the initial uptake phase (t=1 min, p=0.029; t=1 min 15 s, p=0.001; t=1 min 30 s, p=0.014) and at the end of the dynamic scan (t=27.5 min, p=0.029; t=35 min, p=0.009; t=45 min, p=0.009; t=55 min, p=0.009).

The tumor TACs were normalized to the area under the plasma activity curve, thereby removing variability occurring due to differences in injected doses of ^{18}F-FDG. The normalized TACs for the two groups evidenced a large difference in ^{18}F-FDG uptake between untreated and irradiated tumors, with the irradiated tumors presenting an increased rate of dynamic ^{18}F-FDG uptake, thus, this semi-quantitative measure deduced useful information on the tumor's treatment response. The stronger p-values found between the untreated and irradiated tumors for this semi-quantitative measure, as compared to the kinetic parameters, indicate that this measure is a good and maybe better measure of treatment response. However, we believe that kinetic parameters, separately and in combination, may provide valuable biological information that may help explaining the differences in normalized tumor TACs, by taking underlying pharmacokinetic mechanisms into account.

A prerequisite for performing high-quality compartmental modeling of radiotracer uptake in PET is accurate determination of the arterial input function (AIF). Previous studies on kinetic modeling has often involved *ex vivo* estimation of a mean AIF from repeated arterial blood sampling. In addition to radiation exposure to the staff, this procedure is technically challenging in small animals, also being limited by the small volume of blood that can be withdrawn without affecting these small animals' physiological function. In our study, ^{18}F-FDG uptake in tumor and heart was imaged simultaneously, allowing three-dimensional individual AIFs to be derived. However, a shortcoming in our study is that our AIFs have not been compared to results from arterial blood sampling. Thus, further investigations to verify the validity of the AIFs are needed.

Using the individually acquired AIFs, the TACs from both untreated and irradiated tumors were well fitted to the kinetic model, as demonstrated by goodness of fit values above 0.91 in all tumors. ^{18}F-FDG uptake is increased in hyperglycolyzed regions, but the exact mechanisms are complicated and influenced by several microenvironmental parameters, such as the GLUT activity, intracellular ^{18}F-FDG phosphorylation capability, but also by tumor oxygenation status, blood flow and permeability [6,7,21]. Changes

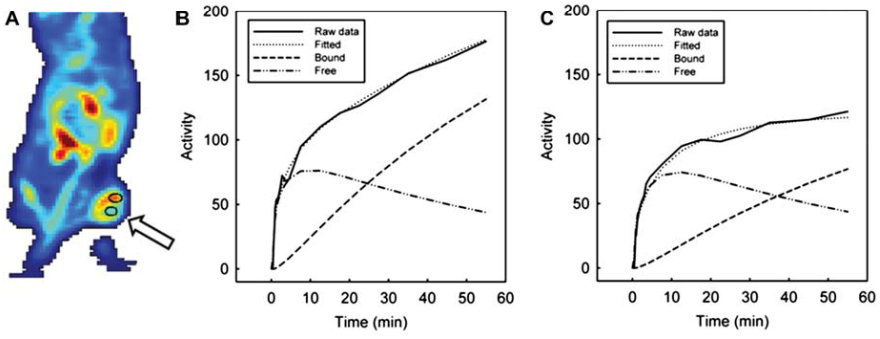

Figure 3. Tumor regions with high and low uptake of ^{18}F-FDG (A). Different TAC was detected in the high uptake region (B) and the low uptake region (C), including different free and bound components. The kinetic parameters of the high uptake region were k_1=0.189 min^{-1}, k_2=0.616 min^{-1}, and k_3=0.072 min^{-1}, whereas in the low uptake region the parameters were k_1=0.098 min^{-1}, k_2=0.425 min^{-1}, and k_3=0.048 min^{-1}.

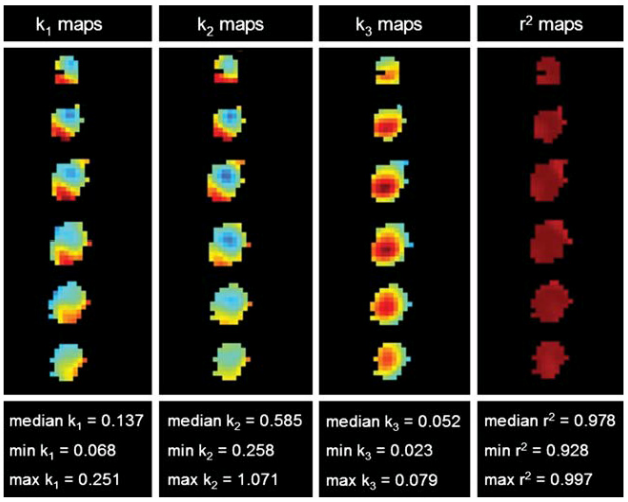

Figure 4. Parametrical maps of k_1, k_2,k_3 and r^2 extracted from the kinetic analysis of dynamic ^{18}F-FDG PET. Six slices of an irradiated CWR22 xenograft are shown, together with the tumor's corresponding median and range values for each parameter (in units of min^{-1} for k_1, k_2 and k_3).

in any of these factors will consequently affect the uptake pattern of ^{18}F-FDG, and thus, also the parameters extracted from kinetic analysis. The forward (k_1) and backward (k_2) diffusion of ^{18}F-FDG are known to be perfusion-dependent constants, and k_1 has previously been shown to significantly correlate with blood flow in a dynamic PET study evaluating chemotherapy in breast cancer [22]. After irradiation, blood vessels become more permeable, allowing injected substances to more easily diffuse into the extravascular space [23]. Since blood flow in general, and permeability in particular, increases ^{18}F-FDG uptake, the elevated k_1 and k_2 in our irradiated tumors (Figure 5A and B) could have been caused by increased permeability.

The k_3 parameter, reflecting the rate of ^{18}F-FDG phosphorylation, was also significantly increased in the irradiated tumors as compared to the untreated. Two tumors with substantially higher k_3 values than the other tumors in the irradiation group might have contributed strongly to this result. Thus, further investigations are needed in order to conclude. Increased expression of GLUTs and glycolytic enzymes, for example HKs, increases the ^{18}F-FDG phosphorylation, which will affect the k_3 parameter. Studies have shown that metabolic alterations are strongly correlated to hypoxia. Since tumor hyperglycosis, reflected by expression of GLUTs and HKs, is driven by activation of the master regulator of oxygen homeostasis under hypoxic conditions,

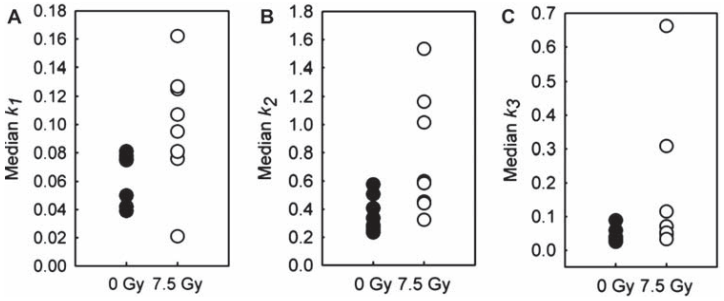

Figure 5. Homogeneous intra-group median values of the k_1 (min^{-1}) (A), k_2 (min^{-1}) (B) and k_3 (min^{-1}) (C) parameters in the untreated xenografts (black), whereas k_1 ($p=0.028$), k_2 ($p=0.010$) and k_3 ($p=0.028$) values changed significantly after irradiation (white).

the hypoxia-inducible factor (HIF-1), the ^{18}F-FDG uptake in tumors might indirectly reflect hypoxia [24]. Co-expression of HIF-1α with GLUTs and HKs has been reported [25], supporting the hypothesis that regions with increased hypoxia may have elevated k_3 values. Zhao et al. have in an experimental study found that regional expression levels of GLUT1, GLUT3 and HK enzymes were elevated in HIF-1α expressing tumor regions, which was suggested to be the cause of intense ^{18}F-FDG uptake in the same regions [5]. Positive correlation between ^{18}F-FDG uptake and hypoxia as detected by pimonidazole staining has also previously been found [21,26,27]. Known irradiation-induced changes in tumor biology 24 h post-irradiation include acute hypoxia, which might be one of the factors explaining the high k_3 parameter values in irradiated tumors. Other studies fail to demonstrate such a correlation between ^{18}F-FDG uptake and hypoxia. However, we believe that application of kinetic modeling and extraction of the k_3 parameter may be a more reliable biomarker of tumor hypoxia than SUV and ^{18}F-FDG uptake in general, but this hypothesis necessitates further investigations.

Hypoxia is a common feature of biologically aggressive tumors that more likely metastasize and represent worse prognosis. If these aggressive tumor regions could be reliably identified it may have consequences for treatment planning and evaluation [28–30]. In particular, intensity modulated radiotherapy (IMRT) and selective boosting of regions showing e.g. high k_3 values may prove valuable. Currently, advances in radiotherapy delivery technology allow realization of image adapted three-dimensional dose distributions based on PET images and kinetic parameter maps [11]. However, so far no large studies have investigated the potential use of such kinetic parameter maps in radiotherapy design, monitoring and/or prediction, representing an under-investigated application that warrants further evaluation.

In conclusion, this study has investigated the performance of a kinetic two-tissue compartment model in analysis of dynamic ^{18}F-FDG PET images in a preclinical model. The extracted parametrical maps and the interpretation of these require a rigorous validation involving correlation to histopathology. Upon validation, this analytic tool may non-invasively depict beneficiary information about tumor microenvironmental status and changes following therapy, and thereby facilitate treatment adaptation.

Acknowledgements

The authors thank Professor F. Saatcioglu at Department of Molecular Biosciences, University of Oslo, for providing the CWR22 xenograft model. Financial support received from the South-Eastern Norway Regional Health Authority (grant 2009070 to K. Røe and grant 2010079 to L. B. Nilsen) and the Norwegian Cancer Society (grant 80114001 to T. Seierstad).

Declaration of interest: The authors report no conflicts of interest. The authors alone are responsible for the content and writing of the paper.

References

[1] Greco C, Ling C. Broadening the scope of image-guided radiotherapy (IGRT). Acta Oncol 2008;47:1193–200.
[2] Bjurberg M, Gustavsson A, Ohlsson T, Brun T. FDG-PET in the detection of residual disease and relapse in patients with Hodgkin's lymphoma. Experience from at Swedish centre. Acta Oncol 2006;45:743–9.
[3] Bomanji JB, Costa DC, Ell PJ. Clinical role of positron emission tomography in oncology. Lancet Oncol 2001;2:157–64.
[4] Fletcher JW, Djulbegovic B, Soares HP, Siegel BA, Lowe VJ, Lyman GH, et al. Recommendations on the use of 18F-FDG PET in oncology. J Nucl Med 2008;49:480–508.
[5] Warburg O. On the origin of cancer cells. Science 1956;123: 309–14.
[6] Plathow C, Weber WA. Tumor cell metabolism imaging. J Nucl Med 2008;49(Suppl 2):S43–S63.
[7] Zhao S, Kuge Y, Mochizuki T, Takahashi T, Nakada K, Sato M, et al. Biologic correlates of intratumoral heterogeneity in 18F-FDG distribution with regional expression of glucose transporters and hexokinase-II in experimental tumor. J Nucl Med 2005;46:675–82.
[8] Krak NC, Boellaard R, Hoekstra OS, Twisk JW, Hoekstra CJ, Lammertsma AA. Effects of ROI definition and reconstruction method on quantitative outcome and applicability in a response monitoring trial. Eur J Nucl Med Mol Imaging 2005;32:294–301.
[9] Boellaard R, Krak NC, Hoekstra OS, Lammertsma AA. Effects of noise, image resolution, and ROI definition on the accuracy of standard uptake values: A simulation study. J Nucl Med 2004;45:1519–27.
[10] Keyes JW Jr. SUV: Standard uptake or silly useless value? J Nucl Med 1995;36:1836–9.
[11] Sovik A, Malinen E, Olsen DR. Strategies for biologic image-guided dose escalation: A review. Int J Radiat Oncol Biol Phys 2009;73:650–8.
[12] Kumar R, Dhanpathi H, Basu S, Rubello D, Fanti S, Alavi A. Oncologic PET tracers beyond [(18)F]FDG and the novel quantitative approaches in PET imaging. Q J Nucl Med Mol Imaging 2008;52:50–65.
[13] Pantaleo MA, Nannini M, Maleddu A, Fanti S, Ambrosini V, Nanni C, et al. Conventional and novel PET tracers for imaging in oncology in the era of molecular therapy. Cancer Treat Rev 2008;34:103–21.
[14] Wainstein MA, He F, Robinson D, Kung HJ, Schwartz S, Giaconia JM, et al. CWR22: Androgen-dependent xenograft model derived from a primary human prostatic carcinoma. Cancer Res 1994;54:6049–52.
[15] Nagabhushan M, Miller CM, Pretlow TP, Giaconia JM, Edgehouse NL, Schwartz S, et al. CWR22: The first human prostate cancer xenograft with strongly androgen-dependent and relapsed strains both in vivo and in soft agar. Cancer Res 1996;56:3042–6.
[16] Qi J, Leahy RM. Resolution and noise properties of MAP reconstruction for fully 3-D PET. IEEE Trans Med Imaging 2000;19:493–506.

[17] Qi J, Leahy RM, Cherry SR, Chatziioannou A, Farquhar TH. High-resolution 3D Bayesian image reconstruction using the microPET small-animal scanner. Phys Med Biol 1998; 43:1001–13.
[18] Markwardt CB. Non-linear least squares fitting in IDL with MPFIT. In: "Astronomical" data analysis software and systems XVIII", editors Bohlender D, Dowler P, Durand D. ASP Conference Series 2008; 411. Quebec, Canada. pp. 251–4.
[19] Kamasak ME, Bouman CA, Morris ED, Sauer K. Direct reconstruction of kinetic parameter images from dynamic PET data. IEEE Trans Med Imaging 2005;24:636–50.
[20] Phelps ME, Huang SC, Hoffman EJ, Selin C, Sokoloff L, Kuhl DE. Tomographic measurement of local cerebral glucose metabolic rate in humans with (F-18)2-fluoro-2-deoxy-D-glucose: Validation of method. Ann Neurol 1979;6:371–88.
[21] Pugachev A, Ruan S, Carlin S, Larson SM, Campa J, Ling CC, et al. Dependence of FDG uptake on tumor microenvironment. Int J Radiat Oncol Biol Phys 2005;62: 545–53.
[22] Tseng J, Dunnwald LK, Schubert EK, Link JM, Minoshima S, Muzi M, et al. 18F-FDG kinetics in locally advanced breast cancer: Correlation with tumor blood flow and changes in response to neoadjuvant chemotherapy. J Nucl Med 2004;45: 1829–37.
[23] Baker DG, Krochak RJ. The response of the microvascular system to radiation: A review. Cancer Invest 1989;7:287–94.
[24] Dierckx RA, Van De Wiele C. FDG uptake, a surrogate of tumour hypoxia? Eur J Nucl Med Mol Imaging 2008;35: 1544–9.
[25] Dang CV, Semenza GL. Oncogenic alterations of metabolism. Trends Biochem Sci 1999;24:68–72.
[26] Clavo AC, Brown RS, Wahl RL. Fluorodeoxyglucose uptake in human cancer cell lines is increased by hypoxia. J Nucl Med 1995;36:1625–32.
[27] Burgman P, Odonoghue JA, Humm JL, Ling CC. Hypoxia-induced increase in FDG uptake in MCF7 cells. J Nucl Med 2001;42:170–5.
[28] Kim Y, Tomé WA. Dose-painting IMRT optimization using biological parameters. Acta Oncol 2010 (in press).
[29] Røe K, Muren LP, Rørvik J, Olsen DR, Dahl O, Bakke A, et al. Dynamic contrast enhanced magnetic resonance imaging of bladder cancer and implications for biological image-adapted radiotherapy. Acta Oncol 2008;47:1257–64.
[30] Toma-Dasu I, Dasu A, Brahme A. Dose prescription and optimisation based on tumour hypoxia. Acta Oncol 2009; 48:1181–92.

A.2 Checklist for animal experiments

Animal:
Arrival date: -
Species: Nude mice
Strain: BALB/c
Supplier: Bred at the Radium hospital
Number: 10/13
Age and weight at start of experiment: 30-35 g, 6-8 weeks old
Sex: Male/
Quality category: SPF
Fasted before experiment: 10hours before PET imaging
Environment:
Type: barrier
Temperature: 21 +/- 1 C^{o}
Daylight in the animal room: No
Light/Dark cycle: 12 hours light cycle starting at 07:00, giving 200lux in the middle of the room and about 100lux in the cages.
Relative humidity: 60 +/- 5%
Air recycling: -
Cages/Housing:
Cage location: Cages were kept inside a cabinet
Cage type and size: Type III
Number of animals in each cage: 8-10
Environmental enrichment: paper and cardboard houses
Cage changes per week: 2 times a week
Feed:
Producer: Special diet services, UK
Consistence: Pellets
Availability: ad libitum
Litter/bedding:
Product name: Scanbur BK
Type: Shavings
Sterility: Heated
Consistency: chips
Water:
Type: Tap water
Sterility: some added HCL
Availability: ad libitum
Health assessment:
A list of information at the lab for each individual animal
Euthanasia:
Date: At end of experiment
Method: Swift dislocation of the neck

A.2 Codes in Interactive Data Language

Main program for obtaining tumor data.

```
DEVICE, DECOMPOSED = 0
common art, arter
!EXCEPT=0
print, 'Choose folder for data extraction'
fileloc=''
read, fileloc, prompt="Enter extraction location"
cd, fileloc
files = FILE_SEARCH('*', COUNT=n_images)
obj = OBJ_NEW('IDLffDICOM')
read = obj->Read(files(0))
date_dic = obj->GetValue('0008'x, '0020'x)
date_dic = *date_dic[0]
dim_xy = obj->GetValue('0028'x, '0010'x)
dim_xy = *dim_xy[0]
dim_z = obj->GetValue('0054'x, '0081'x)
dim_z = *dim_z[0]
dim_time = obj->GetValue('0054'x, '0101'x)
dim_time = *dim_time[0]
res_z= obj->GetValue('0018'x, '0050'x)
res_z = float(strcompress(strmid(*res_z[0], 0,6), /REMOVE_ALL))
res_xy= obj->GetValue('0028'x, '0030'x)
res_xy = float(strcompress(strmid(*res_xy[0], 0,6), /REMOVE_ALL))
inst=intarr(n_images)
for i=0, n_images-1 do begin
        read = obj->Read(files(i))
        dum = obj->GetValue('0054'x, '1330'x)
        inst(i) = *dum[0]
        ptr_free, dum
endfor
sort_ind=sort(inst)
bilder=dblarr(dim_xy, dim_xy, dim_z, dim_time)
time=fltarr(dim_time)
z_ind=0
time_ind=0
for i=0, n_images-1 do begin
        ind=sort_ind(i)
   read = obj->Read(files(ind))
```

```
                dum = obj->GetValue('7fe0'x, '0010'x)
            bilder(*,*, z_ind, time_ind)=double(rotate(*dum[0], 7))
        ;Scaling korreksjon
            resc = obj->GetValue('0028'x, '1053'x)
            ;resca=double(strcompress(strmid(*resc[0], 0, 10), /REMOVE_ALL))
            resca=double(*resc[0])
            bilder(*,*, z_ind, time_ind)=bilder(*,*, z_ind, time_ind)*resca
            z_ind=z_ind+1
            if z_ind eq dim_z then begin
              tim = obj->GetValue('0018'x, '1242'x)
              time(time_ind)=*tim[0]
              time_ind=time_ind+1
              z_ind=0
                    ptr_free, tim
            endif
            ptr_free, dum, resc
        endfor
OBJ_DESTROY, obj
        ;These lines make a new time array, where the new time is the time called "image time" in the tag plus
        ;half the "actual frame duration"
        timeElapsed=0
        for i=0, dim_time-1 do begin
                timeDummy=time(i)
                time(i)=timeElapsed+(1/2.0)*time(i)
                timeElapsed=timeElapsed+timeDummy
        endfor
        time(0)=0
        time=time/1000
        print, tim
        time=time/60.

        ;Because of memory problems, we'll try to cut up the picture a bit
        window, 0, xsize=dim_xy*4, ysize=dim_xy*4, TITLE = 'click bottom left corner of new image(make it
quadratic)'
        tvscl, rebin(bilder(*,*,60,round(dim_time/2.0)), 4*dim_xy, 4*dim_xy, 1, 1, /SAMPLE)
        cursor, xpo, ypo, 4, /DEVICE
        xpo=round(xpo/4.0)
        ypo=round(ypo/4.0)
        startx=xpo
        starty=ypo
        window, 0, xsize=dim_xy*4, ysize=dim_xy*4, TITLE = 'click upper right corner of new image'
        tvscl, rebin(bilder(*,*,60,round(dim_time/2.0)), 4*dim_xy, 4*dim_xy, 1, 1, /SAMPLE)
        cursor, xpo, ypo, 4, /DEVICE
        xpo=round(xpo/4.0)
```

```
ypo=round(ypo/4.0)
endx=xpo
endy=ypo
newdimx=endx-startx
newdimy=endy-starty
if newdimx gt newdimy then begin
        dim_xy=newdimx
endif else begin
        dim_xy=newdimy
endelse
alreadycutted =0
print, 'Did you alredy do that for this mouse?'
read, alreadycutted, prompt="Type 1 for yes, or 0 for no"
if alreadycutted then begin
        print, 'Then gimmi the folder name!!!!!!!!'
        fileloc101=''
        read, fileloc101, prompt="I am waiting..."
        cd, fileloc101
        restore, filename='bildecutting.sav'
        startx=bildecutting(0)
        starty=bildecutting(1)
        dim_xy=bildecutting(2)
endif else begin
        bildecutting=[startx,starty,dim_xy]
endelse
xcounter=startx
ycounter=starty
newbilder=dblarr(dim_xy,dim_xy,dim_z,dim_time)
for timemake = 0, dim_time-1 do begin
        for zmake = 0, dim_z-1 do begin
                for xmakeover = 0, dim_xy-1 do begin
                        for ymakeover = 0, dim_xy-1 do begin

newbilder(xmakeover,ymakeover,zmake,timemake)=bilder(xcounter,ycounter,zmake,timemake)
                                ycounter=ycounter+1
                        endfor
                        ycounter=starty
                        xcounter=xcounter+1
                endfor
                xcounter=startx
        endfor
endfor
bilder=0
bilder=newbilder
```

```
newbilder=0
;These 3 lines call upon functions that will find the intensity function of the heart and the turmour region.
arterieF=findheartfunction(dim_xy,dim_z,time,bilder)
bildesett=bilder(*,*,*,dim_time-1)
TumourR=findtumorregion(bildesett)
;TumourR=findtumorregionboost(bildesett)
stop
save, filename='bildecutting.sav', bildecutting
save, filename='arterieF.sav', arterieF
save, filename='tumorRegion.sav', TumourR
;restore, filename='tumorRegion.sav'
;This is an adittional set of data made in the previous funtion that is needed later.
restore, filename='kartkoord.sav'
loadct, 0
;The follwing is the steps to calculate the tumour functions free, bound and the k-values
index=where(TumourR)
parinfo = replicate({value:0.0D, fixed:0, limited:[0,0], limits:[0.D,0], relstep: 0.0D, tied:''}, 5)
;parinfo = replicate({value:0.0D, fixed:0, limited:[0,0], limits:[0.D,0], relstep: 0.0D, tied:''}, 4) ;Change this
when...
parinfo[0:2].limited[0] = 1
parinfo[0:2].limits[0]  = 0.D
parinfo[0:2].relstep = double(1.0e-4)
parinfo[3].fixed=1
parinfo[4].limited[0] = 1 ;Change this when switching artery parameter on/off
parinfo[4].limits[0]  = 0.D ;Change this when switching artery parameter on/off


k1_in=0.3
k2_in=0.5
k3_in=0.1
k4_in=0.0
vb_in=0.05 ;Change this when switching artery parameter on/off
func=fltarr(dim_time)
func_err=fltarr(dim_time)
stat=intarr(dim_xy,dim_xy, dim_z)
rkv=fltarr(dim_xy,dim_xy, dim_z)
k1=fltarr(dim_xy,dim_xy, dim_z)
k2=fltarr(dim_xy,dim_xy, dim_z)
k3=fltarr(dim_xy,dim_xy, dim_z)
k4=fltarr(dim_xy,dim_xy, dim_z)
CF=fltarr(dim_xy,dim_xy, dim_z, dim_time)
CB=fltarr(dim_xy,dim_xy, dim_z, dim_time)
bilder_fit=fltarr(dim_xy,dim_xy, dim_z, dim_time)
fak=8
```

```
time_interpol=dindgen(fak*dim_time)*(max(time)-min(time))/(fak*dim_time-1)
arter=interpol(arterieF, time, time_interpol)
func_err_inter=time_interpol*0+0.001
func_err=dblarr(dim_time)
par=double([k1_in, k2_in, k3_in, k4_in, vb_in]);, t0]) Change this when switching artery parameter on/off
;par=double([k1_in, k2_in, k3_in, k4_in]);, t0])
i1=long(0)
i=long(0)
fi=1
while i lt n_elements(index) do begin
        ind=array_indices(stat, index(i))
        start_z=ind(2)-fi
        if start_z lt 0 then begin
                start_z=0
                dum=fltarr(2*fi+1,2*fi+1,fi+1, dim_time)
        endif else begin
                dum=fltarr(2*fi+1,2*fi+1,2*fi+1, dim_time)
        endelse
        dum(*,*,*,*)=bilder(ind(0)-fi:ind(0)+fi, ind(1)-fi:ind(1)+fi,start_z:ind(2)+fi,*)
        for j=0, dim_time-1 do begin
                func(j)=mean(double(dum(*,*,*,j)))
                func_err(j)=stdev(double(dum(*,*,*,j)))
        endfor
   func_inter=double(interpol(func, time, time_interpol))
   func_err_inter=0*double(interpol(func_err, time, time_interpol))+1.0
   res=MPFITFUN('trekomp', time_interpol, func_inter, func_err_inter, par, PARINFO=parinfo,
YFIT=func_fit, STATUS=status, QUIET=1, MAXITER=200, FTOL=1e-3, /DOUBLE)
   bilder_fit(ind(0), ind(1),ind(2),*)=interpol(func_fit, time_interpol, time)
   k1(index(i))=res(0)
        k2(index(i))=res(1)
        k3(index(i))=res(2)
        k4(index(i))=res(3)
        stat(index(i))=status
        rkv(index(i))=correlate(interpol(func_fit, time_interpol, time), func)^2.0
        CF(ind(0), ind(1),ind(2),*)=interpol(free(time_interpol, res), time_interpol, time)
        CB(ind(0), ind(1),ind(2),*)=interpol(bound(time_interpol, res), time_interpol, time)
        func_avg=fltarr(dim_time)
        func_fit_avg=fltarr(dim_time*8)
        func_free_avg=fltarr(dim_time*8)
        func_bound_avg=fltarr(dim_time*8)
        i=i+1
endwhile
save, filename='k1.sav', k1
save, filename='k2.sav', k2
```

```
save, filename='k3.sav', k3
save, filename='rkv.sav', rkv
save, filename='status.sav', stat
;This next part will choose voxels containing tumour functions with rkv greater than 0.5,
;and print out the median function and k-values for the entire tumour
index=where(TumourR gt 0 and rkv gt 0.5)
func_avg=fltarr(dim_time)
func_fit_avg=fltarr(dim_time)
func_free_avg=fltarr(dim_time)
func_bound_avg=fltarr(dim_time)
dum=fltarr(dim_xy, dim_xy, dim_z)
for i=0, dim_time-1 do begin
        dum(*,*,*)=bilder(*,*,*,i)
        func_avg(i)=median(dum(index))
        dum(*,*,*)=bilder_fit(*,*,*,i)
        func_fit_avg(i)=median(dum(index))
        dum(*,*,*)=CF(*,*,*,i)
        func_free_avg(i)=median(dum(index))
        dum(*,*,*)=CB(*,*,*,i)
        func_bound_avg(i)=median(dum(index))
endfor
res(0)=median(k1(where(k1 gt 0)))
res(1)=median(k2(where(k2 gt 0)))
res(2)=median(k3(where(k3 gt 0)))
rkvmean=median(rkv(where(rkv gt 0)))
loadct, 0
window, 0, xsize=768, ysize=700
plot, time,func_avg, psym=4,  BACKGROUND=255, COLOR=0, CHARSIZE=2, YTITLE='Relative
Activity', XTITLE='Time (min)'
oplot, time,func_fit_avg, COLOR=0, THICK=2
oplot, time,func_free_avg, COLOR=0, linestyle=1, THICK=2
oplot, time,func_bound_avg, COLOR=150, linestyle=2, THICK=2
xyouts, 220,610, 'k1',  CHARSIZE=2, COLOR=0, /DEVICE
xyouts, 320,610, 'k2',  CHARSIZE=2, COLOR=0, /DEVICE
xyouts, 420,610, 'k3',  CHARSIZE=2, COLOR=0, /DEVICE
xyouts, 520,610, 'k4',  CHARSIZE=2, COLOR=0, /DEVICE
xyouts, 620,610, 'r2',  CHARSIZE=2, COLOR=0, /DEVICE
xyouts, 190,580, strmid(strcompress(string(res(0))), 0, 6),  CHARSIZE=2, COLOR=0, /DEVICE
xyouts, 290,580, strmid(strcompress(string(res(1))), 0, 6),  CHARSIZE=2, COLOR=0, /DEVICE
xyouts, 390,580, strmid(strcompress(string(res(2))), 0, 6),  CHARSIZE=2, COLOR=0, /DEVICE
xyouts, 490,580, strmid(strcompress(string(res(3))), 0, 6),  CHARSIZE=2, COLOR=0, /DEVICE
xyouts, 590,580, strmid(strcompress(string(rkvmean)), 0, 5),  CHARSIZE=2, COLOR=0, /DEVICE
TumorF_jpg=TVREAD(Filename = 'TumourF', /JPEG, QUALITY = 100)
;window, 3, xsize=4*dim_xy, ysize=4*dim_z
```

```
;The following 9 lines creates the k-value maps
;As you can see below, the size of the picture arrays decrease for each new k-parameter. This is in order to show
;them all in the same picture, without the ones applied later writes over the image of the ones printed earlier.
;need to fix something, but idc atm so I just restore iriginal value to the dimension thingy;)
dim_xy=128
rkvmap=fltarr(dim_xy+30,1,dim_z+30)
k1map=fltarr(dim_xy+30,1,dim_z)
k2map=fltarr(dim_xy+30,1,dim_z-30)
k3map=fltarr(dim_xy+30,1,dim_z-60)

;The Array NeedVs is the one restored from the kartkoords.sav files, containing 4 variables describing the
;location and approximate size of the tumour. newz is the number of slices in the z plane that is contains tumour tissue
;to be accurate, it contains the start and stop of the z range, and what is hopefully the center value in the x and y direction.
;This part of the program will unfourtunatly have to be rewritten if the size of the tumours is larger than the ones I've looked at.
newz=NeedVs(2)-NeedVs(1)
;Theese lines places slices of the tumour into the k-maps, the are placed next to eachother in ascending order.
for j1=0, 8  do begin
                rkvmap(1+(12*j1):9+(12*j1),0,(dim_z-newz-2)+20:(dim_z-2)+20)=rkv(NeedVs(3)-4:NeedVs(3)+4,NeedVs(0)-4+j1,NeedVs(1):NeedVs(2))
                k1map(1+(12*j1):9+(12*j1),0,(dim_z-newz-2)-10:(dim_z-2)-10)=k1(NeedVs(3)-4:NeedVs(3)+4,NeedVs(0)-4+j1,NeedVs(1):NeedVs(2))
                k2map(1+(12*j1):9+(12*j1),0,(dim_z-newz-2)-40:(dim_z-2)-40)=k2(NeedVs(3)-4:NeedVs(3)+4,NeedVs(0)-4+j1,NeedVs(1):NeedVs(2))
                k3map(1+(12*j1):9+(12*j1),0,(dim_z-newz-2)-70:(dim_z-2)-70)=k3(NeedVs(3)-4:NeedVs(3)+4,NeedVs(0)-4+j1,NeedVs(1):NeedVs(2))
endfor
;All the stuff below is just spesifics to create the Kmap picture with text and all that
loadct, 33
XPalette, /BLOCK
window, 3, xsize=4*(dim_xy+30), ysize=4*(dim_z+30)
tvscl, rebin(rkvmap(*,0,*),4*(dim_xy+30), 1, 4*(dim_z+30), 1, /SAMPLE)
tvscl, rebin(k1map(*,0,*),4*(dim_xy+30), 1, 4*dim_z, 1, /SAMPLE)
tvscl, rebin(k2map(*,0,*),4*(dim_xy+30), 1, 4*(dim_z-30), 1, /SAMPLE)
tvscl, rebin(k3map(*,0,*),4*(dim_xy+30), 1, 4*(dim_z-60), 1, /SAMPLE)
loadct, 0
xyouts, 15,475, 'rkv map',  CHARSIZE=2, COLOR=255, /DEVICE
xyouts, 15,355, 'k1 map',  CHARSIZE=2, COLOR=255, /DEVICE
```

```
xyouts, 15,235, 'k2 map',  CHARSIZE=2, COLOR=255, /DEVICE
xyouts, 15,115, 'k3 map',  CHARSIZE=2, COLOR=255, /DEVICE
xyouts, 15,20, 'Yvalues from bottom up --------->',  CHARSIZE=2, COLOR=255, /DEVICE
heirkv=rkv(where(rkv gt 0))
heik1=k1(where(k1 gt 0))
heik2=k2(where(k2 gt 0))
heik3=k3(where(k3 gt 0))
xyouts, 70,465, 'mean rkv:',  CHARSIZE=1, COLOR=255, /DEVICE
xyouts, 70,345, 'mean k1:',  CHARSIZE=1, COLOR=255, /DEVICE
xyouts, 70,225, 'mean k2:',  CHARSIZE=1, COLOR=255, /DEVICE
xyouts, 70,105, 'mean k3:',  CHARSIZE=1, COLOR=255, /DEVICE
xyouts, 110,465, mean(heirkv),  CHARSIZE=1, COLOR=255, /DEVICE
xyouts, 110,345, mean(heik1),  CHARSIZE=1, COLOR=255, /DEVICE
xyouts, 110,225, mean(heik2),  CHARSIZE=1, COLOR=255, /DEVICE
xyouts, 110,105, mean(heik3),  CHARSIZE=1, COLOR=255, /DEVICE
xyouts, 200,465, ',min rkv:',  CHARSIZE=1, COLOR=255, /DEVICE
xyouts, 200,345, ',min k1:',  CHARSIZE=1, COLOR=255, /DEVICE
xyouts, 200,225, ',min k2:',  CHARSIZE=1, COLOR=255, /DEVICE
xyouts, 200,105, ',min k3:',  CHARSIZE=1, COLOR=255, /DEVICE
xyouts, 250,465, min(heirkv),  CHARSIZE=1, COLOR=255, /DEVICE
xyouts, 250,345, min(heik1),  CHARSIZE=1, COLOR=255, /DEVICE
xyouts, 250,225, min(heik2),  CHARSIZE=1, COLOR=255, /DEVICE
xyouts, 250,105, min(heik3),  CHARSIZE=1, COLOR=255, /DEVICE
xyouts, 350,465, ',max rkv:',  CHARSIZE=1, COLOR=255, /DEVICE
xyouts, 350,345, ',max k1:',  CHARSIZE=1, COLOR=255, /DEVICE
xyouts, 350,225, ',max k2:',  CHARSIZE=1, COLOR=255, /DEVICE
xyouts, 350,105, ',max k3:',  CHARSIZE=1, COLOR=255, /DEVICE
xyouts, 390,465, max(heirkv),  CHARSIZE=1, COLOR=255, /DEVICE
xyouts, 390,345, max(heik1),  CHARSIZE=1, COLOR=255, /DEVICE
xyouts, 390,225, max(heik2),  CHARSIZE=1, COLOR=255, /DEVICE
xyouts, 390,105, max(heik3),  CHARSIZE=1, COLOR=255, /DEVICE
ParamsMap_jpg=TVREAD(Filename = 'ParamsMap', /JPEG, QUALITY = 100)
;And these lines makes histograms of the k-values and save em as images
n_bins=40
k1_hist = HISTOGRAM(heik1, NBINS = n_bins)
k1_stolpestr = DOUBLE((MAX(heik1) - MIN(heik1))/(n_bins))
k1_stolper = k1_stolpestr*FINDGEN(n_bins)
WINDOW, 5, TITLE = 'k1 histogram'
PLOT, k1_stolper, k1_hist, YRANGE = [0, MAX(k1_hist)+1], PSYM = 10, BACKGROUND = 255,
COLOR = 0, XTITLE = 'k1 value', YTITLE = 'intensity'
k1hist_jpg = TVREAD(filename = 'k1hist', /JPEG, QUALITY = 100)
n_bins=40
k2_hist = HISTOGRAM(heik2, NBINS = n_bins)
k2_stolpestr = DOUBLE((MAX(heik2) - MIN(heik2))/(n_bins))
```

```
k2_stolper = k2_stolpestr*FINDGEN(n_bins)
WINDOW, 6, TITLE = 'k2 histogram'
PLOT, k2_stolper, k2_hist, YRANGE = [0, MAX(k2_hist)+1], PSYM = 10, BACKGROUND = 255,
COLOR = 0, XTITLE = 'k2 value', YTITLE = 'intensity'
k2hist_jpg = TVREAD(filename = 'k2hist', /JPEG, QUALITY = 100)
n_bins=40
k3_hist = HISTOGRAM(heik3, NBINS = n_bins)
k3_stolpestr = DOUBLE((MAX(heik3) - MIN(heik3))/(n_bins))
k3_stolper = k3_stolpestr*FINDGEN(n_bins)
WINDOW, 7, TITLE = 'k3 histogram'
PLOT, k3_stolper, k3_hist, YRANGE = [0, MAX(k3_hist)+1], PSYM = 10, BACKGROUND = 255,
COLOR = 0, XTITLE = 'k3 value', YTITLE = 'intensity'
k3hist_jpg = TVREAD(filename = 'k3hist', /JPEG, QUALITY = 100)
n_bins=40
rkv_hist = HISTOGRAM(heirkv, NBINS = n_bins)
rkv_stolpestr = DOUBLE((MAX(heirkv) - MIN(heirkv))/(n_bins-1))
rkv_stolper = min(heirkv)+rkv_stolpestr*FINDGEN(n_bins)
WINDOW, 8, TITLE = 'rkv histogram'
PLOT, rkv_stolper, rkv_hist, YRANGE = [0, MAX(rkv_hist)+1], PSYM = 10, BACKGROUND = 255,
COLOR = 0, XTITLE = 'rkv value', YTITLE = 'intensity'
rkvhist_jpg = TVREAD(filename = 'rkvhist', /JPEG, QUALITY = 100)
print,
median(heik1),min(heik1),max(heik1),median(heik2),min(heik2),max(heik2),median(heik3),min(heik3),max(heik3),
median(heirkv)
end
```

Method for finding the plasmafunction

```
function findheartfunction ,dim_xy, dim_z, time, bilder
dim_time=n_elements(time)
unsatisf1=1
default=1
print, 'Have you already got a heartfunction for this mouse?'
alreadyHF=0
read, alreadyHF, prompt="Do you got a heartfunction for this mouse? "
if alreadyHF then begin
        print, 'Choose folder for heartfunction extraction'
        fileloc2=''
        read, fileloc2, prompt="Enter extracion location"
        cd, fileloc2
        unsatisf1=0
        restore, filename='centreOfHeart.sav'
                bilde=fltarr(dim_xy, dim_xy, dim_z)
        for i=0, 4 do begin
```

```
                bilde=bilde+bilder(*,*,*, i)
        endfor
endif
loadct, 33
while unsatisf1 do begin
        print, 'Do you want to use default settings?'
        read, default, prompt="Use default settings? "
        if not default then begin
                print, 'Choose start and stop for time averaging'
                read, start, stopp, prompt="Enter start and stop for time averaging: "
        endif
        if default then begin
                start=0
                stopp=4
        endif
        bilde=fltarr(dim_xy, dim_xy, dim_z)
        for i=start, stopp do begin
                bilde=bilde+bilder(*,*,*, i)
        endfor
        scalar=1

        if not default then begin
                print, 'Choose imgage scaling (default is 1)'
                read, scalar, prompt="Enter new image scaling: "
        endif
        window, 0, TITLE = 'Choose Y-value'
        tvscl, rebin(bilde(*,*,40), 4*dim_xy, 4*dim_xy,  1, /SAMPLE) < scalar*max(bilde)
        cursor, xpo, ypo, 4, /DEVICE
        yvalue=round(ypo/4.0)
        window, 0, xsize=512, ysize=512, TITLE = 'Choose Slice'
        tvscl, rebin(bilde(*,yvalue,*), 4*dim_xy, 1, 4*dim_z, /SAMPLE) < scalar*max(bilde)
        cursor, xpo, ypo, 4, /DEVICE
        xpo=round(xpo/4.0)
        ypo=round(ypo/4.0)
        snitt=ypo
        print, 'snitt valgt;'
        print, snitt
        window, 0, TITLE = 'Choose Seed Location'
        tvscl, rebin(bilde(*,*,snitt), 4*dim_xy, 4*dim_xy, 1, /SAMPLE) < scalar*max(bilde)
        ;tv, rebin(bild_btscl(*,72,*, 19),4*dim_xy, 1, 4*dim_z, 1, /SAMPLE)
        cursor, xpo, ypo, 4, /DEVICE
        xpo=round(xpo/4.0)
        ypo=round(ypo/4.0)
        reg=intarr(dim_xy, dim_xy)
```

```
		reg(xpo-1:xpo+1, ypo)=1
		reg(xpo, ypo-1:ypo+1)=1
		print, xpo
		print, ypo
		reg_3d=intarr(dim_xy, dim_xy, dim_z)
		reg_3d(*,*,snitt)=reg(*,*)
		cross_3d=where(reg_3d eq 1)


		print, 'Are you unsatisfied with the seed location?'
		read, mhm, prompt="Are you unsatisfied with the seed location? "
		unsatisf1 = mhm
	endwhile
	heartregion=REGION_GROW(bilde,cross_3d, STDDEV_MULTIPLIER=7.0)
	displayGrown_3d=intarr(dim_xy, dim_xy, dim_z)
	displayGrown_3d(heartregion)=1
	if not default then begin
		print, 'Do you want to see a video of the grown region?
		read, videogrown, prompt="Do you want to see a video of the grown region? "
		if videogrown then begin
			window, 1, xsize=512, ysize=512, TITLE = 'grown'
			for i=ypo-7, ypo+7 do begin
				;tvscl, rebin(bilde(*,i,*), 4*dim_xy, 1, 4*dim_z, /SAMPLE) < 0.2*max(bilde)
				;stop
				tvscl, rebin(bilde(*,i,*)*((1-displayGrown_3d(*,i,*))), 4*dim_xy, 1, 4*dim_z,
/SAMPLE) < 0.7*max(bilder)
				;stop
				wait, 1
			endfor
		endif
	endif
	;Shall we try to limit the region then?
	centre=array_indices(bilde, cross_3d(2))
	print, 'Choose where to save data'
	fileloc=''
	read, fileloc, prompt="Enter save location"
	cd, fileloc
	save, filename='centreOfHeart.sav', cross_3d
	wantlimit=1
	entiresphere=0
	radius=3
	if not default then begin
		print, 'Do you want to limit the region to a sphere, with the choosen seed location as the centre?'
```

```
		read, wantlimit, prompt="Do you want to limit the region to a sphere, with the choosen seed location as the centre?: "
		if wantlimit then begin
			print, 'In that case, do you want to use the entire sphere as your new heartregion?'
			read, entiresphere, prompt="Use entire sphere as new heartregion?"
			print, 'Oh and btw, you must give the radius of the sphere. A radius of 5 voxels shoud contain the entire heart and then some'
			read, radius, prompt="Enter raduis of sphere: "
		endif
	endif
	if entiresphere then begin
		heartregion=REGION_GROW(bilde,cross_3d, STDDEV_MULTIPLIER=100.0)
	endif
	time_cut=5
	i=long(0)
	ind_time_cut=lonarr(n_elements(heartregion))
	forhold=fltarr(n_elements(heartregion))
	j=long(0)
	while i lt n_elements(heartregion)-1 do begin
		index=array_indices(bilde, heartregion(i))
		time_ind_pre=where(time le time_cut)
		maks_pre_cut=float(max(bilder(index(0), index(1), index(2), min(time_ind_pre):max(time_ind_pre))))
		time_ind_post=where(time gt time_cut)
		maks_post_cut=float(max(bilder(index(0), index(1), index(2), min(time_ind_post):max(time_ind_post))))

		if wantlimit then begin
			distance=sqrt(((index(0)-centre(0))^2)+((index(1)-centre(1))^2)+((index(2)-centre(2))^2))
			if distance lt (radius+0.0001) and maks_pre_cut gt maks_post_cut then begin
				ind_time_cut(j)=heartregion(i)
				tall_pre=max(bilder(index(0), index(1), index(2), min(time_ind_pre):max(time_ind_pre)))
				tall_post=float(mean(bilder(index(0), index(1), index(2), dim_time-6:dim_time-1)))
				forhold(j)=tall_pre/tall_post
			j=j+1
			endif
		endif
		i=i+1
	endwhile

	sorte=reverse(sort(forhold))
```

```
func_average=0
k=long(0)
k5=0
n_functions=3
if not default then begin
	print, 'How many individual plasmafunctions do you want to display?'
	read, n_functions, prompt="Enter number of displayed plasmafunctions: "
endif
while k lt j do begin
	ind_max=sorte(k)
	ind_max_3d=ind_time_cut(ind_max)
	ind_max_3d_xyz=array_indices(bilde, ind_max_3d)
	func_orig=reform(bilder(ind_max_3d_xyz(0), ind_max_3d_xyz(1), ind_max_3d_xyz(2), *))
	if k lt n_functions and not alreadyHF then begin
		loadct, 0
		oplot, time, func_orig
	endif
	if forhold(sorte(k)) gt 4 then begin
		func_average=func_average+func_orig
		k5=k5+1
	endif
	k=k+1
endwhile
func_average=func_average/k5
;print, func_average
;time(where(time lt 100))=time(where(time lt 100))*100/60.
;time=time/100.
ind_min=where(func_average eq max(func_average))
ind_min=ind_min(0)
parinfo = replicate({value:0.0D, fixed:0, limited:[0,0], limits:[0.D,0], relstep:0.0D, tied:''}, 4)
parinfo[0:3].limited[0] = 1
parinfo[0:3].limits[0]  = 0.D
parinfo[0:3].relstep[0]  = double(1e-4)
parinfo[2].tied = strcompress(string(max(func_average)), /REMOVE_ALL)+'-P[0]' ; DETTE ER
'TRIKSET'!!!!
a_in=0.8*max(func_average)
b_in=2.0
c_in=0.2*max(func_average)
d_in=0.1
par=double([a_in, b_in, c_in, d_in])
func_err=time(ind_min:dim_time-1)*0+1.0
min_time=time(ind_min)
loadct, 0
```

```
res=MPFITFUN('arterie', time(ind_min:dim_time-1)-min_time(0),
double(func_average(ind_min:dim_time-1)), func_err, par, PARINFO=parinfo, YFIT=func_fit, STATUS=status,
QUIET=1, MAXITER=500, FTOL=1e-6, /DOUBLE)
window, 2, xsize=512, ysize=512
plot, time, func_average, PSYM=4
loadct, 33
oplot, time(ind_min:dim_time-1), func_fit, thick=2
heartF_jpg=TVREAD(Filename = 'heartF', /JPEG, QUALITY = 100)
func=func_average
func(ind_min:dim_time-1)=func_fit
return, func
END
```

Method for delinating the tumor

```
function findtumorregion, bilder
region=fix(bilder)
region(*)=0
si=size(bilder)
dim_xy=si(1)
dim_z=si(3)
dim_time=n_elements(time)
unsatisf1=1
scalar=0.02
choise=0
while unsatisf1 do begin
        reg=0
        region(*)=0
        window, 0, TITLE = 'Choose Y-value'
        tvscl, rebin(bilder(*,*,60), 4*dim_xy, 4*dim_xy, 1, /SAMPLE) < scalar*max(bilder)
        cursor, xpo, ypo, 4, /DEVICE
        yvalue=round(ypo/4.0)
        if choise eq 2 then begin
        print, 'Do you want to eter yvalue found in video instead?'
        print, 'Current yvalue is: ', yvalue
        read, yvalue, prompt="Enter new yvalue: "
        endif
        bild_btscl=bytscl(bilder, MAX=scalar*max(bilder))
        tv, rebin(bild_btscl(*,yvalue,*),4*dim_xy, 1, 4*dim_z, /SAMPLE)
        window, 0, xsize=dim_xy*4, ysize=dim_z*4, TITLE = 'Choose first slice of tumor region'
  tv, rebin(bild_btscl(*,yvalue,*),4*dim_xy, 1, 4*dim_z, /SAMPLE)
        cursor, xpo, ypo, 4, /DEVICE
        xpo=round(xpo/4.0)
        ypo=round(ypo/4.0)
```

```
        xvalue=xpo
        firstslice=ypo
        print, 'firstslice:'
        print, firstslice

        window, 0,  TITLE = 'Choose last slice of tumor region'
        tv, rebin(bild_btscl(*,yvalue,*),4*dim_xy, 1, 4*dim_z,  /SAMPLE)
        cursor, xpo, ypo, 4, /DEVICE
        xpo=round(xpo/4.0)
        ypo=round(ypo/4.0)
        lastslice=ypo
        print, 'lastslice:'
        print, lastslice
        tsk=intarr(2, 3, 2)
        for i=firstslice, lastslice do begin
                window, 0, xsize=dim_xy*4, ysize=dim_z*4, TITLE = 'Draw ROI around tumor'
                tvscl, rebin(bilder(*,*,i), 4*dim_xy, 4*dim_xy, 1,/SAMPLE) < scalar*max(bilder)
                ;tegn inn interesseområde - roi er en liste endimesjonale adresser i et 512x512 bilde
                roi=DEFROI(4*dim_xy,4*dim_xy, /RESTORE)
                reg=intarr(4*dim_xy,4*dim_xy)
                reg(roi)=1
                reg=rebin(reg, dim_xy, dim_xy, /sample)
                region(*,*,i)=reg

                endfor
        print, 'Are you unsatisfied with your tumor region?'
        read, mhm, prompt="Are you unsatisfied with your tumor region? "
        unsatisf1 = mhm
        if unsatisf1 then begin
                print, 'Choose new image scaling (default was 0.02)'
                read, scalar, prompt="Enter new image scaling: "
                print, 'Do you want to see video 1 or 2 too look for tumor?'
                read, choise, prompt ="Enter videonumber: "
                ok=videos(dim_xy,dim_z,dim_time,bilder,choise, time,scalar)
        endif
endwhile
NeedVs=intarr(4)
NeedVs(0)=yvalue
NeedVs(1)=firstslice
NeedVs(2)=lastslice
NeedVs(3)=xvalue
save, filename='kartkoord.sav', NeedVs
return, region
END
```

Method for obtaining arrays containing all normalized TACs wanted

```
DEVICE, DECOMPOSED = 0
common art, arter
!EXCEPT=0
;loadct, 33
;XPalette, /BLOCK
print, 'Choose dataset'
datset=''
read, datset, prompt="Enter datasetnr"
Dataset=finddataset(datset)
findnumber=size(Dataset)
n_tumours=findnumber(1)/2.
timevector=1.0
Superarray1=1.0
Superarray2=1.0
Superarray3=1.0
Superarray4=1.0
for iii=0, n_tumours-1 do begin
fileloc=Dataset(iii)
cd, fileloc
files = FILE_SEARCH('*', COUNT=n_images)
sort_ind=sort(inst)
bilder=dblarr(dim_xy, dim_xy, dim_z, dim_time)
time=fltarr(dim_time)
if iii eq 0 then begin
        Superarray1=fltarr(10,n_tumours)
        Superarray2=fltarr(10,n_tumours)
        if dim_time gt 20 then begin
                Superarray3=fltarr(10,n_tumours)
                Superarray4=fltarr(10,n_tumours)
        endif
endif
;some recurring code has been deleted
results=findnormalizationconstant(dim_xy,dim_z,time,bilder,Dataset,iii)
normconstant=results(0)
restore, filename='tumorRegion.sav'
print, normconstant
index=where(TumourR)
stat=intarr(dim_xy,dim_xy,dim_z)
tumourfunction=fltarr(dim_time)
i=0
while i lt n_elements(index) do begin
        ind=array_indices(stat, index(i))
```

```
        tumourdummy=reform(bilder(ind(0),ind(1),ind(2),*))
        tumourfunction=tumourfunction+tumourdummy
        i=i+1
endwhile
tumourfunction=tumourfunction/(normconstant*n_elements(index))
print, Dataset(iii+findnumber)
print, normconstant
timeshift=realtime(results(1))
realtime=realtime-timeshift
newtimearray=realtime(results(1):dim_time-1)
newtumourfunction=tumourfunction(results(1):dim_time-1)
tumourfunction=interpol(newtumourfunction,newtimearray,timevector)
for lol=0, n_elements(timevector)-1 do begin
        if lol lt 10 then Superarray1(lol,iii)=tumourfunction(lol)
        if lol lt 20 and lol gt 9 then Superarray2(lol-10,iii)=tumourfunction(lol)
        if lol lt 30 and lol gt 19 then Superarray3(lol-20,iii)=tumourfunction(lol)
        if lol lt 40 and lol gt 29 then Superarray4(lol-30,iii)=tumourfunction(lol)
endfor
endfor
print, Superarray1
print, 'hallllooooeen'
print, Superarray2
print, 'woot'
print, Superarray3
print, 'Oh yeah'
print, Superarray4
cd, 'F:\Gistmus\Data\GruppePercentiler'
save, filename='sa1.sav', Superarray1
save, filename='sa2.sav', superarray2
save, filename='sa3.sav', superarray3
save, filename='sa4.sav', superarray4
; The following part will sadly still have to be ad hoc ie  you have to change source code.
percentilesagain=fltarr(n_elements(timevector))
for i3=0, n_elements(timevector)-1 do begin
        if i3 lt 10 then begin
                g0=Superarray1(i3,0:11)
                g1=Superarray1(i3,12:21)
        endif
        if i3 gt 9 and i3 lt 20 then begin
                g0=Superarray2(i3-10,0:11)
                g1=Superarray2(i3-10,12:21)
        endif
        if i3 gt 19 and i3 lt 30 then begin
                g0=Superarray3(i3-20,0:11)
```

```
                g1=Superarray3(i3-20,12:21)
        endif
        if i3 gt 29 and i3 lt 40 then begin
                g0=Superarray4(i3-30,0:11)
                g1=Superarray4(i3-30,12:21)
        endif
        result=tm_test(g0,g1)
        percentilesagain(i3)=result(1)
endfor
window, 1
plot, percentilesagain , PSYM=4, BACKGROUND=255, COLOR=0
treshold=fltarr(n_elements(timevector))
treshold(0:n_elements(timevector)-1)=0.05
oplot, treshold, COLOR=0
stop
end
```

method for doing the patlak plots

```
;some recurring code has been deleted here
Kfromk=(res(0)*res(2))/(res(1)+res(2))
print, 'K* estimated from k-parameters'
print, Kfromk
KK(iii)=Kfromk
loadct, 0
dim_time=dim_time
func_tissue=func_free_avg+func_bound_avg
Patlakx=fltarr(dim_time)
Patlaky=fltarr(dim_time)
for ij=1, dim_time-1 do begin

        if arterieF(ij) gt 0 then begin
                ind=where(time lt (time(ij)+0.01))
                Patlakx(ij)=(int_tabulated(time(ind), arterieF(ind)))/arterieF(ij)
                Patlaky(ij)=func_tissue(ij)/arterieF(ij)
        endif
endfor
window, 0, xsize=700, ysize=700
;plot, Patlakx, Patlaky
plot, Patlakx, Patlaky, psym=4
Patlakxend=Patlakx((dim_time-4):(dim_time-1))
Patlakyend=Patlaky((dim_time-4):(dim_time-1))
KfromP=linfit(Patlakxend,Patlakyend)
```

```
print, 'K* estimated from Patlak plot'
print, KfromP(1)
PatlakK(iii)=KfromP(1)
lala=KfromP(1)*Patlakxend
lala=lala+KfromP(0)
oplot, Patlakxend, lala
stop
endfor
end
```

Method for creating the percentile charts

```
DEVICE, DECOMPOSED = 0
;This program is to do the ultimate test, check the percentile
print, 'Choose dataset (5)'
datset=''
read, datset, prompt="Enter datasetnr"
Dataset=finddataset(datset)
findnumber=(size(Dataset))
n_tumors=findnumber(1)/2
Percentilearrayk1=fltarr(102)
Percentilearrayk1(0)=0
Percentilearrayk1(101)=0
Percentilearrayk2=fltarr(102)
Percentilearrayk2(0)=0
Percentilearrayk2(101)=0
Percentilearrayk3=fltarr(102)
Percentilearrayk3(0)=0
Percentilearrayk3(101)=0
for i1=1, 100 do begin
ArrayG0k1=fltarr(12)
ArrayG1k1=fltarr(8)
ArrayG0k2=fltarr(12)
ArrayG1k2=fltarr(8)
ArrayG0k3=fltarr(12)
ArrayG1k3=fltarr(8)
g0counter=0
g1counter=0
for i=0, n_tumors-1 do begin
        cd, Dataset(i+n_tumors)
        restore, filename='k1.sav'
        restore, filename='k2.sav'
        restore, filename='k3.sav'
        k1array=k1(where (k1 gt 0))
```

```
                k2array=k2(where (k2 gt 0))
                k3array=k3(where (k3 gt 0))
                if Dataset(i) eq 0 then begin
                        perck1=prank(k1array,i1)
                        perck2=prank(k2array,i1)
                        perck3=prank(k3array,i1)
                        ArrayG0k1(g0counter)=perck1
                        ArrayG0k2(g0counter)=perck2
                        ArrayG0k3(g0counter)=perck3
                        g0counter=g0counter+1
                endif
                if Dataset(i) eq 1 then begin
                        perck1=prank(k1array,i1)
                        perck2=prank(k2array,i1)
                        perck3=prank(k3array,i1)
                        ArrayG1k1(g1counter)=perck1
                        ArrayG1k2(g1counter)=perck2
                        ArrayG1k3(g1counter)=perck3
                        g1counter=g1counter+1
                endif
        endfor
        resultk1=TM_TEST(ArrayG0k1,ArrayG1k1)
        resultk2=TM_TEST(ArrayG0k2,ArrayG1k2)
        resultk3=TM_TEST(ArrayG0k3,ArrayG1k3)
        if i1 eq 50 then stop
        Percentilearrayk1(i1)=resultk1(1)
        Percentilearrayk2(i1)=resultk2(1)
        Percentilearrayk3(i1)=resultk3(1)
        endfor
        hello=fltarr(102)
        hello[0:101]=0.05
        ;t test (mean-test)/(std/(sqrt(n)))
        ;TM_TEST gir [t,p]
        n_bins=102
        Stolpestr = 1
        Stolper = FINDGEN(n_bins)
        loadct, 0
        cd, 'F:\DATA PET forsøk\Grupperpercentiler'
        WINDOW, 1, TITLE = 'Percentiles k1'
        PLOT, Stolper, Percentilearrayk1, YRANGE = [0, 1.1*Max(Percentilearrayk1)], PSYM = 10,
BACKGROUND = 255, COLOR = 0, XTITLE = 'Percentiles k1', YTITLE = 'p-value'
        ;FinalAllk1g0hist_jpg = TVREAD(filename = 'FinalAllk1g0hist', /JPEG, QUALITY = 100)
        loadct, 33
        oplot, hello, color = 220
```

```
loadct, 0
Percentilearrayk1_jpg = TVREAD(filename = 'Percentilearrayk1', /JPEG, QUALITY = 100)
WINDOW, 2, TITLE = 'Percentiles k2'
PLOT, Stolper, Percentilearrayk2, YRANGE = [0, 1.1*Max(Percentilearrayk2)], PSYM = 10,
BACKGROUND = 255, COLOR = 0, XTITLE = 'Percentiles k2', YTITLE = 'p-value'
loadct, 33
oplot, hello, color=220
loadct, 0
Percentilearrayk2_jpg = TVREAD(filename = 'Percentilearrayk2', /JPEG, QUALITY = 100)
WINDOW, 3, TITLE = 'Percentiles k3'
PLOT, Stolper, Percentilearrayk3, YRANGE = [0, 1.1*Max(Percentilearrayk3)], PSYM = 10,
BACKGROUND = 255, COLOR = 0, XTITLE = 'Percentiles k3', YTITLE = 'p-value'
loadct, 33
oplot, hello, color=220
loadct, 0
Percentilearrayk3_jpg = TVREAD(filename = 'Percentilearrayk3', /JPEG, QUALITY = 100)
End
```

Method for checking radiell dependency

```
DEVICE, DECOMPOSED = 0
print, 'Choose dataset'
datset=''
read, datset, prompt="Enter datasetnr"
Dataset=finddataset(datset)
findnumber=size(Dataset)
n_tumours=findnumber(1)/2.
CorrArr=fltarr(n_tumours)
MaxDistArr=fltarr(n_tumours)
;MegaDistanceg0=fltarr(10000)
Megak1g0=fltarr(8)
Megak2g0=fltarr(8)
Megak3g0=fltarr(8)
MegaMeRag0=fltarr(8)
MegaCountg0=0
Megak1g1=fltarr(8)
Megak2g1=fltarr(8)
Megak3g1=fltarr(8)
MegaMeRag1=fltarr(8)
MegaCountg1=0
for iii=0, n_tumours-1 do begin
cd, Dataset(iii+n_tumours)
restore, filename='k1.sav'
```

```
restore, filename='k2.sav'
restore, filename='k3.sav'
restore, filename='tumorRegion.sav'
dim_xy=128
dim_z=9
MeRa=fltarr(dim_xy,dim_xy,dim_z)
for xlol = 0, dim_xy-1 do begin
        for ylol = 0, dim_xy-1 do begin
                for zlol =0, dim_z-1 do begin
                k1val=k1(xlol,ylol,zlol)
                k2val=k2(xlol,ylol,zlol)
                k3val=k3(xlol,ylol,zlol)
                if k1val gt 0 and k2val gt 0 and k3val gt 0 then begin
                        MeRa(xlol,ylol,zlol)=(k1val*k3val)/(k2val+k3val)
                endif
                endfor
        endfor
endfor
;MeRa=((k1(where(k2))*k3(where(k2)))/(k2(where(k2))+k3(where(k2))))
save, filename='MeRa.sav', MeR
jaha=where(TumourR gt 0)
xretning=intarr(n_elements(jaha))
yretning=intarr(n_elements(jaha))
zretning=intarr(n_elements(jaha))
;restore den tingen tingen
;dim_xy=bildecutting(2)
dim_z=95
noe=intarr(dim_xy,dim_xy,dim_z)
for ix=0, n_elements(jaha)-1 do begin
        ind=array_indices(noe, jaha(ix))
        xretning(ix)=ind(0)
        yretning(ix)=ind(1)
        zretning(ix)=ind(2)
endfor
xret=xretning(where(xretning gt 0))
yret=yretning(where(yretning gt 0))
zret=zretning(where(zretning gt 0))
index=fltarr(3)
index(0)=median(xret)
index(1)=median(yret)
index(2)=median(zret)
DistArr=fltarr(n_elements(jaha))
k1Arr=fltarr(n_elements(jaha))
k2Arr=fltarr(n_elements(jaha))
```

```
k3Arr=fltarr(n_elements(jaha))
MeRaArr=fltarr(n_elements(jaha))
for xi=0, n_elements(jaha)-1 do begi
        ;Allright, then to make an insane thingy to calculate a cricular thing
        distance=sqrt((((index(0)-xret(xi))*0.87)^2)+(((index(1)-yret(xi))*0.87)^2)+(((index(2)-
zret(xi))*0.8)^2))
        DistArr(xi)=distance
        k1Arr(xi)=k1(xret(xi),yret(xi),zret(xi))
        k2Arr(xi)=k2(xret(xi),yret(xi),zret(xi))
        k3Arr(xi)=k3(xret(xi),yret(xi),zret(xi))
        MeRaArr(xi)=MeRa(xret(xi),yret(xi),zret(xi))
endfor
window, 0
plot, DistArr, k1Arr, psym=4
xyouts, 10,256, 'k1',  CHARSIZE=1, COLOR=255, /DEVICE
xyouts, 180,8, 'Distance->',  CHARSIZE=1, COLOR=255, /DEVICE
xyouts, 250,8, 'Correlation',  CHARSIZE=1, COLOR=255, /DEVICE
xyouts, 300,8, correlate(DistArr, k1Arr),  CHARSIZE=1, COLOR=255, /DEVICE
k1radiell = TVREAD(filename = 'k1radiell', /JPEG, QUALITY = 100)
window, 1
plot, DistArr, k2Arr, psym=4
xyouts, 10,256, 'k2',  CHARSIZE=1, COLOR=255, /DEVICE
xyouts, 180,8, 'Distance->',  CHARSIZE=1, COLOR=255, /DEVICE
xyouts, 250,8, 'Correlation',  CHARSIZE=1, COLOR=255, /DEVICE
xyouts, 300,8, correlate(DistArr, k2Arr),  CHARSIZE=1, COLOR=255, /DEVICE
k2radiell = TVREAD(filename = 'k2radiell', /JPEG, QUALITY = 100)
window, 2
plot, DistArr, k3Arr, psym=4
xyouts, 10,256, 'k3',  CHARSIZE=1, COLOR=255, /DEVICE
xyouts, 180,8, 'Distance->',  CHARSIZE=1, COLOR=255, /DEVICE
xyouts, 250,8, 'Correlation',  CHARSIZE=1, COLOR=255, /DEVICE
xyouts, 300,8, correlate(DistArr, k3Arr),  CHARSIZE=1, COLOR=255, /DEVICE
k3radiell = TVREAD(filename = 'k3radiell', /JPEG, QUALITY = 100)
window, 3
plot, DistArr, MeRaArr, psym=4
xyouts, 10,256, 'Metabloic Rate',  CHARSIZE=1, COLOR=255, /DEVICE
xyouts, 180,8, 'Distance->',  CHARSIZE=1, COLOR=255, /DEVICE
xyouts, 250,8, 'Correlation',  CHARSIZE=1, COLOR=255, /DEVICE
xyouts, 300,8, correlate(DistArr, MeRaArr),  CHARSIZE=1, COLOR=255, /DEVICE
MeRaradiell = TVREAD(filename = 'MetabolicRateRradiell', /JPEG, QUALITY = 100
print, correlate(DistArr, k3Arr)
print, Dataset(iii+n_tumours)
print,max(DistArr)
CorrArr(iii)=correlate(DistArr, k3Arr)
```

```
MaxDistArr(iii)=max(DistArr)
lulz=0
if Dataset(iii) eq 0 then begin



                    Megak1g0(Megacountg0)=correlate(DistArr, k1Arr)
                    Megak2g0(Megacountg0)=correlate(DistArr, k2Arr)
                    Megak3g0(Megacountg0)=correlate(DistArr, k3Arr)
                    MegaMeRag0(Megacountg0)=correlate(DistArr, MeRaArr)
                    Megacountg0=Megacountg0+1
          ;endfor
endif
if Dataset(iii) eq 1 then begin

                    ;MegaDistanceg1(Megacountg1)=DistArr(lulz)
                    Megak1g1(Megacountg1)=correlate(DistArr, k1Arr)
                    Megak2g1(Megacountg1)=correlate(DistArr, k2Arr)
                    Megak3g1(Megacountg1)=correlate(DistArr, k3Arr)
                    MegaMeRag1(Megacountg1)=correlate(DistArr, MeRaArr)
                    Megacountg1=Megacountg1+1

endif

endfor
print, 'mean k1g0'
print, median(Megak1g0)
print, 'mean k2g0'
print, median(Megak2g0)
print, 'mean k3g0'
print, median(Megak3g0)
print, 'mean MeRag0'
print, median(MegaMeRag0)
print, 'mean k1g1'
print, median(Megak1g1)
print, 'mean k2g1'
print, median(Megak2g1)
print, 'mean k3g1'
print, median(Megak3g1)
print, 'mean MeRag1'
print, median(MegaMeRag1)
print, 'then the p-values'
result=tm_test(Megak1g0,Megak1g1)
print, result(1)
```

```
result=tm_test(Megak2g0,Megak2g1)
print, result(1)
result=tm_test(Megak3g0,Megak3g1)
print, result(1)
result=tm_test(MegaMeRag0,MegaMeRag1)
print, result(1)
end
```

support porgrams, arterie

```
Function arterie, x, par, F
a=par(0)
b=par(1)
c=par(2)
d=par(3)
F=a*exp(-b*x)+c*exp(-d*x)
return, F
end
```

bound

```
Function bound, x, par, F
common art
k1=par(0)
k2=par(1)
k3=par(2)
alfa1=0.5*(k2+k3+k4-sqrt(((k2+k3+k4)^2)-4*k2*k4))
alfa2=0.5*(k2+k3+k4+sqrt(((k2+k3+k4)^2)-4*k2*k4))
nel=n_elements(x)
F=fltarr(nel)
fak=k1*k3/(alfa2-alfa1)
F1_h=exp(-alfa1*x(1:*))*total((x(1:*)-x(0:nel-2))*arter(1:*)*exp(alfa1*x(1:*)), /CUMULATIVE, /DOUBLE)
F2_h=exp(-alfa2*x(1:*))*total((x(1:*)-x(0:nel-2))*arter(1:*)*exp(alfa2*x(1:*)), /CUMULATIVE, /DOUBLE)
F1_v=exp(-alfa1*x(0:nel-2))*total((x(1:*)-x(0:nel-2))*arter(0:nel-2)*exp(alfa1*x(0:nel-2)), /CUMULATIVE,
/DOUBLE)
F2_v=exp(-alfa2*x(0:nel-2))*total((x(1:*)-x(0:nel-2))*arter(0:nel-2)*exp(alfa2*x(0:nel-2)), /CUMULATIVE,
/DOUBLE)
F(1:*)=fak*0.5*(F1_h+F1_v-F2_h-F2_v)
return, F
end
```

free

```
Function free, x, par, F
common art
k1=par(0)
k2=par(1)
k3=par(2)
k4=par(3)
```

```
alfa1=0.5*(k2+k3+k4-sqrt(((k2+k3+k4)^2)-4*k2*k4))
alfa2=0.5*(k2+k3+k4+sqrt(((k2+k3+k4)^2)-4*k2*k4))
nel=n_elements(x)
F=fltarr(nel)
F1_h=(k1/(alfa2-alfa1))*(k4-alfa1)*exp(-alfa1*x(1:*))*total((x(1:*)-x(0:nel-2))*arter(1:*)*exp(alfa1*x(1:*)),
/CUMULATIVE, /DOUBLE)
F2_h=(k1/(alfa2-alfa1))*(alfa2-k4)*exp(-alfa2*x(1:*))*total((x(1:*)-x(0:nel-2))*arter(1:*)*exp(alfa2*x(1:*)),
/CUMULATIVE, /DOUBLE)
F1_v=(k1/(alfa2-alfa1))*(k4-alfa1)*exp(-alfa1*x(0:nel-2))*total((x(1:*)-x(0:nel-2))*arter(0:nel-
2)*exp(alfa1*x(0:nel-2)), /CUMULATIVE, /DOUBLE)
F2_v=(k1/(alfa2-alfa1))*(alfa2-k4)*exp(-alfa2*x(0:nel-2))*total((x(1:*)-x(0:nel-2))*arter(0:nel-
2)*exp(alfa2*x(0:nel-2)), /CUMULATIVE, /DOUBLE
F(1:*)=0.5*(F1_h+F1_v+F2_h+F2_v)
return, F
end
```

trekomp

```
Function trekomp, x, par, F
common ar
F=free(x, par)+bound(x,par)
F=F+(par(4)*arter)  ;Change this when switching artery parameter on/off
return, F
end
```